



## 저작자표시-비영리-변경금지 2.0 대한민국

이용자는 아래의 조건을 따르는 경우에 한하여 자유롭게

- 이 저작물을 복제, 배포, 전송, 전시, 공연 및 방송할 수 있습니다.

다음과 같은 조건을 따라야 합니다:



저작자표시. 귀하는 원저작자를 표시하여야 합니다.



비영리. 귀하는 이 저작물을 영리 목적으로 이용할 수 없습니다.



변경금지. 귀하는 이 저작물을 개작, 변형 또는 가공할 수 없습니다.

- 귀하는, 이 저작물의 재이용이나 배포의 경우, 이 저작물에 적용된 이용허락조건을 명확하게 나타내어야 합니다.
- 저작권자로부터 별도의 허가를 받으면 이러한 조건들은 적용되지 않습니다.

저작권법에 따른 이용자의 권리는 위의 내용에 의하여 영향을 받지 않습니다.

이것은 [이용허락규약\(Legal Code\)](#)을 이해하기 쉽게 요약한 것입니다.

[Disclaimer](#)

**Doctoral Thesis**

**Exploitation of Cyclostationarity  
and Impropropriety in Optimal System  
Design**

Jeongho Yeo (여 정 호)

Department of Electrical Engineering

Pohang University of Science and Technology

2014



주기정상성과 복소이상성을 이용한  
최적 시스템 설계

**Exploitation of Cyclostationarity  
and Impropropriety in Optimal System  
Design**



# **Exploitation of Cyclostationarity and Impropriety in Optimal System Design**

by

Jeongho Yeo

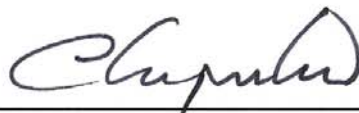
Department of Electrical Engineering  
Pohang University of Science and Technology

A thesis submitted to the faculty of Pohang University of Science and Technology in partial fulfillment of the requirements for the degree of Doctor of Philosophy in the Department of Electrical Engineering.

Pohang, Korea

June 11, 2014

Approved by



Joon Ho Cho  
Academic Advisor



# Exploitation of Cyclostationarity and Impropriety in Optimal System Design

Jeongho Yeo

The undersigned have examined this thesis and hereby  
certify that it is worthy of acceptance for a doctoral degree  
from POSTECH.

6/11/2014

Committee Chair    조 준 호

(Seal)

Member    김 경 태

(Seal)

Member    박 부 건

(Seal)

Member    송 황 준

(Seal)

Member    임 기 홍

(Seal)

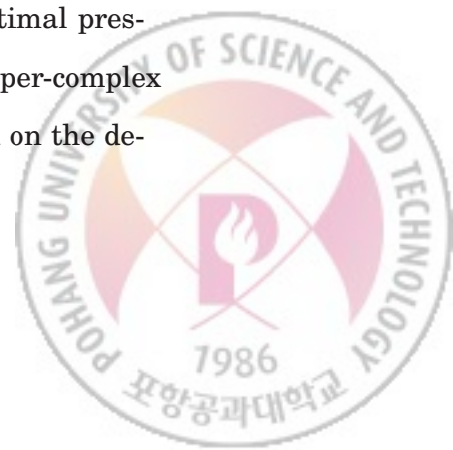


DEE 20062243 여 정 호, Jeongho Yeo, Exploitation of Cyclostationarity and Impropropriety in Optimal System Design, 주기정상성과 복소이상성을 이용한 최적 시스템 설계, Department of Electrical Engineering, 2014, 128 p,  
Advisor: 조 준 호 (Joon Ho Cho). Text in English.

## **Abstract**

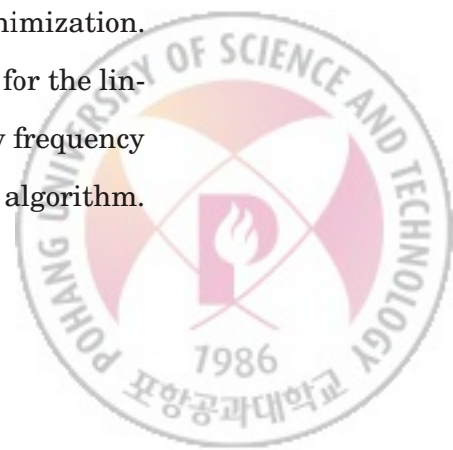
In this thesis, the optimal system design is considered for transmission and reception of digitally modulated signals. Digitally modulated signals are well modeled by second-order cyclostationary (SOCS) random processes whose complex envelopes possess periodicity in all variables of the mean, the auto-covariance, and the complementary auto-covariance functions. The periodicity in these second-order statistics and the property of nonvanishing complementary auto-covariance function are called cyclostationarity and impropropriety, respectively. The objective of this thesis is to propose the optimal and the asymptotically optimal system designs by efficiently exploiting the cyclostationarity and the impropropriety of SOCS random processes.

First, an invertible linear-conjugate linear (LCL) or a widely linear (WL) periodically time-varying operator named a continuous-time (CT) FREquency SHift (FRESH) properizer is proposed. It is shown that this operator converts a CT SOCS random process, whether it is proper or improper, can be always converted to an equivalent CT proper-complex SOCS random process with twice the cycle period. As an application, the presence detection of an improper-complex SOCS random process is considered. In particular, the optimal presence detector that utilizes the FRESH properizer is derived for improper-complex SOCS Gaussian random processes, which provides the lower bound on the detection error probabilities.



Second, the block processing of a discrete-time (DT) SOCS random process is considered. An invertible LCL operator named the DT FRESH properizer is proposed by extending the CT FRESH properizer. Then, an invertible LCL block processing operator named the asymptotic FRESH properizer is proposed that mimics the operation of the DT FRESH properizer but processes a finite number of consecutive samples of a DT improper-complex SOCS random process. It is shown that the output of the asymptotic FRESH properizer is not proper but asymptotically proper and that its frequency-domain covariance matrix converges to a highly-structured block matrix with diagonal blocks as the block size tends to infinity. Two representative estimation and detection problems are presented to demonstrate that asymptotically optimal low-complexity post-processors can be easily designed by exploiting the asymptotic FRESH properizer.

Lastly, the transmission of an improper-complex second-order stationary data sequence is considered over a strictly band-limited frequency-selective channel. It is assumed that the transmitter employs linear modulation and that the channel output is corrupted by additive proper-complex cyclostationary noise. Under the average transmit power constraint, the problem of minimizing the mean-squared error at the output of an LCL receiver is formulated in the time domain to find the optimal transmit and receive waveforms. This optimization problem is converted into a frequency-domain problem by using the vectorized Fourier transform technique and put into the form of a double minimization. After the LCL receiver is optimized, the optimal transmit waveform for the linear modulator is derived by introducing the notion of the impropriety frequency function and by performing a line search combined with an iterative algorithm.



**To My Family**



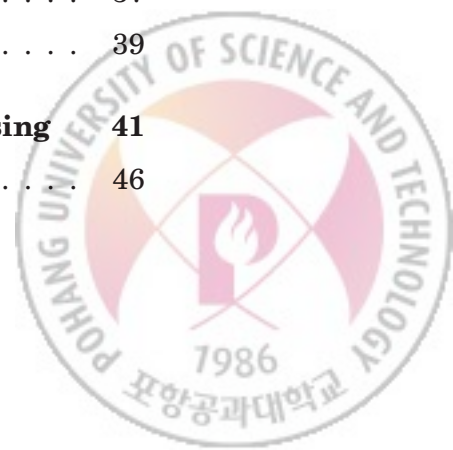


---

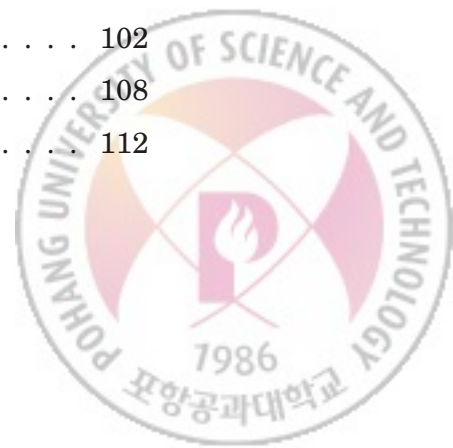
## Contents

---

<b>1</b>	<b>Introduction</b>	<b>1</b>
1.1	Backgrounds and Related Works . . . . .	3
1.1.1	Definitions Related with Complex-Valued Random Processes	3
1.1.2	Improper-Complex Random Processes . . . . .	5
1.1.3	Second-Order Cyclostationary Random Process . . . . .	7
1.1.4	Vectorized Fourier Transform (VFT) . . . . .	18
1.1.5	Properizing Frequency-Shift (p-FRESH) Vectorizer . . . . .	20
1.2	Thesis Outline . . . . .	24
<b>2</b>	<b>CT FRESH Properizer and Its Application to Presence Detection</b>	<b>26</b>
2.1	FRESH Properizer . . . . .	27
2.2	Application to Signal Presence Detection . . . . .	33
2.3	Numerical Results . . . . .	37
2.4	Summary . . . . .	39
<b>3</b>	<b>Asymptotic Frequency-Shift Properizer for Block Processing</b>	<b>41</b>
3.1	DT FRESH Properizer . . . . .	46



3.2	Asymptotic FRESH Properizer . . . . .	51
3.2.1	Asymptotic FRESH Properizer and Its Inverse Operator . . . . .	52
3.2.2	Second-Order Properties of Output of Asymptotic FRESH Properizer . . . . .	55
3.3	Application of Asymptotic FRESH Properizer to Signal Estimation Problem . . . . .	62
3.3.1	Asymptotically Optimal Low-Complexity Estimator . . . . .	63
3.3.2	Numerical Results . . . . .	70
3.4	Application of Asymptotic FRESH Properizer to Signal Presence Detection Problem . . . . .	72
3.4.1	Asymptotically Optimal Low-Complexity Detector . . . . .	73
3.4.2	Numerical Results . . . . .	77
3.5	Discussions . . . . .	80
3.6	Summary . . . . .	86
<b>4</b>	<b>Joint Transmitter and Receiver Optimization for Improper-Complex Second-Order Stationary Data Sequence</b>	<b>87</b>
4.1	System Model and Problem Formulation . . . . .	91
4.1.1	System Model . . . . .	91
4.1.2	Problem Formulation in Time Domain . . . . .	93
4.2	Problem Reformulation in Frequency Domain . . . . .	94
4.3	Optimization of Transmit and Receive Waveforms . . . . .	98
4.3.1	Optimization of Widely Linear Receiver . . . . .	98
4.3.2	Impropriety Frequency Function . . . . .	99
4.3.3	Optimization of Transmitter . . . . .	102
4.4	Numerical Results . . . . .	108
4.5	Summary . . . . .	112



## **CONTENTS**

---

**iii**

**5 Conclusions** **114**

**Bibliography** **116**

**Glossary** **124**

한글 요약문 **127**

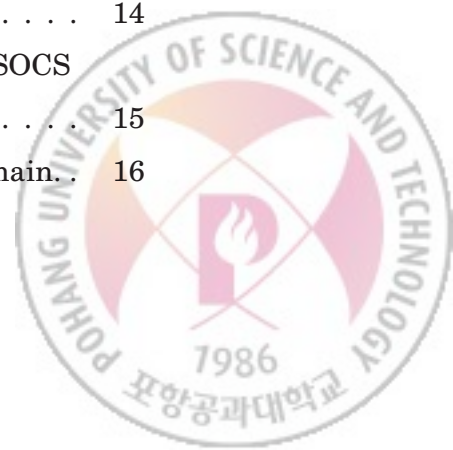


---

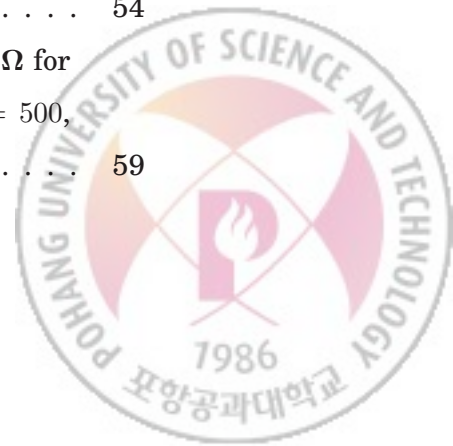
## List of Figures

---

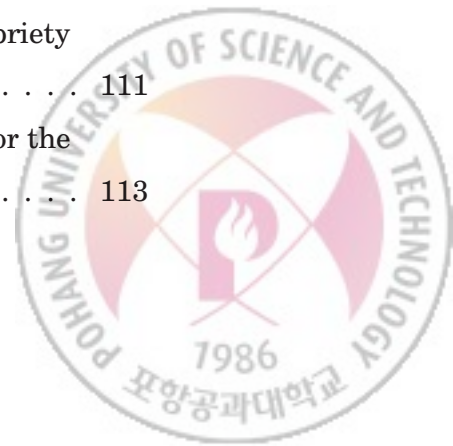
1.1	Comparison of (upper two subfigures) proper- and (lower two subfigures) improper-complex Gaussian random variable . . . . .	7
1.2	Canonical representation of improper-complex random variables	8
1.3	Classification of complex-valued random processes. . . . .	9
1.4	Contour plot of magnitude of (a) the auto-correlation and (b) the complementary auto-correlation functions of BPSK signal and (c) the auto-correlation and (d) the complementary auto-correlation functions of QPSK signal with SRRC having roll-off $\beta = 0.5$ . . .	10
1.5	Comparison of second-order properties in the time domain. . . . .	11
1.6	Magnitude of (a) the 2-D PSD and (b) the 2-D complementary PSD of BPSK signal and (c) the 2-D PSD and (d) the 2-D complementary PSD of QPSK signal with SRRC pulse shape having roll-off $\beta = 0.5$ . . . . .	14
1.7	Correlation between frequency-domain components of an SOCS random process due to its cyclostationarity. . . . .	15
1.8	Comparison of second-order properties in the frequency domain. . . . .	16



1.9	FRESH vectorization and scalarization for a deterministic signal $s(t)$ in the frequency domain. . . . .	19
1.10	p-FRESH vectorization viewed in the time domain [21, Fig. 2]. . .	22
1.11	p-FRESH vectorization and scalarization for a deterministic signal $s(t)$ in the frequency domain. . . . .	23
2.1	(a) Frequency response of the FD-RSW filter. (b) FRESH properizer viewed in the time domain. . . . .	28
2.2	The output of the FRESH properizer for a deterministic signal $s(t)$ viewed in the frequency domain. . . . .	29
2.3	(a) Conventional optimal detector that consists of an LCL cyclic Wiener filter followed by a correlator. (b) Proposed detector that consists of a FRESH properizer followed by an estimator-correlator with single cyclic Wiener filter. . . . .	34
2.4	Comparison of the deflections of the proposed detector and the conventional linear estimator-correlator. . . . .	38
2.5	Comparison of the ROCs of the proposed detector and the conventional linear estimator-correlator. . . . .	39
3.1	Frequency response of the FD-RSW filter with reference frequency $1/M$ . . . . .	48
3.2	DT FRESH properizer with reference frequency $1/M$ viewed in the time domain. . . . .	49
3.3	Illustration that shows how the asymptotic FRESH properizer works in the frequency domain. . . . .	54
3.4	Magnitudes of exemplary (a) $\bar{\mathbf{W}}_{MN} \mathbf{R}_{\bar{\mathbf{x}}} \bar{\mathbf{W}}_{MN}^H$ for $N = 50$ , (b) $\Omega$ for $N = 50$ , (c) $\bar{\mathbf{W}}_{MN} \mathbf{R}_{\bar{\mathbf{x}}} \bar{\mathbf{W}}_{MN}^H$ for $N = 500$ , and (d) $\Omega$ for $N = 500$ , when $M = 2$ . . . . .	59



3.5	Magnitudes of exemplary (a) $\bar{\mathbf{W}}_{MN} \tilde{\mathbf{R}}_{\tilde{\mathbf{x}}} \bar{\mathbf{W}}_{MN}^T$ for $N = 50$ , (b) $\tilde{\Omega}$ for $N = 50$ , (c) $\bar{\mathbf{W}}_{MN} \tilde{\mathbf{R}}_{\tilde{\mathbf{x}}} \bar{\mathbf{W}}_{MN}^T$ for $N = 500$ , and (d) $\tilde{\Omega}$ for $N = 500$ , when $M = 2$ . . . . .	60
3.6	Illustrations that show how to construct (a) $\mathbf{R}_{\hat{\mathbf{y}}}$ and (b) $\tilde{\mathbf{R}}_{\hat{\mathbf{y}}}$ from $\bar{\mathbf{W}}_{MN} \mathbf{R}_{\tilde{\mathbf{x}}} \bar{\mathbf{W}}_{MN}^H \sim \Omega$ and $\bar{\mathbf{W}}_{MN} \tilde{\mathbf{R}}_{\tilde{\mathbf{x}}} \bar{\mathbf{W}}_{MN}^T \sim \tilde{\Omega}$ , respectively. Thick diagonal and anti-diagonal lines represent all possible non-zero entries of $\Omega$ and $\tilde{\Omega}$ , respectively. . . . .	61
3.7	Computational complexities of the WMMSE and the proposed estimators. . . . .	71
3.8	Average MSEs of the LMMSE, the WMMSE and the proposed estimators. . . . .	72
3.9	Statistical averages of the exact LRT and the proposed test statistics versus $N$ for $E_s/N_0 = 0, -5$ , and $-10$ [dB], under (a) $\mathcal{H}_0$ and (b) $\mathcal{H}_1$ . . . . .	78
3.10	Empirical CDFs of the difference of the proposed test statistic from the exact LRT statistic for $N = 100, 200$ , and $400$ , under (a) $\mathcal{H}_0$ and (b) $\mathcal{H}_1$ . . . . .	79
3.11	ROC curves of the optimal and the proposed detectors. . . . .	80
4.1	System block diagram. . . . .	91
4.2	Comparison of squared-magnitudes of the optimal transmit and receive waveforms for (a) $k(f) = 0, \forall f$ and single interferer, (b) $k(f) = 0.8, \forall f$ and single interferer, and (c) $k(f) = 0.8, \forall f$ and two uncorrelated interferers. . . . .	110
4.3	Comparison of MSE (a) versus $E_s/N_0$ and (b) versus propriety $k(f) = k, \forall f$ . . . . .	111
4.4	Comparison of BER versus $E_b/N_0$ for BPSK data sequence for the transmit band (a) $[-2/T, 2/T)$ and (b) $[-1.9/T, 1.9/T)$ . . . . .	113



---

## List of Tables

---

4.1	An Algorithm to Construct Candidate Density Function at $\nu \in (0, \nu_{\max}]$ . . . . .	107
-----	---	-----



# CHAPTER 1

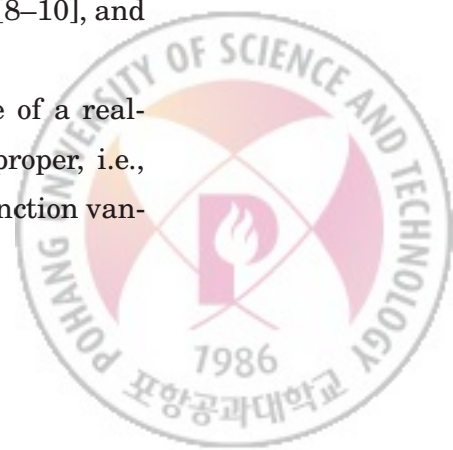
---

## Introduction

---

Many digitally modulated signals are well modeled by wide-sense cyclostationary (WSCS) random processes [1], whose complex envelopes possess periodicity in all variables of the mean and the auto-covariance functions. In [2], it is shown that a WSCS random process can be represented by an equivalent WSS vector random process. In [3], to efficiently extract the correlation structure of a WSCS random process in the time and the frequency domains, the translation series representation (TSR) and the harmonic series representation (HSR) are proposed, which are based on linear periodically time-varying (PTV) processings. Such second-order structure of a proper-complex WSCS random process has long been exploited in the design of many communications and signal processing systems [4,5] including presence detectors [6,7], estimators [8–10], and optimal transceivers [11–13] under various criteria.

On the other hand, it is well known that the complex envelope of a real-valued bandpass wide-sense stationary (WSS) random process is proper, i.e., its complementary auto-covariance (a.k.a. the pseudo-covariance) function van-

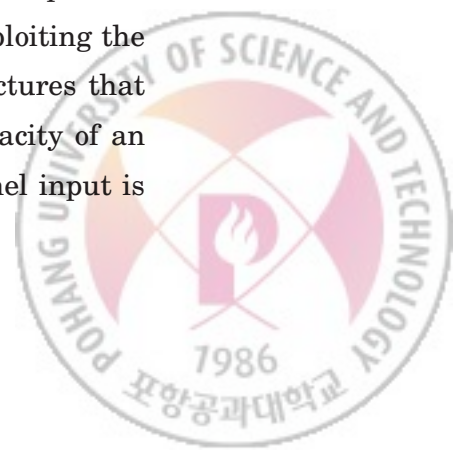




ishes [14]. However, there are a lot of important improper-complex random processes that do not have vanishing complementary auto-covariance functions [15–17]. For example, the complex envelope of a real-valued bandpass non-stationary signal is not necessarily proper and even the complex envelope of a real-valued bandpass WSS signal becomes improper in the presence of the imbalance between its in-phase and quadrature components [18]. In order to fully capture the statistical properties of a complex-valued signal, including all the second-order statistics, the filtering of augmented signals has been proposed. This so-called widely linear (WL) filtering processes either the signal augmented by its complex conjugate or the real part of the signal augmented by the imaginary part [18, 19], where the former is referred to as the linear-conjugate linear (LCL) filtering [20].

The complex envelopes of the majority of digitally modulated signals are proper and WSS. However, as well documented in [18], there still remain many other digitally modulated signals such as pulse amplitude modulation (PAM), offset quaternary phase-shift keying (OQPSK), and Gaussian minimum shift keying (GMSK), that are not only improper-complex WSS but also second-order cyclostationary (SOCS) [21], i.e., the complementary auto-covariance function is also periodic in all its variables with the same period as the mean and the auto-covariance functions. To exploit both cyclostationarity and impropriety, the LCL FREquency Shift (FRESH) filter has been proposed in [22] that combines signal augmentation and linear PTV processing.

Recently, another LCL PTV operator called the properizing FRESH (p-FRESH) vectorizer is proposed in [21, 23] by non-trivially extending the HSR. The p-FRESH vectorizer converts an *improper-complex* SOCS scalar random process to an equivalent *proper-complex* WSS vector random process by exploiting the frequency-domain correlation and complementary correlation structures that are rigorously examined in [16]. By successfully deriving the capacity of an SOCS Gaussian noise channel, it is shown that the optimal channel input is



improper-complex SOCS in general when the interfering signal is improper-complex SOCS. It is also well demonstrated that such properization provides the advantage of enabling the adoption of the conventional signal processing techniques and algorithms that utilize only the correlation but not the complementary correlation structure. These results warrant further research in communications and signal processing on the efficient construction and processing of improper-complex SOCS random processes.

## 1.1 Backgrounds and Related Works

In this section, we first provide definitions of continuous-time (CT) and discrete-time (DT) complex-valued random processes. Then, we review definitions and properties of improper-complex random processes and SOCS random processes. Finally, we review the vectorized Fourier transform (VFT) and the properizing frequency-shift (p-FRESH) vectorizer techniques that effectively exploit the second-order statistical properties of SOCS random processes.

### 1.1.1 Definitions Related with Complex-Valued Random Processes

The mean, the auto-correlation, the auto-covariance, the complementary auto-correlation, and the complementary auto-covariance functions of a CT complex-valued random process  $X(t)$  are defined, respectively, as,

$$\mu_X(t) \triangleq \mathbb{E}\{X(t)\}, \quad (1.1a)$$

$$r_X(t, s) \triangleq \mathbb{E}\{X(t)X(s)^*\}, \quad (1.1b)$$

$$c_X(t, s) \triangleq \mathbb{E}\{(X(t) - \mu_X(t))(X(s) - \mu_X(s))^*\}, \quad (1.1c)$$

$$\tilde{r}_X(t, s) \triangleq \mathbb{E}\{X(t)X(s)\}, \text{ and} \quad (1.1d)$$

$$\tilde{c}_X(t, s) \triangleq \mathbb{E}\{(X(t) - \mu_X(t))(X(s) - \mu_X(s))\}. \quad (1.1e)$$

Throughout this thesis, all CT complex-valued random processes are assumed to be of finite power, i.e.,  $|r_X[t, s]| \leq \mathbb{E}\{|X[t]|^2\} < \infty, \forall t, \forall s$ .



**Definition 1** *The two-dimensional (2-D) power spectral density (PSD)  $R_X(f, f')$  and the 2-D complementary PSD  $\tilde{R}_X(f, f')$  of a CT complex-valued random process  $X(t)$  are defined as*

$$R_X(f, f') \triangleq \int_{-\infty}^{\infty} \int_{-\infty}^{\infty} r_X(t, s) e^{-j2\pi(ft - f's)} \quad (1.2a)$$

and

$$\tilde{R}_X(f, f') \triangleq \int_{-\infty}^{\infty} \int_{-\infty}^{\infty} \tilde{r}_X(t, s) e^{-j2\pi(ft + f's)}, \quad (1.2b)$$

respectively, if they exist.<sup>1</sup>

The 2-D PSD has also been referred to as bifrequency spectral correlation function [24], cointensity spectrum [25], generalized spectrum [26], and Loève bifrequency spectrum [27]. Similarly, the 2-D complementary PSD has also been referred to as complementary Loève spectrum [28].

Similar to a CT random process, definitions related with a DT complex-valued random process are provided as follows.

**Definition 2** *Given a DT complex-valued random process  $X[n]$  with a finite power, i.e.,  $\mathbb{E}\{|X[n]|^2\} < \infty, \forall n$ , the mean, the auto-correlation, the auto-covariance, the complementary auto-correlation, and the complementary auto-covariance functions of  $X[n]$  are defined, respectively, as*

$$\mu_X[n] \triangleq \mathbb{E}\{X[n]\}, \quad (1.3a)$$

$$r_X[n, m] \triangleq \mathbb{E}\{X[n]X[m]^*\}, \quad (1.3b)$$

$$c_X[n, m] \triangleq \mathbb{E}\{(X[n] - \mu_X[n])(X[m] - \mu_X[m])^*\}, \quad (1.3c)$$

$$\tilde{r}_X[n, m] \triangleq \mathbb{E}\{X[n]X[m]\}, \text{ and} \quad (1.3d)$$

$$\tilde{c}_X[n, m] \triangleq \mathbb{E}\{(X[n] - \mu_X[n])(X[m] - \mu_X[m])\}. \quad (1.3e)$$

Throughout this thesis, all DT complex-valued random processes are assumed to be of finite power, i.e.,  $|r_X[n, m]| \leq \mathbb{E}\{|X[n]|^2\} < \infty, \forall n, \forall m$ .

<sup>1</sup>In [21],  $\tilde{R}_X(f, f')$  is defined as  $\tilde{R}_X(f, f') \triangleq \int_{-\infty}^{\infty} \int_{-\infty}^{\infty} \tilde{r}_X(t, s) e^{-j2\pi(ft + f's)}$  by substituting  $-f'$  into  $f'$ .



**Definition 3** *The 2-D PSD  $R_X(f, f')$  and the 2-D complementary PSD  $\tilde{R}_X(f, f')$  of a DT complex-valued random process  $X[n]$  are defined as*

$$R_X(f, f') \triangleq \sum_{m=-\infty}^{\infty} \sum_{n=-\infty}^{\infty} r_X[n, m] e^{-j2\pi(fn - f'm)} \quad (1.4a)$$

and

$$\tilde{R}_X(f, f') \triangleq \sum_{m=-\infty}^{\infty} \sum_{n=-\infty}^{\infty} \tilde{r}_X[n, m] e^{-j2\pi(fn + f'm)}, \quad (1.4b)$$

respectively, if they exist.

Since the 2-D PSD and the 2-D complementary PSD are the DT double Fourier transforms of  $r_X[n, m]$  and  $\tilde{r}_X[n, m]$ , respectively, they are always periodic in both variables  $f$  and  $f'$  with the common period 1. The set of all DT complex-valued random processes can be partitioned into two subsets by using the following definition.

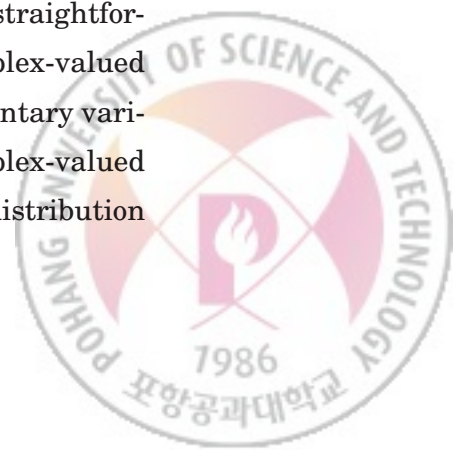
### 1.1.2 Improper-Complex Random Processes

The set of all CT complex-valued random processes can be partitioned into two subsets by using the following definition.

**Definition 4** [14, Definition 2] *A CT complex-valued random process  $X(t)$  is proper if its complementary auto-correlation function vanishes, i.e.,  $\tilde{c}_X(t, s) = 0, \forall t, \forall s$ , and is improper otherwise.*

Similar to a CT random process, a DT complex-valued random process  $X[n]$  is proper if its complementary auto-covariance function vanishes, i.e.,  $\tilde{r}_X[n, m] = 0, \forall n, \forall m$ , and is improper otherwise.

The definition of the improper-complex random process can be straightforwardly extended to a complex-valued random variable. Given a complex-valued random variable  $X$ , the random variable  $X$  is proper if its complementary variance  $\mathbb{E}\{X^2\}$  vanishes and is improper otherwise. Note that a complex-valued random variable  $X$  is called circular if it has the same probability distribution



as  $Xe^{j\theta}$ ,  $\forall \theta \in \mathbb{R}$ . Note also that, if a complex-valued random variable is a circular, then it is zero-mean and proper. A parameter to describe how improper a random variable is can be defined as follows.

**Definition 5** *Given an improper-complex random variable with the variance  $\sigma^2$  and the complementary variance  $\tau$ , its impropriety  $k$  is defined as*

$$k \triangleq \frac{|\tau|}{\sigma^2}. \quad (1.5)$$

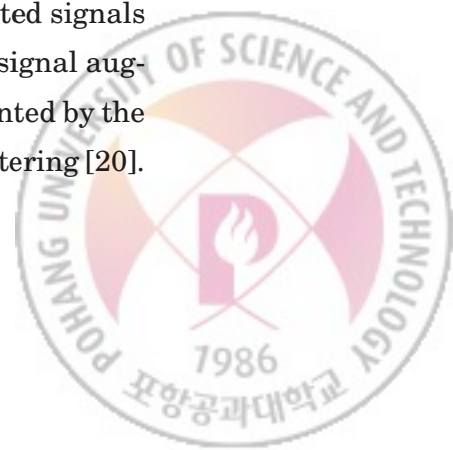
Then, the impropriety  $k$  is a positive real number between 0 and 1. If the impropriety of  $X$  is 0, then it implies the random variable  $X$  is proper. When  $X$  is a real-valued random variable, its impropriety becomes 1. Fig. 1.1 shows the probability density function (PDF) of improper-complex random Gaussian random variables. For the improper-complex case, a random variable with impropriety 0.8 is used, i.e., it has the variance  $\sigma^2 = 1$  and the complementary variance  $\tau = 0.8e^{j\pi/4}$ .

An improper-complex Gaussian random variable can be written by using a canonical representation as follows. For a given improper Gaussian random variable  $X$  with the variance  $\sigma^2$  and the complementary variance  $\tau$ , there exists a pair of complex numbers  $X_p$  and  $X_i$  such that

$$X = aX_p + bX_i, \quad (1.6)$$

where  $X_p \sim \mathcal{CN}(0, 1)$ ,  $X_i \sim \mathcal{N}(0, 1)$ , and  $X_p$  and  $X_i$  are independent. Fig. 1.2 shows the realizations of improper-complex Gaussian random variables. This canonical representation can be straightforwardly extended to complex-valued random vectors and processes.

In order to fully capture the statistical properties of a complex-valued signal, including all the second-order statistics, the filtering of augmented signals has been proposed. This so-called WL filtering processes either the signal augmented by its complex conjugate or the real part of the signal augmented by the imaginary part [18,19], where the former is referred to as the LCL filtering [20]. For details, see [18] and references therein.



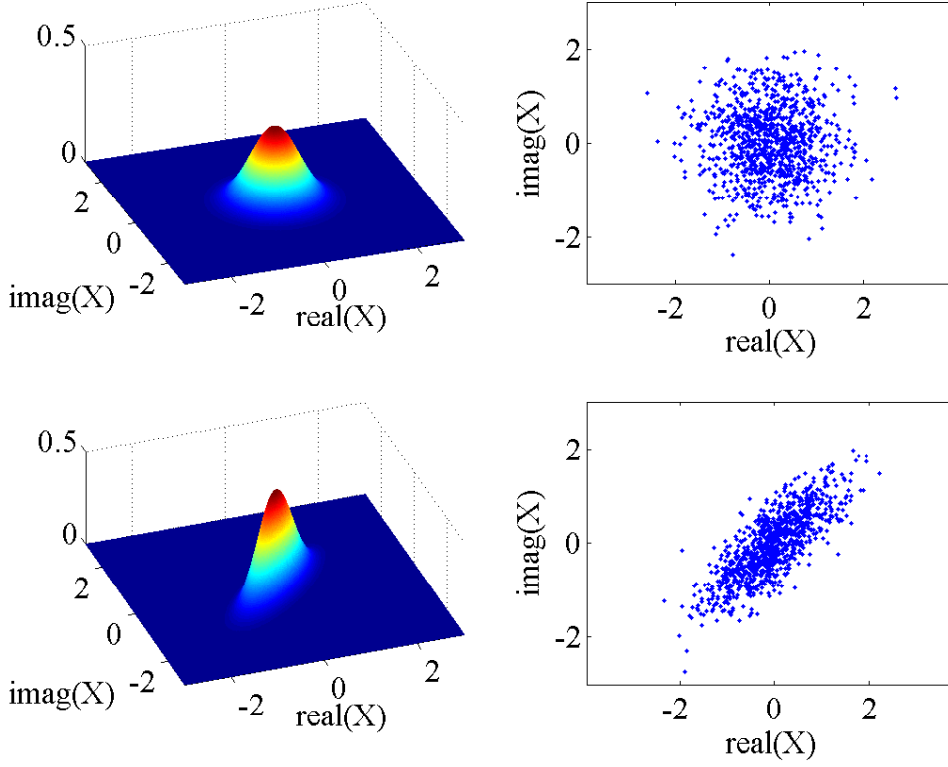


**Fig. 1.1** Comparison of (upper two subfigures) proper- and (lower two subfigures) improper-complex Gaussian random variable

### 1.1.3 Second-Order Cyclostationary Random Process

A complex-valued random process  $X(t)$  is wide-sense stationary (WSS) if,  $\forall t, \forall s$ ,

$$\mu_X(t) = \mu_X(0), \text{ and} \quad (1.7a)$$

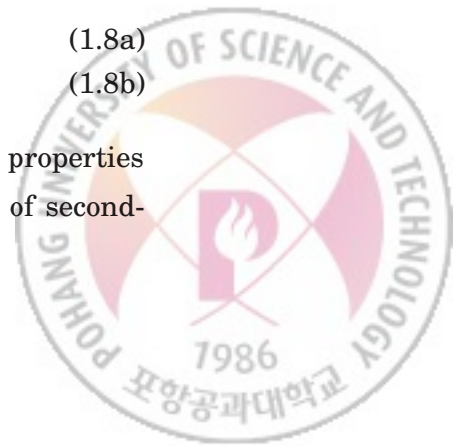
$$c_X(t, s) = c_X(t - s, 0), \quad (1.7b)$$

and is WSCS with cycle period  $T > 0$  if,  $\forall t, \forall s$ ,

$$\mu_X(t) = \mu_X(t + T), \text{ and} \quad (1.8a)$$

$$c_X(t, s) = c_X(t + T, s + T). \quad (1.8b)$$

In addition to these standard definitions related to the second-order properties of complex-valued random processes, we use the following notions of second-





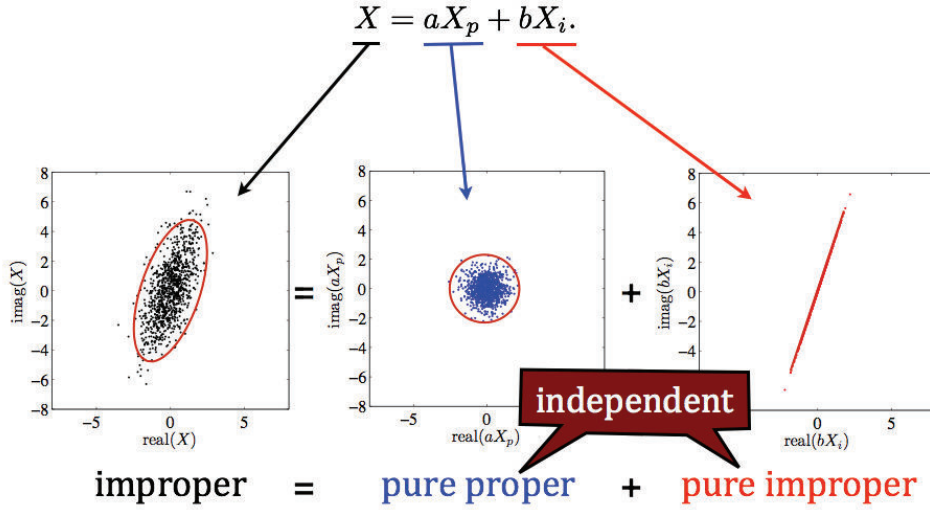


**Fig. 1.2** Canonical representation of improper-complex random variables

order stationarity and cyclostationarity.

**Definition 6** [29, Section II-B] A CT complex-valued random process  $X(t)$  is second-order stationary (SOS) if,  $\forall t, \forall s$ ,

$$\mu_X(t) = \mu_X(0), \quad (1.9a)$$

$$c_X(t, s) = c_X(t - s, 0), \text{ and} \quad (1.9b)$$

$$\tilde{c}_X(t, s) = \tilde{c}_X(t - s, 0). \quad (1.9c)$$

**Definition 7** A CT complex-valued random process  $X(t)$  is SOCS with cycle period  $T > 0$  if  $\forall t, \forall s$ ,

$$\mu_X(t) = \mu_X(t + T), \quad (1.10a)$$

$$c_X(t, s) = c_X(t + T, s + T), \text{ and} \quad (1.10b)$$

$$\tilde{c}_X(t, s) = \tilde{c}_X(t + T, s + T). \quad (1.10c)$$

Note that the conditions on  $c_X(t, s)$  and  $\tilde{c}_X(t, s)$  can be substituted by the conditions on  $r_X(t, s)$  and  $\tilde{r}_X(t, s)$ , respectively. Extending the above definitions to vector-valued random processes is straightforward.



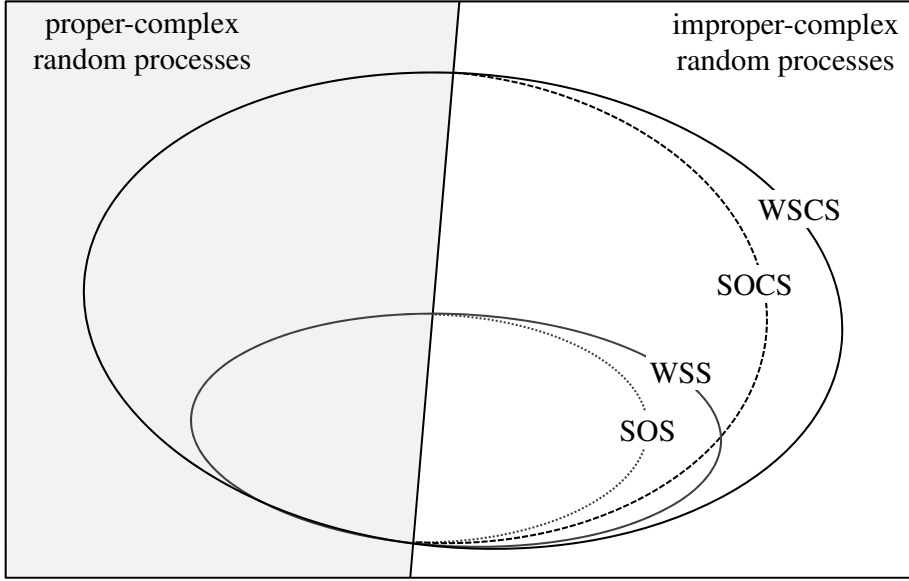


**Fig. 1.3** Classification of complex-valued random processes.

Due to the condition, an SOCS random process can be either proper or improper. Since  $\tilde{c}_X(t, s) = 0, \forall t, \forall s$  satisfies the condition of the SOCS random process, it can be easily seen that the set of all SOCS random processes includes the set of all proper-complex SOCS random processes. In the literature, such an SOCS random process with a vanishing complementary auto-covariance function has been termed a proper-complex WSCS random process, and has long been used in system design and analysis for various communications and signal processing problems. Thus, the notion of the second-order cyclostationarity can be viewed as a natural extension of that of the well-known proper-complex wide-sense cyclostationarity.

Fig. 1.3 shows the Venn diagram to illustrate the relationship among the above notions of complex-valued random processes. The sets of the proper-complex and the improper-complex random processes are mutually exclusive by the definition. Since (1.9a)–(1.9c) can be rewritten as  $\mu_X(t) = \mu_X(t + \tau)$ ,





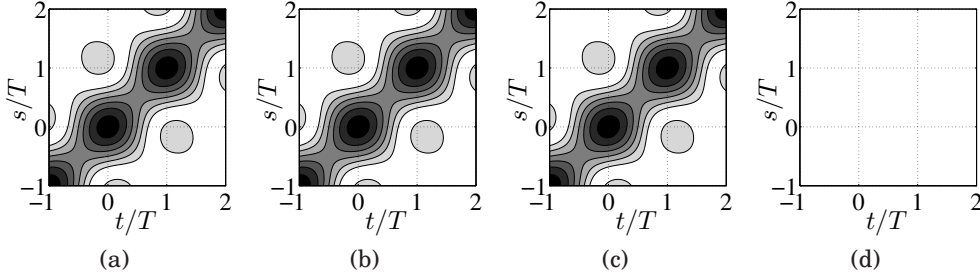


**Fig. 1.4** Contour plot of magnitude of (a) the auto-correlation and (b) the complementary auto-correlation functions of BPSK signal and (c) the auto-correlation and (d) the complementary auto-correlation functions of QPSK signal with SRRC having roll-off  $\beta = 0.5$

$c_X(t, s) = c_X(t + \tau, s + \tau)$ , and  $\tilde{c}_X(t, s) = \tilde{c}_X(t + \tau, s + \tau)$ ,  $\forall t, \forall s, \forall \tau$ , respectively, the mean, the auto-correlation, and the complementary auto-correlation functions of an SOS random process can be viewed as periodic functions for any period, so that the second-order stationarity implies the second-order cyclostationarity. Similarly, the wide-sense stationarity implies the wide-sense cyclostationarity. Since the condition  $\tilde{c}_X(t, s) = 0, \forall t, \forall s$ , satisfies the condition (1.10c), it can be easily seen from the above definitions that the set of all SOCS random processes includes the set of all proper-complex WSCS random processes. In the literature, such an SOCS random process with a vanishing complementary auto-covariance function has been termed as a proper-complex WSCS random process, and long been used in the signal modeling for various communications and signal processing problems. Thus, the notion of the second-order cyclostationarity can be viewed as a natural extension of that of the well-known proper-complex wide-sense cyclostationarity.

In the following example, the auto-correlation and the complementary auto-correlation functions of a proper- and an improper-complex zero-mean SOCS random processes are provided. Throughout this thesis, complex-valued random processes are assumed to have zero mean, unless otherwise specified. The zero-mean assumption is well justified when we are interested in the process-



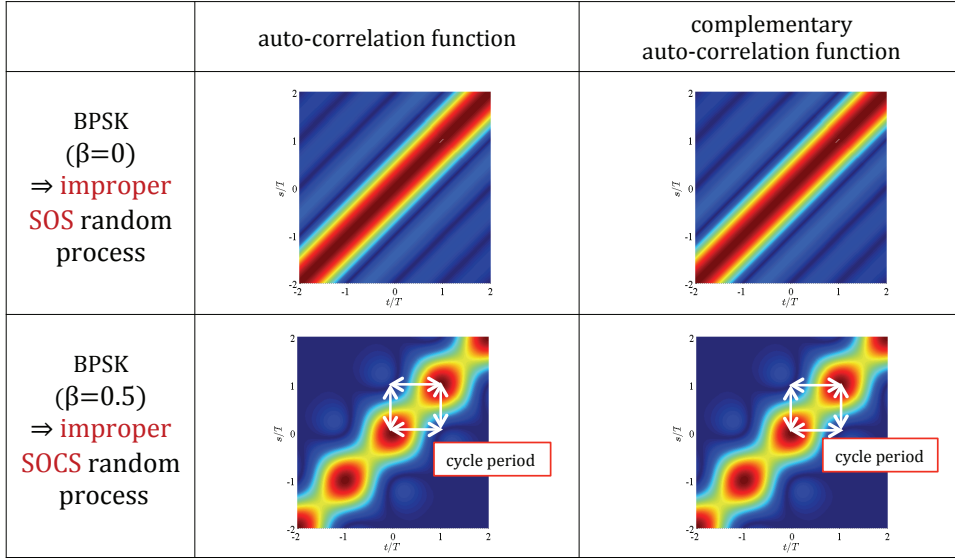


**Fig. 1.5** Comparison of second-order properties in the time domain.

ing of a digitally modulated signal, of which the mean function is often set to zero, in order not to waste any signal power.

**Example 1** An SOCS random process can be observed when a transmitter employs a linear modulation scheme such as double sideband (DSB) PAM, single sideband (SSB) PAM, vestigial sideband (VSB) PAM, QAM, MSK, SQPSK, etc. Note that these linear modulation schemes are among the most popular digital modulation schemes and that their complex envelopes are all in the form of

$$X(t) \triangleq \sum_{n=-\infty}^{\infty} \{c_1[n]p_1(t - nT) + jc_2[n]p_2(t - nT)\}, \quad (1.11)$$

where  $j$  denotes  $\sqrt{-1}$ ,  $(c_1[n])_n$  and  $(c_2[n])_n$  are modeled by jointly WSS real-valued random data sequences, and  $p_1(t)$  and  $p_2(t)$  are the transmit waveforms with excess bandwidth  $\beta$ . Particularly when  $p_1(t) = p_2(t)$ , the auto-correlation and the complementary auto-correlation functions of  $X(t)$  can be written, respec-



tively, as

$$r_X(t, s) = \sum_{n=-\infty}^{\infty} \sum_{m=-\infty}^{\infty} r_c[n-m]p(t-nT)p(s-mT)^* \quad (1.12a)$$

and

$$\tilde{r}_X(t, s) = \sum_{n=-\infty}^{\infty} \sum_{m=-\infty}^{\infty} \tilde{r}_c[n-m]p(t-nT)p(s-mT), \quad (1.12b)$$

where  $p(t) \triangleq p_1(t) = p_2(t)$ , and  $r_c[n-m] \triangleq \mathbb{E}\{c[n]c[m]^*\}$  and  $\tilde{r}_c[n-m] \triangleq \mathbb{E}\{c[n]c[m]\}$  are, respectively, the auto-correlation and the complementary auto-correlation functions of the complex-valued sequence  $(c[n])_n$  satisfying  $c[n] \triangleq c_1[n] + jc_2[n]$ ,

If  $(c[n])_n$  consists of improper-complex data symbols,  $X(t)$  becomes an improper-complex SOCS random process. Figs. 1.4-(a) and 1.4-(b) are the contour plots of the magnitudes of the auto-correlation and the complementary auto-correlation functions, when uncorrelated BPSK symbols and the square-root raised cosine (SRRC) transmit pulse with roll-off factor  $\beta = 0.5$  are used. As expected, both  $r_X(t, s)$  and  $\tilde{r}_X(t, s)$  exhibit the periodicity in  $t$  and  $s$  with the same period  $T$ . On the contrary, if  $(c[n])_n$  consists of proper-complex data symbols,  $X(t)$  becomes a proper-complex SOCS random process. Figs. 1.4-(c) and 1.4-(d) are the contour plots, when uncorrelated proper-complex QPSK symbols and the SRRC pulse with  $\beta = 0.5$  are used. Again,  $r_X(t, s)$  exhibits periodicity in  $t$  and  $s$  with period  $T$ . However,  $\tilde{r}_X(t, s)$  now vanishes. Fig. 1.5 shows the auto-correlation and the complementary auto-correlation functions for the roll-off factor of the BPSK signal  $\beta = 0$  and  $\beta = 0.5$ . It can be seen that the BPSK signal becomes SOS for  $\beta = 0$  and SOCS for  $\beta = 0.5$ , respectively.

In the following lemmas, the implications of the second-order cyclostationarity are provided in the time and the frequency domains, respectively.

**Lemma 1** For a CT SOCS random process  $X(t)$  with cycle period  $T > 0$ , there



exist  $r_X^{(k)}(\tau), k \in \mathbb{Z}$  and  $\tilde{r}_X^{(k)}(\tau), k \in \mathbb{Z}$  such that

$$r_X(t, s) = \sum_{k=-\infty}^{\infty} r_X^{(k)}(t-s) e^{j2\pi kt/T}, \quad (1.13a)$$

and

$$\tilde{r}_X(t, s) = \sum_{k=-\infty}^{\infty} \tilde{r}_X^{(k)}(t-s) e^{j2\pi kt/T}. \quad (1.13b)$$

*Proof:* Since  $r'_X(t, \tau) \triangleq r_X(t, t - \tau)$  is periodic in  $t$  with period  $T$  and is finite, there exist the CT Fourier series coefficients  $r_X^{(k)}(\tau), k \in \mathbb{Z}$  such that  $r'_X(t, \tau) = \sum_{k=-\infty}^{\infty} r_X^{(k)}(\tau) e^{j2\pi kt/T}$ . By replacing  $\tau$  with  $t - s$ , we obtain (1.13a). Similarly, we obtain (1.13b). Therefore, the conclusion follows.  $\square$

**Lemma 2** For a CT SOCS random process  $X(t)$  with cycle period  $T > 0$ , the 2-D PSD and the 2-D complementary PSD are given, respectively, by

$$R_X(f, f') = \sum_{k=-\infty}^{\infty} R_X^{(k)} \left( f - \frac{k}{T} \right) \delta \left( f - f' - \frac{k}{T} \right) \quad (1.14a)$$

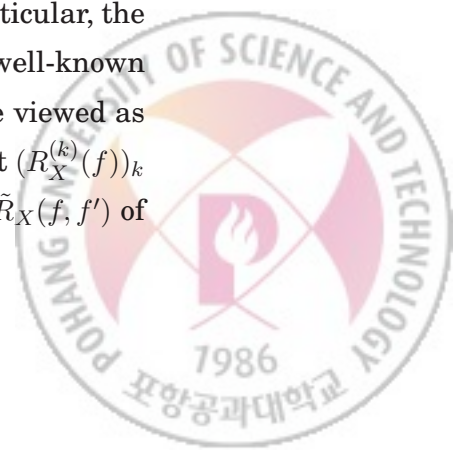
and

$$\tilde{R}_X(f, f') = \sum_{k=-\infty}^{\infty} \tilde{R}_X^{(k)} \left( f - \frac{k}{T} \right) \delta \left( f + f' - \frac{k}{T} \right), \quad (1.14b)$$

where  $R_X^{(k)}(f) \triangleq \mathcal{F}\{r_X^{(k)}(\tau)\}$  and  $\tilde{R}_X^{(k)}(f) \triangleq \mathcal{F}\{\tilde{r}_X^{(k)}(\tau)\}$ .

*Proof:* It is straightforward by applying the definitions (1.2a) and (1.2b) in Definition 1, respectively, to (1.13a) and (1.13b) in Lemma 1.  $\square$

The above lemmas are the extensions of the results in [3] for CT WSCS and SOCS random processes and can be also found in [21]. Note from (1.14) that  $R_X(f, f')$  and  $\tilde{R}_X(f, f')$  consist of  $1/T$ -spaced impulse fences along the lines  $f = f'$  and along the lines  $f = -f' \pm k/M, \forall k \in \mathbb{Z}$ , respectively. In particular, the height  $R_X^{(0)}(f)$  of the impulse fence of  $R_X(f, f')$  is nothing but the well-known PSD of  $X(t)$ . Particularly for an SOS random process, which can be viewed as an SOCS random process with any cycle period, it can be shown that  $(R_X^{(k)}(f))_k$  and  $(\tilde{R}_X^{(k)}(f))_k$  always vanish except for  $k = 0$ . Thus,  $R_X(f, f')$  and  $\tilde{R}_X(f, f')$  of



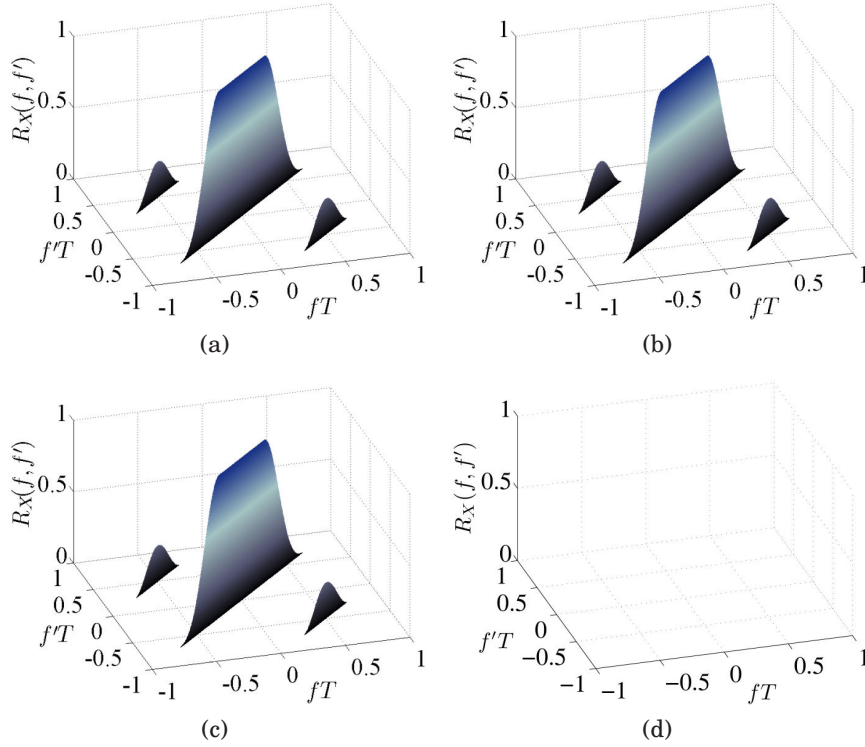


**Fig. 1.6** Magnitude of (a) the 2-D PSD and (b) the 2-D complementary PSD of BPSK signal and (c) the 2-D PSD and (d) the 2-D complementary PSD of QPSK signal with SRRC pulse shape having roll-off  $\beta = 0.5$

an SOS random process consist of a single impulse fence only on the line  $f = f'$  and  $f = -f'$ , respectively, and the heights of these impulse fences contain all the information about the spectral correlation of the process [15].

In the following example, the 2-D PSD and the 2-D complementary PSD of the linearly modulated signal considered in Example 1 are provided. For consistency with [21], we use the 2-D complementary PSD by the definition in [21] as  $\tilde{R}_X(f, f') \triangleq \int_{-\infty}^{\infty} \int_{-\infty}^{\infty} \tilde{r}_X(t, s) e^{-j2\pi(ft+f's)}$ .

**Example 2** By double Fourier transforming (1.12a) and (1.12b), we have

$$R_X(f, f') = \frac{1}{T} R_c(fT) P(f) P(f')^* \sum_{k=-\infty}^{\infty} \delta\left(f - f' - \frac{k}{T}\right) \quad (1.15a)$$



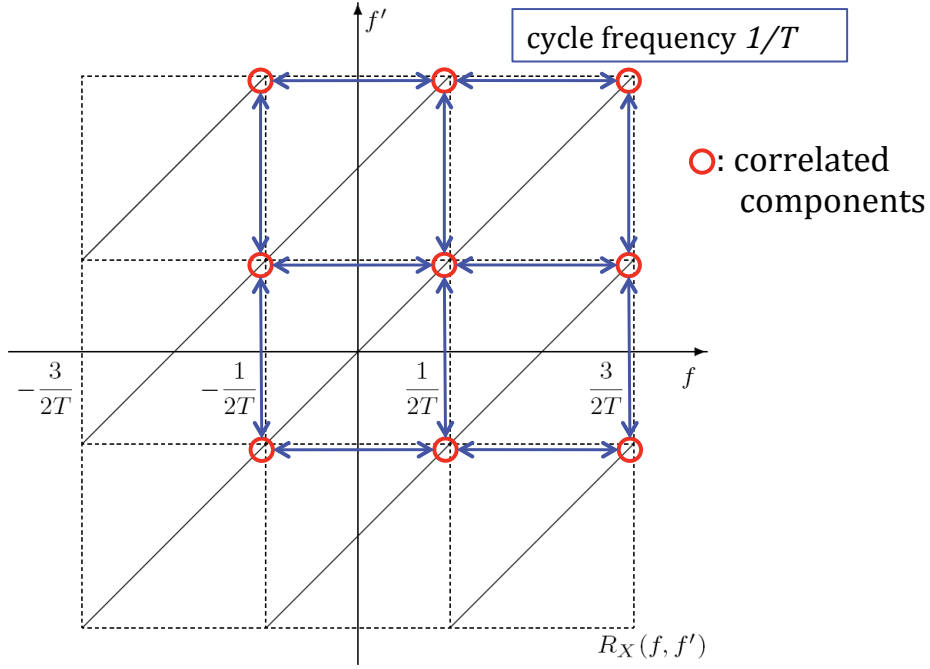
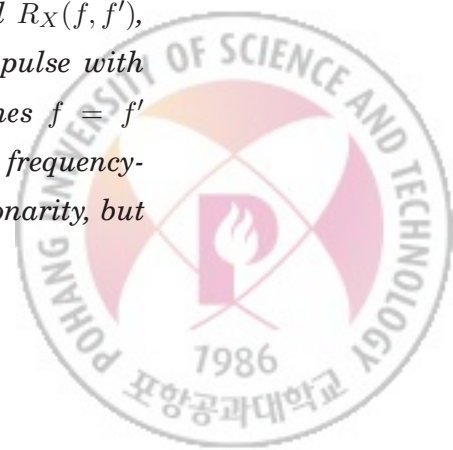


**Fig. 1.7** Correlation between frequency-domain components of an SOCS random process due to its cyclostationarity.

and

$$\tilde{R}_X(f, f') = \frac{1}{T} \tilde{R}_c(fT) P(f) P(-f') \sum_{k=-\infty}^{\infty} \delta\left(f - f' - \frac{k}{T}\right), \quad (1.15b)$$

where  $R_c(f)$  and  $\tilde{R}_c(f)$  are the discrete-time Fourier transform of  $r_c[n]$  and  $\tilde{r}_c[n]$ , respectively. Figs. 1.6-(a) and 1.6-(b) show the heights of the impulse fences of  $R_X(f, f')$  and  $\tilde{R}_X(f, f')$ , when uncorrelated BPSK symbols and the SRRC pulse with  $\beta = 0.5$  are used. As expected, both  $R_X(f, f')$  and  $\tilde{R}_X(f, f')$  have impulse fences not only on the line  $f = f'$  but also on the lines  $f = f' \pm 1/T$ . Figs. 1.6-(c) and 1.6-(d) show the heights of the impulse fences of  $R_X(f, f')$  and  $\tilde{R}_X(f, f')$ , when uncorrelated proper-complex QPSK symbols and the SRRC pulse with  $\beta = 0.5$  are used. Again,  $R_X(f, f')$  has impulse fences on the lines  $f = f'$  and  $f = f' \pm 1/T$ . However,  $\tilde{R}_X(f, f')$  vanishes. Fig. 1.7 shows the frequency-domain correlation of an SOCS random process due to the cyclostationarity, but





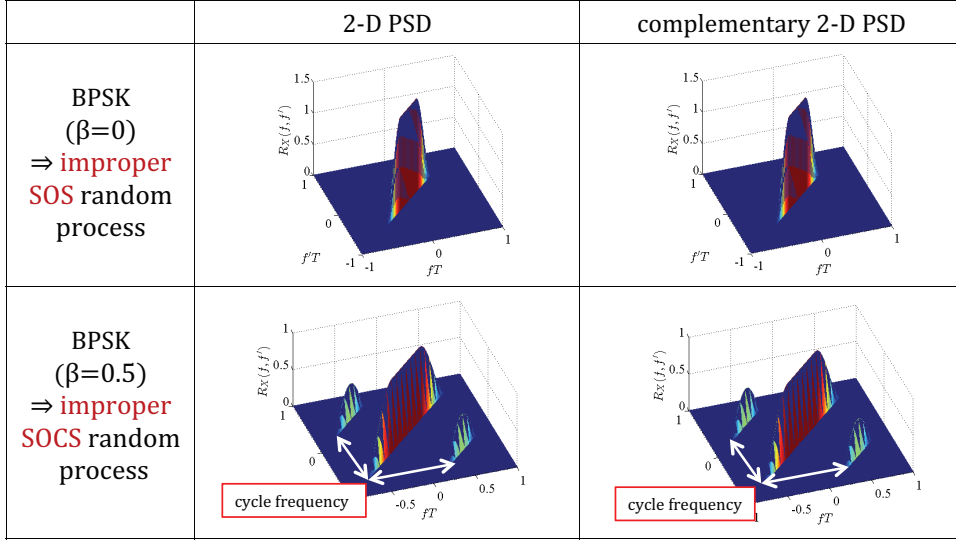


**Fig. 1.8** Comparison of second-order properties in the frequency domain.

not including the frequency-domain symmetric correlation due to the impropriety. Fig. 1.8 shows the auto-correlation and the complementary auto-correlation functions for the roll-off factor of the BPSK signal  $\beta = 0$  and  $\beta = 0.5$ .

Up to this point, we have reviewed CT SOCS random processes both in the time domain and in the frequency domain. Similar to the CT SOCS random processes, definitions and lemmas related to the DT SOCS random processes can be provided as follows.

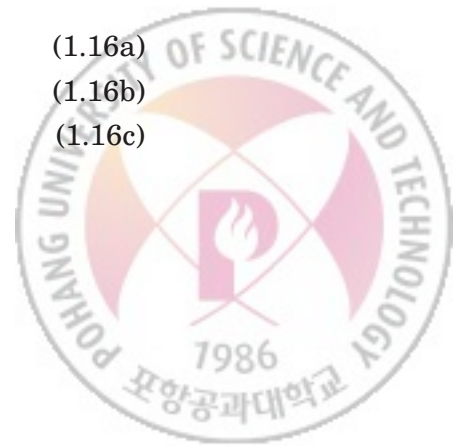
Two types of stationarity can be defined as follows by using the second-order moments of a DT complex-valued random process.

**Definition 8** [29, Section II-B] A DT complex-valued random process  $X[n]$  is second-order stationary (SOS) if,  $\forall m, \forall n$ ,

$$\mu_X[n] = \mu_X[0], \quad (1.16a)$$

$$r_X[n, m] = r_X[n - m, 0], \text{ and} \quad (1.16b)$$

$$\tilde{r}_X[n, m] = \tilde{r}_X[n - m, 0]. \quad (1.16c)$$



**Definition 9** A DT complex-valued random process  $X[n]$  is SOCS with cycle period  $M \in \mathbb{N}$  if,  $\forall n, \forall m$ ,

$$\mu_X[n] = \mu_X[n + M], \quad (1.17a)$$

$$r_X[n, m] = r_X[n + M, m + M], \text{ and} \quad (1.17b)$$

$$\tilde{r}_X[n, m] = \tilde{r}_X[n + M, m + M]. \quad (1.17c)$$

Note that a DT SOS random process can be viewed as a special DT SOCS random process with cycle period 1. For the ease of comparison with the definition of a CT SOCS random process, we use the time indexes  $m$  and  $n$  in the orders appearing in Definitions 2-9.

In the following lemmas, the implications of the second-order cyclostationarity are provided in the time and the frequency domains, respectively.

**Lemma 3** For a DT SOCS random process  $X[n]$  with cycle period  $M \in \mathbb{N}$ , there exist  $(r_X^{(k)}[n])_{k=0}^{M-1}$  and  $(\tilde{r}_X^{(k)}[n])_{k=0}^{M-1}$  such that

$$r_X[n, m] = \sum_{k=0}^{M-1} r_X^{(k)}[n - m] e^{j2\pi kn/M}, \quad (1.18a)$$

and

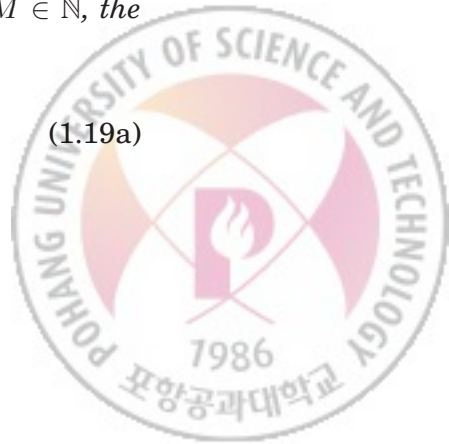
$$\tilde{r}_X[n, m] = \sum_{k=0}^{M-1} \tilde{r}_X^{(k)}[n - m] e^{j2\pi kn/M}. \quad (1.18b)$$

*Proof:* Since  $r'_X[n, l] \triangleq r_X[n, n - l]$  is periodic in  $n$  with period  $M$  and is finite, there exist the DT Fourier series coefficients  $(r_X^{(k)}[l])_{k=0}^{M-1}$  for each  $l$  such that  $r'_X[n, l] = \sum_{k=0}^{M-1} r_X^{(k)}[l] e^{j2\pi kn/M}$ . By replacing  $l$  with  $n - m$ , we obtain (1.18a). Similarly, we obtain (1.18b). Therefore, the conclusion follows.  $\square$

**Lemma 4** For a DT SOCS random process  $X[n]$  with cycle period  $M \in \mathbb{N}$ , the 2-D PSD and the 2-D complementary PSD are given, respectively, by

$$R_X(f, f') = \sum_{l=-\infty}^{\infty} \sum_{k=0}^{M-1} R_X^{(k)} \left( f - \frac{k}{M} \right) \delta \left( f - f' - \frac{k}{M} - l \right) \quad (1.19a)$$

and





$$\tilde{R}_X(f, f') = \sum_{l=-\infty}^{\infty} \sum_{k=0}^{M-1} \tilde{R}_X^{(k)} \left( f - \frac{k}{M} \right) \delta \left( f + f' - \frac{k}{M} - l \right), \quad (1.19b)$$

where  $R_X^{(k)}(f) \triangleq \mathcal{F}\{r_X^{(k)}[n]\}$  and  $\tilde{R}_X^{(k)}(f) \triangleq \mathcal{F}\{\tilde{r}_X^{(k)}[n]\}$ .

*Proof:* It is straightforward by applying the definitions (1.4a) and (1.4b) in Definition 3, respectively, to (1.18a) and (1.18b) in Lemma 3.  $\square$

Note from (1.19) that  $R_X(f, f')$  and  $\tilde{R}_X(f, f')$  consist of  $1/M$ -spaced impulse fences along the lines  $f = f'$  and along the lines  $f = -f' \pm k/M, \forall k \in \mathbb{Z}$ , respectively. The above lemmas are the extensions of the results in [3, 21] for CT WSCS and SOCS random processes.

#### 1.1.4 Vectorized Fourier Transform (VFT)

In this subsection, we briefly review the notions of excess bandwidth, the Nyquist interval, the VFT, and the matrix-valued PSD. For details, see [12].

To exploit such spectral correlation of the WSCS random process, a vectorized Fourier transform (VFT) technique is employed in [12]. This technique is motivated by the harmonic series representation [3] of a WSCS random process, and the use of that representation for joint Tx and Rx optimizations in cyclostationary interference and noise has been examined in [30] and [31].

Given a pair  $(B, 1/T)$  of a bandwidth and a reference rate, the excess bandwidth  $\beta$  is defined as  $\beta \triangleq 2BT - 1$  and the Nyquist interval  $\mathcal{F}$  is defined as

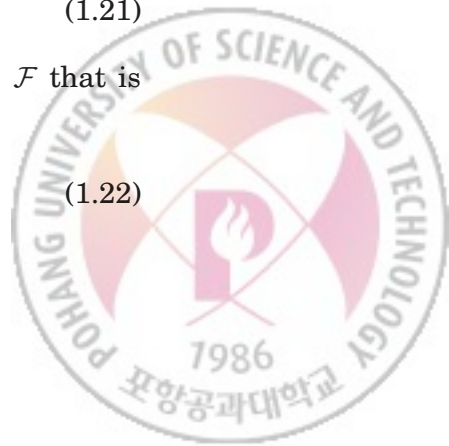
$$\mathcal{F} \triangleq \left\{ f : -\frac{1}{2T} \leq f < \frac{1}{2T} \right\}. \quad (1.20)$$

Given a pair  $(B, 1/T)$  and a deterministic function  $p(t)$  having the continuous-time Fourier transform (CTFT)

$$P(\xi) \triangleq \int_{-\infty}^{\infty} p(t) e^{-j2\pi\xi t} dt, \quad (1.21)$$

the VFT  $\mathbf{p}(f)$  of  $p(t)$  is defined as a vector-valued function of  $f \in \mathcal{F}$  that is equivalent to  $P(\xi)$ . In particular, the  $k$ th entry of  $\mathbf{p}(f)$  is given by

$$[\mathbf{p}(f)]_k \triangleq P \left( f + \frac{k - L - 1}{T} \right) \quad (1.22)$$



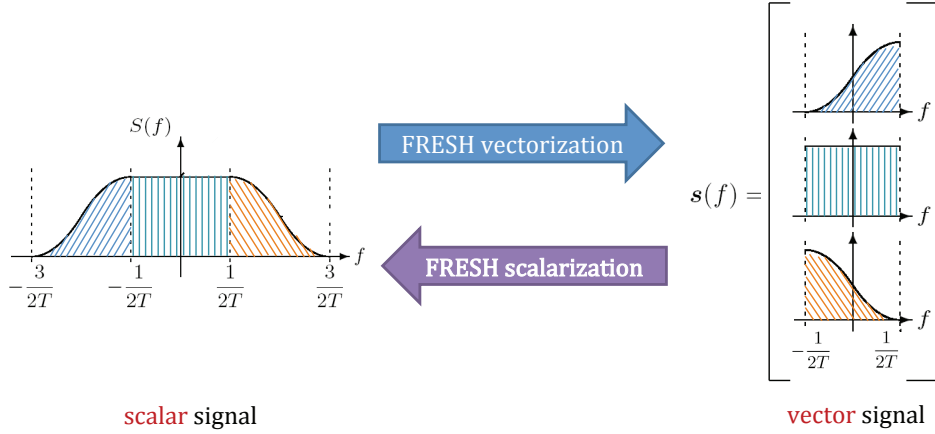


**Fig. 1.9** FRESH vectorization and scalarization for a deterministic signal  $s(t)$  in the frequency domain.

for  $k = 1, 2, \dots, 2L + 1$ , where  $L \triangleq \lceil \beta/2 \rceil$ .

The VFT technique can be viewed as a FRESH vectorization. Fig. 1.9 shows how the FRESH vectorization and scalarization works in the frequency domain. The VFT is an element-wise Fourier transform of the FRESH vectorization output vector of a deterministic signal.

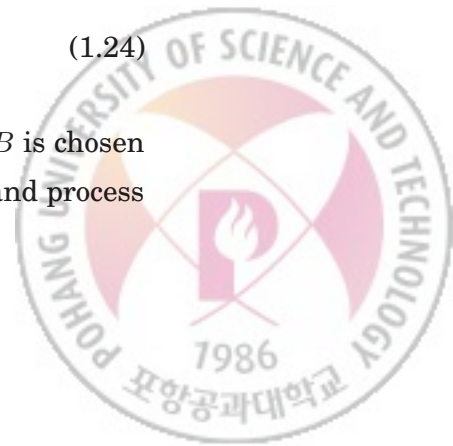
Given a pair  $(B, 1/T)$  and an SOCS random process  $N(t)$  with cycle period  $T$  having the auto-correlation function  $r_N(t, s)$ , the matrix-valued PSD  $\mathbf{R}_N(f)$  of  $N(t)$  is defined as a matrix-valued function of  $f \in \mathcal{F}$ , whose  $(k, l)$ th entry is given by

$$[\mathbf{R}_N(f)]_{k,l} \triangleq R_N^{(k-l)}\left(f + \frac{l-L-1}{T}\right) \quad (1.23)$$

for  $k, l = 1, 2, \dots, 2L + 1$ , where  $R_N^{(k)}(\xi)$  is the CTFT of  $r_N^{(k)}(\tau)$  that is obtained by applying the Fourier series expansion to  $r_N(t, t - \tau)$ , i.e.,

$$r_N(t, s) = \sum_{k=-\infty}^{\infty} r_N^{(k)}(t-s) e^{j2\pi kt/T}. \quad (1.24)$$

In using the above definitions, it is assumed that the parameter  $B$  is chosen as bandwidth in complex baseband over which the Rx can observe and process



a signal and that the parameter  $1/T$  is chosen as the symbol transmission rate of the Tx. It is also assumed that the frequency band over which the Tx can emit non-zero power is identical to the frequency band of the Rx. For a general case where these two frequency bands are different, the notion of virtual legacy Rx's and the orthogonal constraint at the virtual legacy Rx's can be employed as is done in [13] for the transmission of a proper-complex data sequence.

Due to the above assumption on the frequency band that can be used by the Tx and the Rx, the first and the last entries of the VFT of the transmit waveform need to be always zero for  $-1/(2T) \leq f \leq L/T - B$  and  $B - L/T \leq f \leq 1/(2T)$ , respectively. For this, the notion of the effective VFT is employed as discussed in [12, 13], and [32]. The effective VFT is defined as a variable-length vector-valued function of  $f \in \mathcal{F}$  by removing the first and the last entries of the VFT for  $-1/(2T) \leq f \leq L/T - B$  and  $B - L/T \leq f \leq 1/(2T)$ , respectively. In what follows, the length of the effective VFT is denoted by  $\mathcal{N}(f)$ . For details, see [32, Eq. (14)]. Similarly, the effective matrix-valued PSD can be also defined as an  $\mathcal{N}(f)$ -by- $\mathcal{N}(f)$  matrix-valued function of  $f \in \mathcal{F}$  by removing both the first row and column of the matrix-valued PSD for  $-1/(2T) \leq f \leq L/T - B$  and by removing both the last row and column for  $B - L/T \leq f \leq 1/(2T)$ .

### 1.1.5 Properizing Frequency-Shift (p-FRESH) Vectorizer

The LCL-TV operator called p-FRESH vectorizer is introduced in [21] to convert an improper-complex scalar-valued SOCS random process to a proper-complex vector-valued WSS random process. Before proceeding, we define the following terms.

**Definition 10** [21, Definition 4] *Given a pair  $(B, 1/T)$  of a reference bandwidth and a reference rate, the  $l$ th Nyquist zone  $\mathcal{F}_l$ , its center frequency  $f_l$ , the half-Nyquist zone  $\mathcal{F}^+$ , and the  $l$ th half-Nyquist zone  $\mathcal{F}_l^+$  are defined, respectively,*



as

$$\mathcal{F}_l \triangleq \left\{ f : f_l - \frac{1}{2T} \leq f < f_l + \frac{1}{2T} \right\}, \quad (1.24a)$$

$$f_l \triangleq \frac{l - \lfloor L/2 \rfloor - 1}{T}, \quad (1.24b)$$

$$\mathcal{F}^+ \triangleq \left\{ f : 0 \leq f < \frac{1}{2T} \right\}, \text{ and} \quad (1.24c)$$

$$\mathcal{F}_l^+ \triangleq \mathcal{F}^+ + f_l = \left\{ f : f_l \leq f < f_l + \frac{1}{2T} \right\}, \quad (1.24d)$$

for  $l = 1, 2, \dots, L$ , where the integer  $L$  is given by  $L \triangleq \lceil 2BT \rceil$ .

Note that a half-Nyquist zone is just the right-half of the corresponding Nyquist zone. Note also that  $L$  is chosen as the number of length- $1/(2T)$  intervals that can fully cover the one-sided frequency band  $f \in [0, B)$  of interest.

First of all, we define the p-FRESH vectorization that converts a scalar-valued signal to a vector-valued one.

**Definition 11** [21, Definition 5] *Given a reference pair  $(B, 1/T)$  and an input  $Y(t)$ , the p-FRESH vectorizer is defined as a single-input multiple-output (SIMO) LCL-TV system, whose output  $\mathbf{Y}(t)$  is given by  $\mathbf{Y}(t) \triangleq [Y_1(t) Y_2(t) \dots Y_{2L}(t)]^T$ , where the  $l$ th entry  $Y_l(t)$ , for  $l = 1, 2, \dots, 2L$ , is given by*

$$Y_l(t) \triangleq \begin{cases} (Y(t)e^{-j2\pi f_l t}) * g(t), & \text{for } l \leq L, \\ (Y(t)^* e^{-j2\pi f_{l-L} t}) * g(t), & \text{for } l > L, \end{cases} \quad (1.25)$$

with  $g(t)$  being the impulse response of the ideal brickwall filter having the half-Nyquist zone  $\mathcal{F}^+$  as the support, i.e., the Fourier transform  $G(f) \triangleq \mathcal{F}\{g(t)\}$  is given by  $G(f) = 1$  for  $f \in \mathcal{F}^+$  and zero, otherwise.

Fig. 1.10 shows how the p-FRESH vectorizer works in the time domain, where a scalar-valued signal  $Y(t)$  is converted to a  $2L$ -by-1 vector-valued signal  $\mathbf{Y}(t)$ . The p-FRESH vectorizer modulates  $Y(t)$  and its complex conjugate  $Y(t)^*$  each with  $L$  different carriers, of which frequencies are integer multiples of the reference rate  $1/T$ , and filters to form  $\mathbf{Y}(t)$ , of which entries are all band-limited to the half-Nyquist zone  $\mathcal{F}^+$ . Also, Fig. 1.11 shows how the p-FRESH



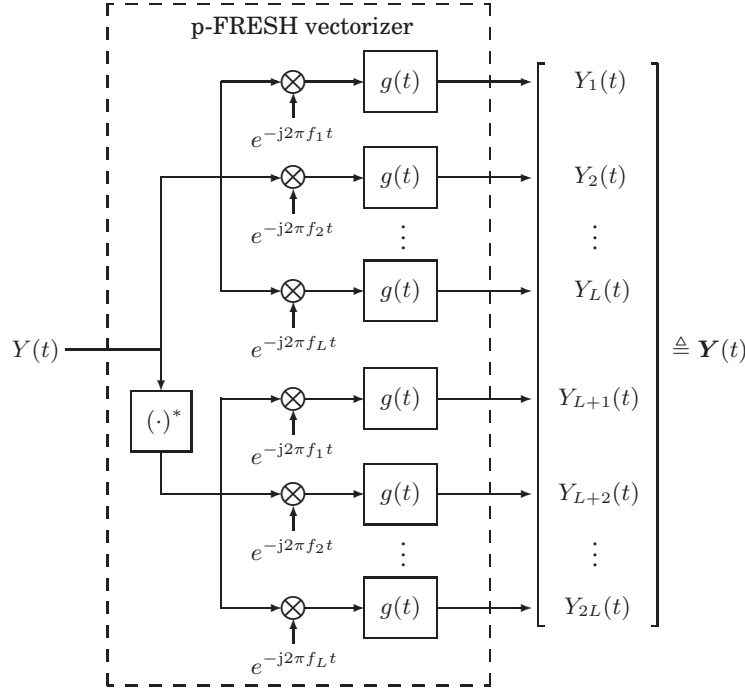
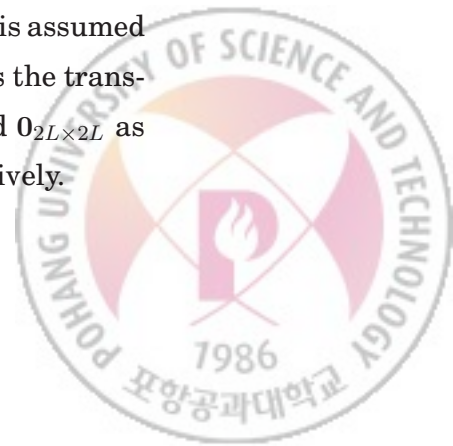


**Fig. 1.10** p-FRESH vectorization viewed in the time domain [21, Fig. 2].

vectorizer works in the frequency domain. Compared to the FRESH vectorization shown in Fig. 1.9, the bandwidth of the output becomes the half.

Note that the p-FRESH vectorizer processes both  $Y(t)$  and  $Y(t)^*$ , like linear-conjugate linear filters [20] or, equivalently, widely linear filters [19] that are devised to process improper-complex random signals. The major difference is that the p-FRESH vectorizer filters out half the signal components in  $Y(t)$  and  $Y(t)^*$  to completely remove the redundancy during the vectorization.

The following lemma shows the crucial property of the output of the p-FRESH vectorizer. Suppose, without loss of generality, that the mean of  $X(t)$  is assumed to be zero for all  $t$ . In what follows, we define superscripts  $\mathcal{T}$  and  $\mathcal{H}$  as the transposition and the Hermitian transposition, respectively, and  $\mathbf{0}_{2L}$  and  $\mathbf{0}_{2L \times 2L}$  as the  $2L$ -by-1 all-zero vector and the  $2L$ -by- $2L$  all-zero matrix, respectively.



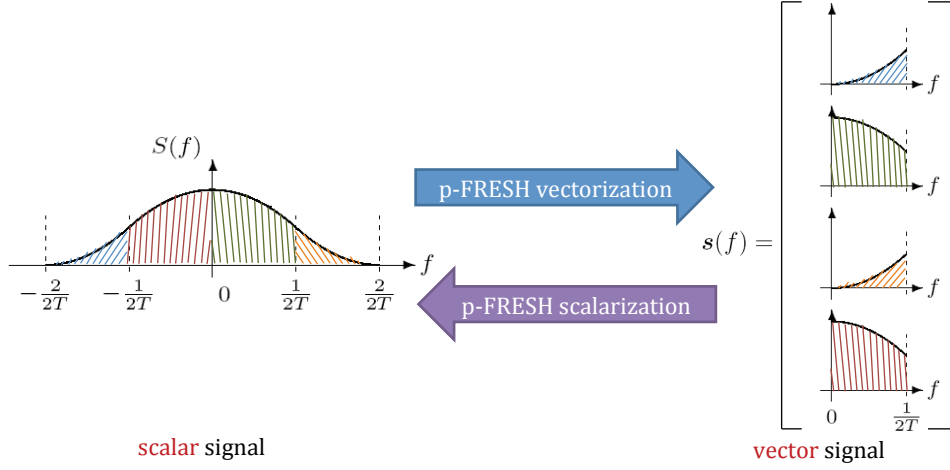


**Fig. 1.11** p-FRESH vectorization and scalarization for a deterministic signal  $s(t)$  in the frequency domain.

**Lemma 5** [21, Lemma 1] *If the fundamental cycle frequency of the input zero-mean SOCS random process  $Y(t)$  is the reference rate  $1/T$  of a p-FRESH vectorizer, then the output  $Y(t)$  becomes a proper-complex zero-mean vector-valued WSS process.*

$$\mu_Y(t) \triangleq \mathbb{E}\{Y(t)\} = \mathbf{0}_{2L}, \forall t, \quad (1.25a)$$

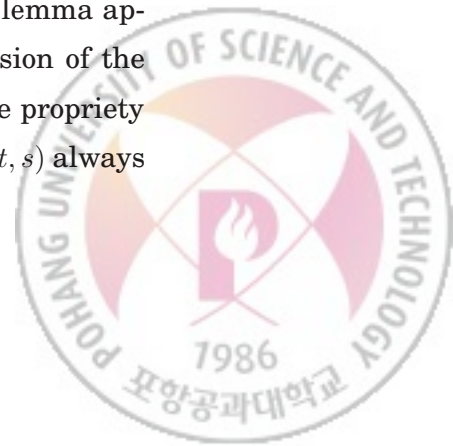
$$\mathbf{r}_Y(t, s) \triangleq \mathbb{E}\{Y(t)Y(s)^H\} = \mathbf{r}_Y(t - s), \forall t, \forall s, \text{ and} \quad (1.25b)$$

$$\tilde{\mathbf{r}}_Y(t, s) \triangleq \mathbb{E}\{Y(t)Y(s)^T\} = \mathbf{0}_{2L \times 2L}, \forall t, \forall s, \quad (1.25c)$$

where  $\mathbf{r}_Y(\tau) \triangleq \mathbf{r}_Y(\tau, 0)$  is a  $2L$ -by- $2L$  matrix-valued function.

*Proof:* The brick-wall filters destroy the excess-bandwidth and correlation between the symmetric components of the input in the frequency domain. Thus, the cyclostationary and improper features vanish. For the detailed proof, see [21].  $\square$

As far as the auto-correlation function  $\mathbf{r}_Y(t, s)$  is concerned, this lemma applying the p-FRESH vectorizer to an SOCS input is a mere extension of the result in [33]. However, it additionally shows that, regardless of the propriety of the SOCS input, the complementary auto-correlation function  $\tilde{\mathbf{r}}_Y(t, s)$  always vanishes.



## 1.2 Thesis Outline

In this thesis, we consider the optimal system design for transmission and reception of the signals that is well modeled as SOCS random processes.

In Chapter 2, we propose an invertible LCL periodically time-varying operator named a CT FRESH properizer. It is shown that this operator converts a CT SOCS random process can be always converted to an equivalent CT proper-complex SOCS random process with twice the cycle period. As an application, the presence detection of an improper-complex SOCS random process is considered. In particular, the optimal presence detector that utilizes the FRESH properizer is derived for improper-complex SOCS Gaussian random processes, which provides the lower bound on the detection error probabilities.

In Chapter 3, we consider the block processing of a DT SOCS random process. We first propose an invertible LCL operator named the DT FRESH properizer by extending the CT FRESH properizer and then propose an invertible LCL block processing operator named the asymptotic FRESH properizer. It is shown that the output of the asymptotic FRESH properizer is not proper but asymptotically proper and that its frequency-domain covariance matrix converges to a highly-structured block matrix with diagonal blocks as the block size tends to infinity. Two representative estimation and detection problems are presented to demonstrate that asymptotically optimal low-complexity post-processors can be easily designed by exploiting the asymptotic FRESH properizer.

In Chapter 4, we consider the transmission of an improper-complex second-order stationary data sequence over a strictly band-limited frequency-selective channel. It is assumed that the transmitter employs linear modulation and that the channel output is corrupted by additive proper-complex cyclostationary noise. We first formulate the problem of minimizing the mean-squared error at the output of an LCL receiver under the average transmit power constraint in the time domain to find the optimal transmit and receive waveforms.





Then, we convert this optimization problem in the time domain into an equivalent frequency-domain problem by using the vectorized Fourier transform technique. After the LCL receiver is optimized, the optimal transmit waveform for the linear modulator is derived by introducing the notion of the improper frequency function and by performing a line search combined with an iterative algorithm. Finally, concluding remarks are given in Chapter 5.

Throughout this thesis, the operator  $\mathbb{E}\{\cdot\}$  denotes the expectation, the operator  $\mathcal{F}\{\cdot\}$  denotes the continuous-time Fourier transform (CTFT) or the discrete-time Fourier transform (DTFT), and the function  $\delta(\cdot)$  denotes the Dirac delta function. The sets  $\mathbb{Z}$  and  $\mathbb{N}$  are the sets of all integers and of all positive integers, respectively. The operator  $\times$  denotes the Cartesian product between two sets. The superscripts  $*$ ,  $\mathcal{T}$ , and  $\mathcal{H}$  denote the complex conjugation, the transpose, and the Hermitian transpose, respectively. The operator  $*$  denotes the convolution.<sup>2</sup> The operators  $\odot$  and  $\otimes$  denote the Hadamard product and the Kronecker product, respectively. The matrices  $\mathbf{1}_N$ ,  $\mathbf{I}_N$ ,  $\mathbf{O}_N$ , and  $\mathbf{O}_{M,N}$  denote the  $N$ -by- $N$  all-one matrix, the  $N$ -by- $N$  identity matrix, the  $N$ -by- $N$  all-zero matrix, and the  $M$ -by- $N$  all-zero matrix, respectively. The matrix  $P_N$  denotes the  $N$ -by- $N$  backward identity matrix whose  $(m, n)$ th entry is given by 1 for  $m + n = N + 1$ , and 0 otherwise. The operator  $[A]_{m,n}$  and  $\text{tr}(A)$  denote the  $(m, n)$ th entry and the trace of a matrix  $A$ , respectively. The operator  $[x]_n$  denotes the  $n$ th entry of a vector  $x$ . To describe the computational complexity, we will use the big-O notation  $\mathcal{O}(g(N))$  defined as  $f(N) = \mathcal{O}(g(N))$  if and only if there exist a positive constant  $M$  and a real number  $N_0$  such that  $|f(N)| \leq M|g(N)|$ ,  $\forall N > N_0$ .

---

<sup>2</sup>There should be no confusion from the superscript  $*$  that denotes the complex conjugation.





## CHAPTER 2

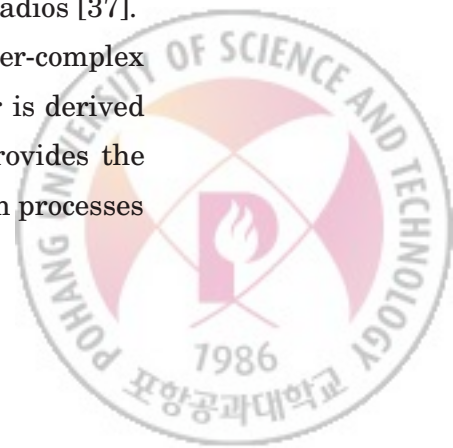
---

### CT FRESH Properizer and Its Application to Presence Detection

---

Recently, physical layer security has attracted a lot of research interests to negate various attacks in wireless networks [34]. In military communications, however, not only devising such counter-attacks but designing passive and active attacks such as eavesdropping and jamming, respectively, has also been critical issues [35, 36]. Eavesdropping that mainly intends to retrieve adversary's secret information initiates with signal presence detection and classification. Jamming that aims to interfere with communications between adversaries can also be much improved in its efficiency by detecting the signal presence in advance. In civilian communications, signal presence detection again may play an important role, e.g., in spectrum sensing for cognitive radios [37].

In this chapter, we consider the presence detection of an improper-complex SOCS random process. In particular, the optimal presence detector is derived for improper-complex SOCS Gaussian random processes, which provides the lower bound on the detection error probabilities for all SOCS random processes

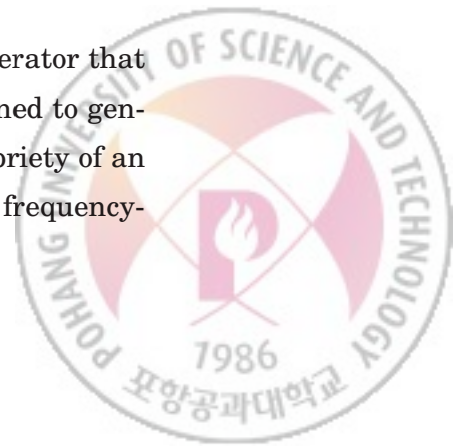


of the same second-order statistics. To capture the cyclostationarity, periodically time-varying filters such as the FREquency SHift (FRESH) filter [9] must be employed. To capture the impropriety, LCL or WL processing [19, 20] is necessary, employing two parallel linear filters that process the complex random process and its complex conjugate separately. Thus, the estimator-correlator structure [40] may straightforwardly be employed that consists of the LCL cyclic Wiener filter [22] followed by a correlator [38].

Unlike the conventional estimator-correlator approach using two parallel linear periodically time-varying filters, we propose an alternative structure of the optimal detector that employs two serially-connected periodically time-varying filters. An LCL periodically time-varying operator precedes that requires the information only about the center frequency and the cycle period of the SOCS random process input. This operator is named a FRESH properizer because it converts the SOCS random process input, whether proper or improper, to an equivalent proper-complex SOCS random process with twice the cycle period. The FRESH properizer is motivated by the recently proposed p-FRESH vectorizer [21] that converts an SOCS random process to an equivalent proper-complex vector-WSS random process. Then, a linear periodically time-varying filter follows that does not require the information about the complementary auto-covariance function of the output of the FRESH properizer. In this way, the use of two parallel linear filters is circumvented in processing the SOCS random process. Of course, the proposed detector achieves the same performance as the conventional optimal detector due to the equivalence.

## 2.1 FRESH Properizer

In this section, we introduce an LCL periodically time-varying operator that converts its input to an equivalent output. In particular, it is designed to generate a proper-complex SOCS random process regardless of the propriety of an SOCS random process input. To proceed, we define the following frequency-



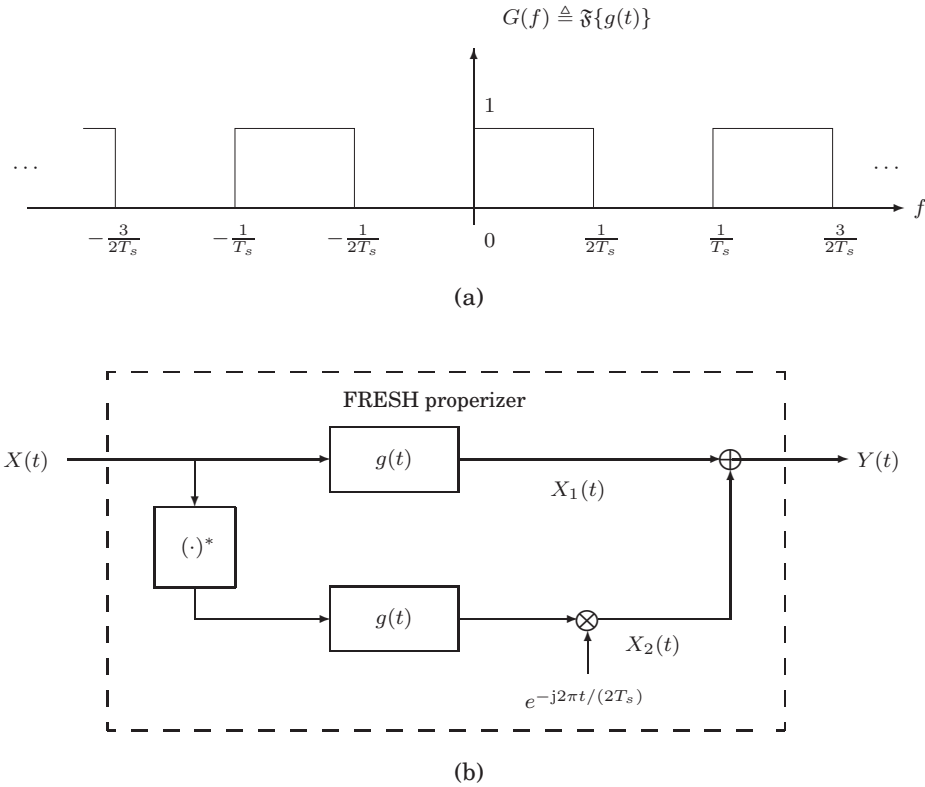


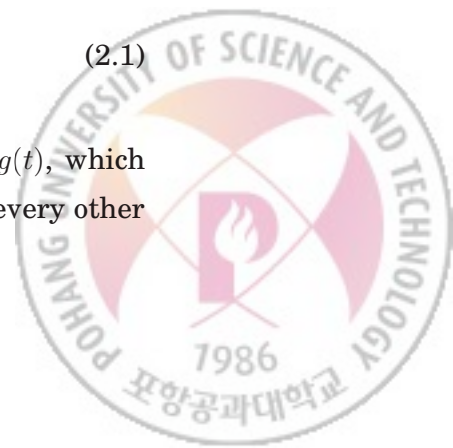
**Fig. 2.1** (a) Frequency response of the FD-RSW filter. (b) FRESH properizer viewed in the time domain.

selective filter that filters out half the signal components in the input.

**Definition 12** Given a reference rate  $1/T_s$ , the frequency-domain raised square wave (FD-RSW) filter  $g(t)$  is defined as a linear time-invariant (LTI) system having the frequency response  $G(f) \triangleq \mathfrak{F}\{g(t)\}$  given by

$$G(f) \triangleq \begin{cases} 0, & \text{for } -\frac{1}{2T_s} \leq f < 0, \\ 1, & \text{for } 0 \leq f < \frac{1}{2T_s}, \text{ and} \\ G\left(f + \frac{1}{T_s}\right), & \text{elsewhere.} \end{cases} \quad (2.1)$$

Fig. 2.1-(a) shows the frequency response of the FD-RSW filter  $g(t)$ , which alternately passes the frequency components of the input signal in every other



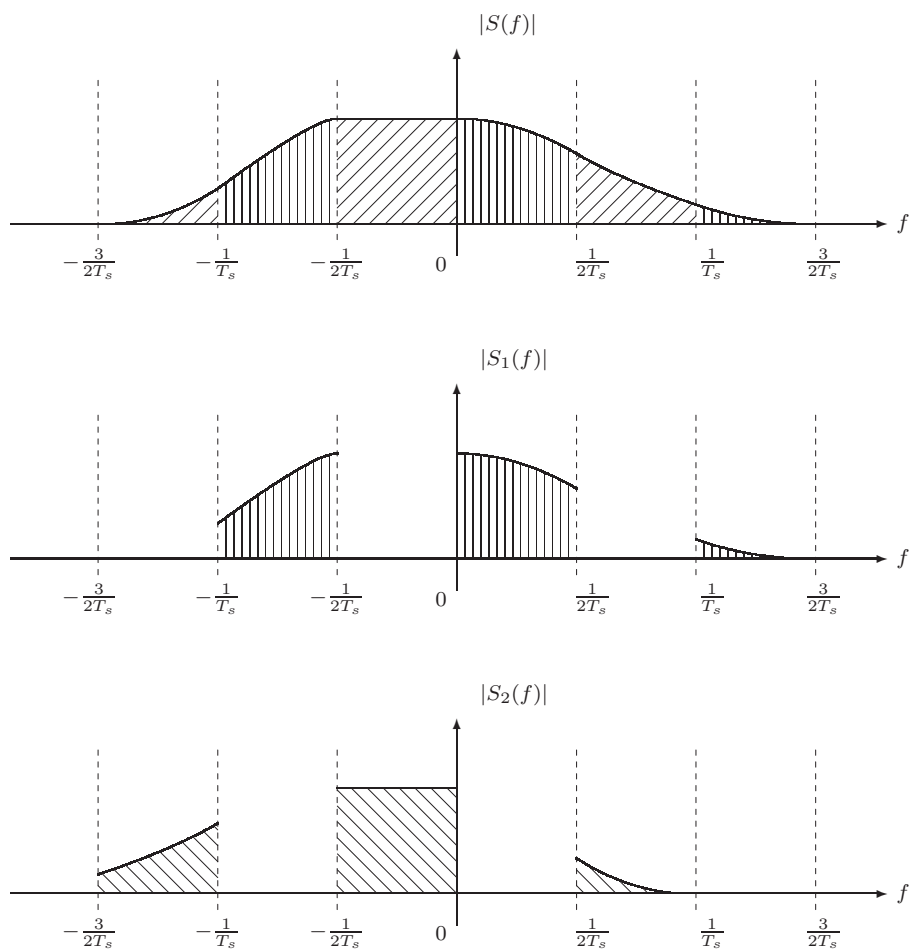


**Fig. 2.2** The output of the FRESH properizer for a deterministic signal  $s(t)$  viewed in the frequency domain.



interval of bandwidth  $1/(2T_s)$ . Hereafter,  $\mathcal{G}$  denotes the support of this FD-RSW filter with a reference rate  $1/T_s$ .

Now, we define an LCL periodically time-varying operator called the FRESH properizer.

**Definition 13** *Given a reference rate  $1/T_s$  and an input  $X(t)$ , the FRESH properizer is defined as a single-input single-output LCL periodically time-varying system, whose output is given by*

$$\mathcal{F}_p\{X(t)\} \triangleq X(t) * g(t) + \{X(t)^* * g(t)\}e^{-j2\pi \frac{t}{2T_s}}, \quad (2.2)$$

where  $g(t)$  is the impulse response of the FD-RSW filter with a reference rate of  $1/T_s$ .

Fig. 2.1-(b) shows how the FRESH properizer works in the time domain, where an input signal  $X(t)$  is converted to an output signal  $Y(t) \triangleq \mathcal{F}_p\{X(t)\}$ . It becomes clear that the output is equivalent to the input when this FRESH properization process is viewed in the frequency domain. Fig. 2.2 shows how the FRESH properizer works in the frequency domain, when the input is a deterministic signal  $s(t)$  with Fourier transform  $S(f) \triangleq \mathfrak{F}\{s(t)\}$ . Note that  $S(f)$  is directly processed by the FD-RSW filter to generate the first term  $S_1(f)$  of the Fourier transform of the FRESH properizer output  $S_1(f) + S_2(f)$  while  $S(-f)^*$  is processed by the FD-RSW filter and shifted in the frequency domain to generate the second term,  $S_2(f)$ . Thus,  $S_1(f)$  contains all the frequency components in  $s(t)$  on the support  $\mathcal{G}$  of the FD-RSW filter, while  $S_2(f)$  contains the remaining frequency components.

Up to this point, the FRESH properizer is no more than a sufficient statistic generator given an observation signal. The following proposition shows the important property of the output of the FRESH properizer when the input is an SOCS random process with cycle period  $T_s$ .



**Proposition 1** *If the input  $X(t)$  to the FRESH properizer with reference rate  $1/T_s$  is a zero-mean SOCS random process with cycle period  $T_s$ , then the output  $Y(t)$  becomes a zero-mean proper-complex SOCS random process with cycle period  $2T_s$ , i.e., the mean, the auto-correlation, and the complementary auto-correlation functions of  $Y(t)$  satisfy*

$$\mu_Y(t) \triangleq \mathbb{E}\{Y(t)\} = 0, \quad (2.3a)$$

$$r_Y(t, s) \triangleq \mathbb{E}\{Y(t)Y(s)^*\} = r_Y(t + 2T_s, s + 2T_s), \text{ and} \quad (2.3b)$$

$$\tilde{r}_Y(t, s) \triangleq \mathbb{E}\{Y(t)Y(s)\} = 0, \quad (2.3c)$$

$\forall t, \forall s$ , respectively.

*Proof:* It is straightforward to show (2.3a) using  $\mu_X(t) = 0, \forall t$ . Define  $X_1(t)$  and  $X_2(t)$  as  $X_1(t) \triangleq X(t) * g(t)$  and  $X_2(t) \triangleq \{X(t)^* * g(t)\}e^{-j2\pi t/(2T_s)}$ . Then, the auto-correlation function  $r_Y(t, s)$  of  $Y(t)$  is given by

$$\begin{aligned} r_Y(t, s) = & \mathbb{E}\{X_1(t)X_1(s)^*\} + \mathbb{E}\{X_1(t)X_2(s)^*\} \\ & + \mathbb{E}\{X_2(t)X_1(s)^*\} + \mathbb{E}\{X_2(t)X_2(s)^*\}, \end{aligned} \quad (2.4a)$$

while the complementary auto-correlation function  $\tilde{r}_Y(t, s)$  of  $Y(t)$  is given by

$$\begin{aligned} \tilde{r}_Y(t, s) = & \mathbb{E}\{X_1(t)X_1(s)\} + \mathbb{E}\{X_1(t)X_2(s)\} \\ & + \mathbb{E}\{X_2(t)X_1(s)\} + \mathbb{E}\{X_2(t)X_2(s)\}. \end{aligned} \quad (2.4b)$$

Let  $R_X(f, f') \triangleq \int_{-\infty}^{\infty} \int_{-\infty}^{\infty} r_X(t, s) e^{-j2\pi(ft-f's)} dt ds$  be the double Fourier transform of  $r_X(t, s)$ . Similarly, define  $\tilde{R}_X(f, f')$  as that of  $\tilde{r}_X(t, s)$ . Then, as shown in [12], there exist  $\{R_X^{(k)}(f)\}_{k \in \mathbb{Z}}$  and  $\{\tilde{R}_X^{(k)}(f)\}_{k \in \mathbb{Z}}$  such that

$$R_X(f, f') = \sum_{k=-\infty}^{\infty} R_X^{(k)}\left(f - \frac{k}{T_s}\right) \delta\left(f - f' - \frac{k}{T_s}\right) \quad (2.5a)$$

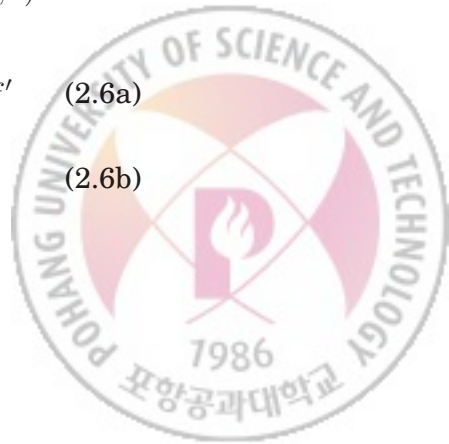
and

$$\tilde{R}_X(f, f') = \sum_{k=-\infty}^{\infty} \tilde{R}_X^{(k)}\left(f - \frac{k}{T_s}\right) \delta\left(f - f' - \frac{k}{T_s}\right), \quad (2.5b)$$

where  $\delta(\cdot)$  denotes the Dirac delta function. The first term in  $r_Y(t, s)$  is then given by

$$\mathbb{E}\{X_1(t)X_1(s)^*\} = \int_{-\infty}^{\infty} \int_{-\infty}^{\infty} G(f) e^{j2\pi ft} R_X(f, f') G(f')^* e^{-j2\pi f's} df df' \quad (2.6a)$$

$$= \sum_{k=-\infty}^{\infty} \left( \int_{\mathcal{G}} R_X^{(k)}\left(f - \frac{k}{T_s}\right) e^{j2\pi f(t-s)} df \right) e^{j2\pi \frac{k}{T_s}s}, \quad (2.6b)$$



which is periodic in both  $t$  and  $s$  with period  $T_s$ , where Parseval's relation is used twice in (2.6a). The second term in  $r_Y(t, s)$  is also given by

$$\mathbb{E}\{X_1(t)X_2(s)^*\} = \int_{-\infty}^{\infty} \int_{-\infty}^{\infty} G(f)e^{j2\pi ft} \tilde{R}_X(f, f')G(f')^* e^{-j2\pi f's} df df' e^{j2\pi \frac{s}{2T_s}} \quad (2.7a)$$

$$= \sum_{k=-\infty}^{\infty} \left( \int_{\mathcal{G}} \tilde{R}_X^{(k)} \left( f - \frac{k}{T_s} \right) e^{j2\pi f(t-s)} df \right) e^{j2\pi \frac{2k+1}{2T_s}s}, \quad (2.7b)$$

which is periodic in both  $t$  and  $s$  with period  $2T_s$ , where Parseval's relation is used again twice in (2.7b). Similarly, we can obtain the other two terms, which again are found to be periodic in  $t$  and  $s$  with period  $2T_s$ .

On the other hand, the first and the second terms in  $\tilde{r}_Y(t, s)$  are given by

$$\mathbb{E}\{X_1(t)X_1(s)\} = \iint_{\mathcal{G} \times \mathcal{G}} \tilde{R}_X(f, -f') e^{j2\pi ft} e^{j2\pi f's} df df' \quad (2.8a)$$

and

$$\mathbb{E}\{X_1(t)X_2(s)\} = \iint_{\mathcal{G} \times \mathcal{G}} R_X(f, -f') e^{j2\pi(f t + f' s)} e^{-j2\pi \frac{1}{2T_s}s} df df' \quad (2.8b)$$

respectively,  $\forall t, \forall s$ . These two terms both have zero values because the impulse fences of  $R_X(f, -f')$  and  $\tilde{R}_X(f, -f')$  on  $f = -f' - m/T_s$  do not cross the integration area  $(f, f') \in \mathcal{G} \times \mathcal{G}$  at all. Similarly, we can obtain the other two terms, which again are both found to have zero values. Thus, the complementary auto-covariance function  $\tilde{r}_Y(t, s)$  of  $Y(t)$  vanishes for all  $t$  and  $s$ . Therefore, the conclusion follows.  $\square$

The following corollary is noteworthy because, although the cyclostationarity with cycle period  $T_s$  implies that with cycle period  $2T_s$ , the converse is not true.

**Corollary 1** *If the input  $X(t)$  to the FRESH properizer with reference rate  $1/T_s$  is a zero-mean proper-complex SOCS random process with cycle period  $T_s$ , then the zero-mean proper-complex SOCS random process  $Y(t)$  has the cycle period  $T_s$ .*

*Proof:* As can be easily seen in (2.6a),  $\tilde{R}_X(f, f') = 0, \forall f, \forall f'$ , makes the second term  $\mathbb{E}\{X_1(t)X_2(s)^*\}$  of  $r_Y(t, s)$  become zero,  $\forall t, \forall s$ . Similarly, the third





term becomes zero. Since the first and the fourth terms of  $r_Y(t, s)$  are periodic in  $t$  and  $s$  with period  $T_s$ ,  $r_Y(t, s) = r_Y(t + T_s, s + T_s), \forall t, \forall s$ . On the other hand,  $\tilde{r}_Y(t, s)$  is still zero,  $\forall t, \forall s$ , by Proposition 1. Therefore, the conclusion follows.  $\square$

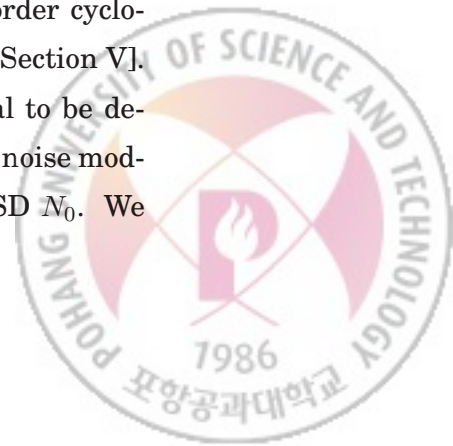
The properization of an SOCS complex random process first appears in [21], where a band-limited SOCS complex random process is converted by a single-input multiple-output LCL periodically time-varying system, called the p-FRESH vectorizer, to an equivalent vector-valued proper-complex WSS random process. Unlike the p-FRESH vectorizer, which performs both the properization and the stationarization of its output, the FRESH properizer does not perform the stationarization but only the properization of its output. However, it has a notable advantage over the p-FRESH vectorizer in that it can convert even a band-unlimited input to a scalar-valued proper-complex random process.

## 2.2 Application to Signal Presence Detection

In this section, we consider a presence detection of improper-complex SOCS Gaussian random processes.

Suppose that there is a communicator that can be either silent or transmitting a digitally modulated signal over a real passband frequency-selective channel. The center frequency of a bandpass digitally modulated signal is assumed to be known to the detector to make the complex envelope an SOCS random process. This assumption is not important for proper-complex cases, as long as no signal component is lost during the down-conversion process to the complex baseband. However, it is crucial for improper-complex SOCS cases, because an arbitrary choice of center frequency does not result in the second-order cyclostationarity of the complex envelope in general, as discussed in [21, Section VI].

Let  $X(t)$  be the complex envelope of a digitally modulated signal to be detected, and  $W(t)$  be the complex baseband equivalent of the ambient noise modeled by a zero-mean proper-complex white Gaussian noise with PSD  $N_0$ . We





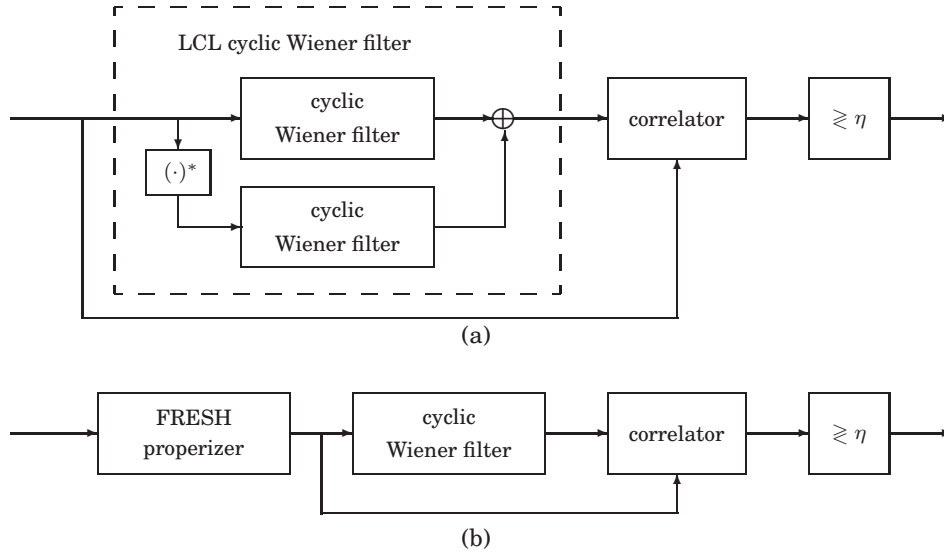
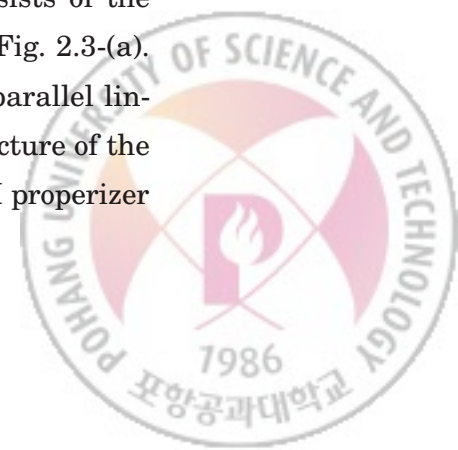


**Fig. 2.3** (a) Conventional optimal detector that consists of an LCL cyclic Wiener filter followed by a correlator. (b) Proposed detector that consists of a FRESH properizer followed by an estimator-correlator with single cyclic Wiener filter.

assume that  $X(t)$  is a zero-mean SOCS Gaussian process with average power  $P$  and the cycle period  $T_s$ . The zero-mean assumption is well justified because our main interest is in the presence detection of a digitally modulated signal, of which the mean function is zero in general, in order not to waste the signal power. The Gaussian assumption not only makes the problem mathematically tractable but also is well justified if  $X(t)$  is generated by digitally modulating data symbols from an optimal Gaussian codebook.

To capture both the cyclostationarity and the impropriety, the estimator-correlator structure may straightforwardly be employed that consists of the LCL cyclic Wiener filter [22] followed by a correlator as shown in Fig. 2.3-(a). Unlike the conventional estimator-correlator approach using two parallel linear periodically time-varying filters, we propose an alternative structure of the optimal detector by using the FRESH properizer. Since the FRESH properizer



results in a proper-complex random process, a conjugate-linear processing of the output of the FRESH properizer is not necessary. Thus, we derive the detector in the structure of the FRESH properizer followed by an estimator-correlator with a linear periodically time-varying filter as shown in Fig. 2.3-(b).

Since we assume that the complex envelope of the received signal passes through the FRESH properizer, the observation model at the output of the FRESH properizer is then given by

$$\begin{aligned} \mathcal{H}_0 : Z(t) &= N(t) \\ \text{versus} \\ \mathcal{H}_1 : Z(t) &= Y(t) + N(t) \end{aligned} \tag{2.9}$$

for  $t \in \mathcal{T}$ , where  $\mathcal{H}_0$  and  $\mathcal{H}_1$  are the null and the alternative hypotheses, respectively,  $N(t)$  and  $Y(t)$  denote the outputs of the FRESH properizer when  $W(t)$  and  $X(t)$  are the inputs, respectively, and  $\mathcal{T}$  denotes the length- $T$  observation interval defined as

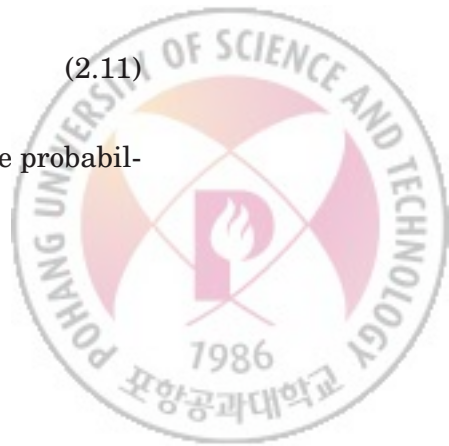
$$\mathcal{T} \triangleq \{t : -T/2 \leq t < T/2\}. \tag{2.10}$$

Note that the FRESH properizer does not introduce additional spectral correlations that did not exist in the input to the FRESH properizer. This is because the FRESH properizer only changes the location of the frequency components of the input. Note also that a proper-complex white noise has no correlation among different frequency components. Thus, it can be easily seen that, if the input  $W(t)$  to the FRESH properizer is a proper-complex white noise, the output  $N(t)$  becomes also a proper-complex white noise.

Given this observation model and the second-order statistics of  $Z(t)$ , our objective is to design the  $\alpha$ -level most powerful detector or the Neyman-Pearson detector that solves the optimization problem

$$\begin{aligned} &\text{maximize} \quad P_D \\ &\text{subject to} \quad P_{FA} \leq \alpha, \end{aligned} \tag{2.11}$$

where  $P_D \triangleq \Pr(\text{declare } \mathcal{H}_1 | \mathcal{H}_1)$  and  $P_{FA} \triangleq \Pr(\text{declare } \mathcal{H}_1 | \mathcal{H}_0)$  are the probability of detection and the probability of false alarm, respectively.



It is assumed that the auto-correlation function  $r_Y(t, s)$  of  $Y(t)$  is bounded, i.e.,  $\mathbb{E}\{|Y(t)|^2\} < \infty$ , and continuous on  $(t, s) \in \mathcal{T} \times \mathcal{T}$ . Because we are using the observation model of the FRESH properizer output, we deal with the proper-complex SOCS random process  $Z(t)$ . Then, the straightforward extension of Mercer's theorem [39, Secion 3.3] for a real-valued random process to the proper-complex random process can provides the representation of  $r_Y(t, s)$  as

$$r_Y(t, s) = \sum_{n=1}^{\infty} \lambda_n \phi_n(t) \phi_n(s)^* \quad (2.12a)$$

for  $(t, s) \in \mathcal{T} \times \mathcal{T}$ , where the eigenvalues  $(\lambda_n)_n$  and the corresponding orthonormal eigenfunctions  $(\phi_n(t))_n$  are the solutions to the Fredholm integral equation

$$\lambda_n \phi_n(t) = \int_{\mathcal{T}} r_Y(t, s) \phi_n(s) ds, \quad \forall t \in \mathcal{T}, \quad (2.12b)$$

$\forall n \in \mathbb{N}$ . The convergence in (2.12a) is absolute and uniform for  $(t, s) \in \mathcal{T} \times \mathcal{T}$  [40].

The optimal solution of the detection problem (2.11) is well known for a real-valued observation [39, 40]. By the straightforward extension to a proper-complex observation, the log-likelihood ratio (LLR)  $l(Z(t))$  can be derived by

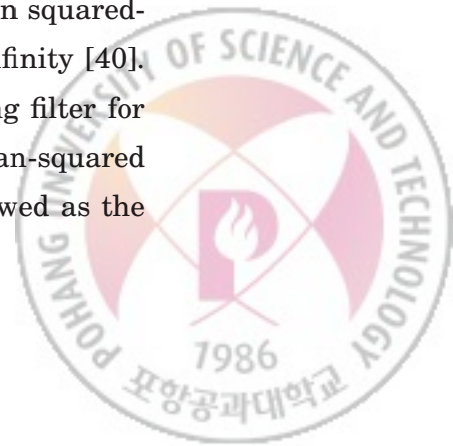
$$l(Z(t)) = \frac{1}{N_0} \int_{\mathcal{T}} \int_{\mathcal{T}} Z(t)^* q(t, s) Z(s) dt ds, \quad (2.13)$$

where the non-negative definite function  $q(t, s)$  is defined by

$$q(t, s) \triangleq \sum_{n=1}^{\infty} \frac{\lambda_n}{\lambda_n + N_0} \phi_n(t) \phi_n(s)^*, \quad \forall t, s \in \mathcal{T}. \quad (2.14)$$

Note that the optimal detector can be performed by comparing the LLR with the threshold that is determined to satisfy  $P_{FA} = \alpha$  [40].

It is interesting that  $\hat{Z}(t) \triangleq \int_{\mathcal{T}} q(t, s) Z(s) ds$  is the minimum mean squared-error estimator of  $Z(t)$  when the observation period  $T$  tends to infinity [40]. A cyclic Wiener filter is an optimal linear periodically time-varying filter for a proper-complex SOCS random process in the sense that the mean-squared error is minimized. Thus, the derived optimal detector can be viewed as the



FRESH properizer followed by an estimator-correlator with single cyclic Wiener filter as shown in Fig. 2.3-(b). Since the proposed detector achieves the same performance as the conventional optimal detector due to the equivalence, the use of two parallel cyclic Wiener filters is circumvented in processing the SOCS random process.

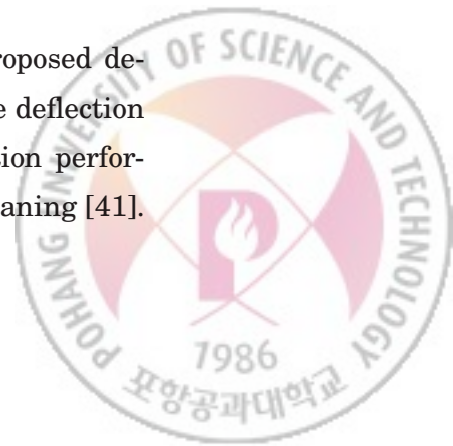
In the next section, the numerical results are provided to demonstrate the effectiveness of the FRESH properizer in a detector in the form of the estimator-correlator with a linear periodically time-varying filter.

## 2.3 Numerical Results

In the previous section, it is shown that the proposed detector achieves the same performance as the conventional estimator-correlator with an LCL cyclic Wiener filter due to the equivalence. In this section, we provide numerical results that demonstrate the effectiveness of the FRESH properizer in exploiting the cyclostationarity and impropriety of an SOCS random process.

We consider the complex envelope of the bandpass signal with the bandwidth  $2B$  that is linearly modulated with an uncorrelated data sequence, which consists of independent and identically distributed zero-mean real Gaussian random variables. The observation period is given by  $T = 200T_s$  and the transmission rate, the center frequency, and the noise variance are assumed to be known to the detector. Throughout this section, the proposed detector means a detector that consists of the FRESH properizer followed by an estimator-correlator with a linear periodically time-varying filter while the conventional linear estimator-correlator means a detector that consists only of a linear periodically time-varying filter followed by a correlator.

The first result in Fig. 2.4 is to compare the deflection of the proposed detector with that of the conventional linear estimator-correlator. The deflection is often used as a mathematically tractable measure of the detection performance even though the deflection does not have a clear physical meaning [41].



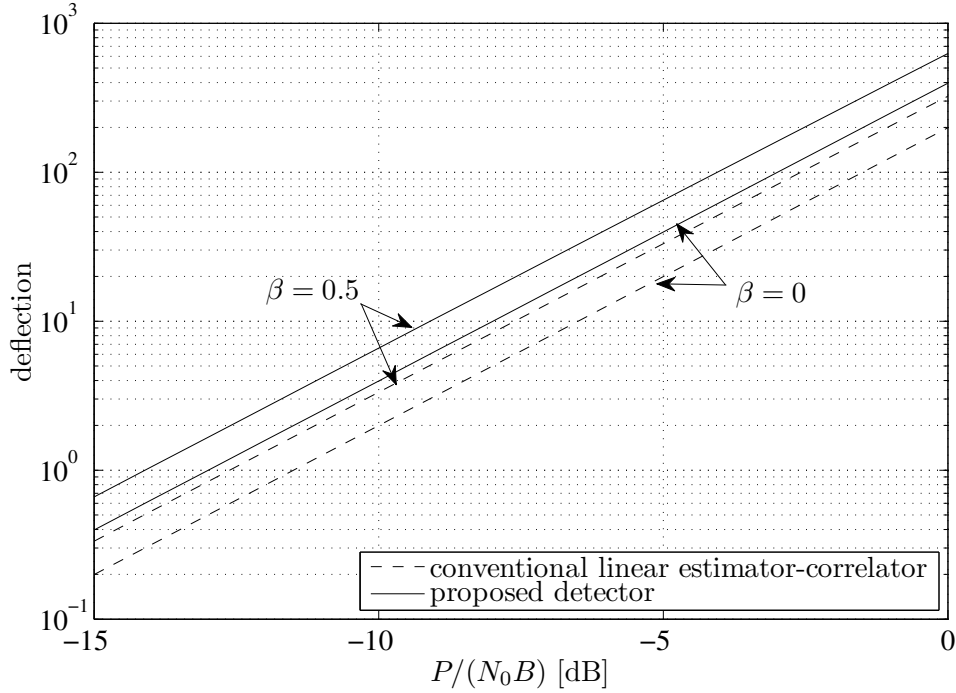


**Fig. 2.4** Comparison of the deflections of the proposed detector and the conventional linear estimator-correlator.

Fig. 2.4 shows that the deflections of both the detectors increase as the excess bandwidth  $\beta$  increases. It is also shown that the proposed detector has deflections greater than the conventional linear estimator-correlator. This is because although both the detectors fully exploit the cyclostationarity of the SOCS random process, the proposed detector can exploit the additional propriety by using the FRESH properizer.

The second result in Fig. 2.5 is to compare the receiver operating characteristic (ROC) curve of the proposed detector with that of the conventional linear estimator-correlator for  $P/(N_0B) = -10$  dB and  $-5$  dB with the excess bandwidth  $\beta = 0.25$ . It is shown that the proposed detector significantly outperforms the conventional linear estimator-correlator. Note that the proposed detector achieves both the probability of miss and the probability of false alarm less than



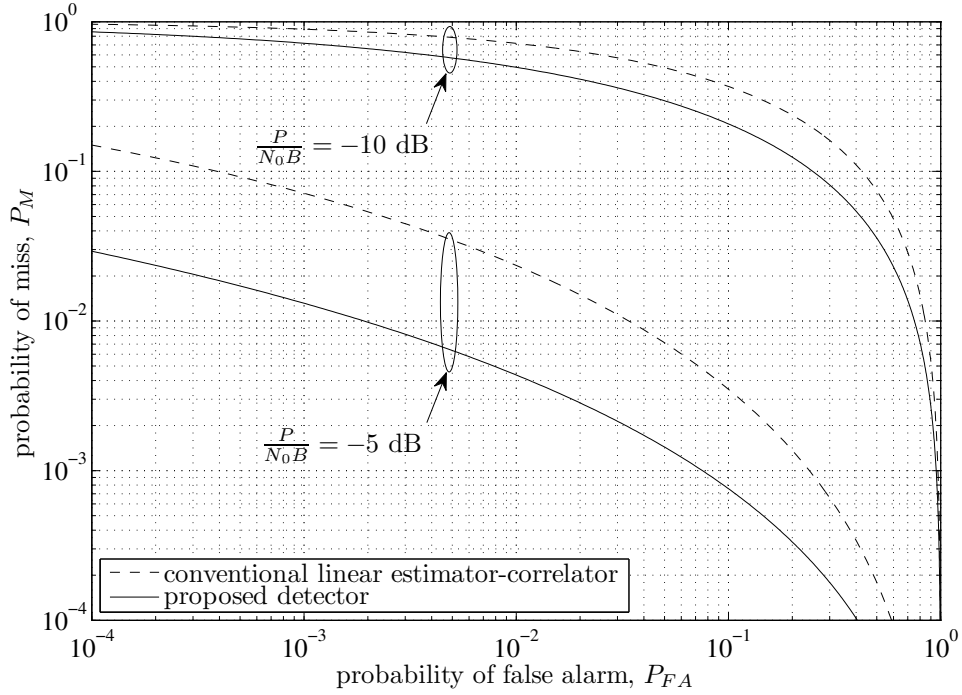


**Fig. 2.5** Comparison of the ROCs of the proposed detector and the conventional linear estimator-correlator.

$10^{-2}$  at  $P/(N_0 B) = 5$  dB while the conventional linear estimator-correlator does not.

## 2.4 Summary

In this chapter, we propose a simple periodically LCL time-varying operator called a FRESH properizer. It is shown that the FRESH properizer always converts an SOCS random process, whether it is proper or improper, into an equivalent proper-complex SOCS random process. As an application, we consider the detection problem of an improper-complex SOCS Gaussian random process and derive the optimal presence detector that consists of a FRESH properizer followed by an estimator-correlator with a linear periodically time-varying filter.



Numerical results show that the proposed detector significantly outperform the conventional linear estimator-correlator.



# CHAPTER 3

---

## Asymptotic Frequency-Shift Properizer for Block Processing

---

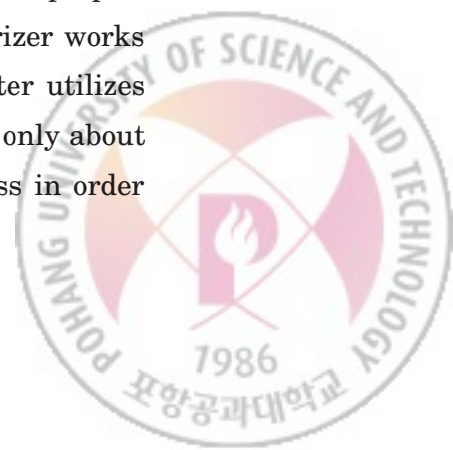
Recently, another LCL PTV operator called the p-FRESH vectorizer is proposed in [21, 23] by non-trivially extending the HSR. The p-FRESH vectorizer converts an *improper-complex* SOCS scalar random process to an equivalent *proper-complex* WSS vector random process by exploiting the frequency-domain correlation and complementary correlation structures that are rigorously examined in [16]. By successfully deriving the capacity of an SOCS Gaussian noise channel, it is shown that the optimal channel input is improper-complex SOCS in general when the interfering signal is improper-complex SOCS. It is also well demonstrated that such properization provides the advantage of enabling the adoption of the conventional signal processing techniques and algorithms that utilize only the correlation but not the complementary correlation structure. These results warrant further research in communications and signal processing on the efficient construction and processing of improper-complex SOCS random processes.





In this chapter, we consider the block processing of a complex-valued random vector that is obtained by taking a finite, but a very large, number of consecutive samples from a DT improper-complex SOCS random process. To proceed, the p-FRESH vectorization developed for CT SOCS random processes is first extended to DT improper-complex SOCS random processes. Instead of straightforwardly modifying the CT p-FRESH vectorizer that properizes as well as vectorizes the input CT improper-complex SOCS random process, an invertible LCL operator is proposed in this chapter that does not vectorize but only properizes the input DT improper-complex SOCS random process. Thus, unlike the p-FRESH vectorizer, this LCL operator named the DT FRESH properizer generates a scalar-valued random process. Specifically, the DT FRESH properizer transforms a DT improper-complex SOCS scalar random process into an equivalent proper-complex SOCS scalar random process with the cycle period that is twice the cycle period of the input process. Similar to the p-FRESH vectorizer, the DT FRESH properizer also enables the adoption of the conventional signal processing techniques and algorithms that are already developed for the filtering of proper-complex random processes.

To make this idea of pre-processing by properization better suited for digital signal processing, an invertible LCL block processing operator is then proposed that mimics the operation of the DT FRESH properizer. Although the augmentation of the improper-complex random vector by its complex conjugate can generate a sufficient statistic [18], it is not only a redundant information of twice the length of the original observation vector but also improper. Thus, the augmenting pre-processor does not allow the direct application of the conventional techniques and algorithms dedicated to the block processing of proper-complex random vectors. Motivated by how the DT FRESH properizer works in the frequency domain, the pre-processor proposed in this chapter utilizes the centered discrete Fourier transform (DFT) and the information only about the cycle period of the DT improper-complex SOCS random process in order



to convert a finite number of consecutive samples of the random process to an equivalent random vector. Unlike the simple augmentation of the improper-complex random vector by its complex conjugate, the output of this LCL block processing operator is not redundant in that it has the same length as its input. Unlike the output of the DT FRESH properizer, the output of this LCL block processing operator is not proper but approximately proper for sufficiently large block size. Thus, the pre-processor is named the asymptotic FRESH properizer. Specifically, the asymptotic FRESH properizer makes the sequence of the complementary covariance matrices of the output asymptotically equivalent [42] to the sequence of all-zero matrices.

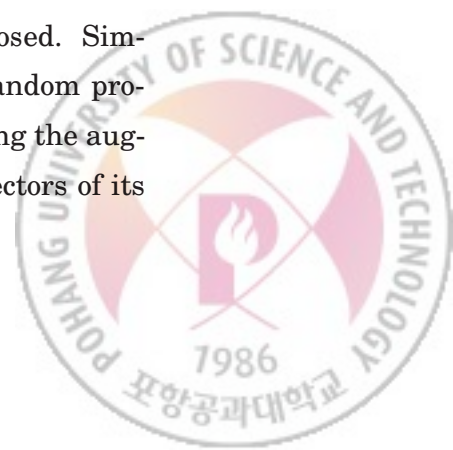
In [43], it is shown that the complex-valued random vector consisting of a finite number of consecutive samples of a DT proper-complex SOCS random process has its frequency-domain covariance matrix that approaches a block matrix with diagonal blocks as the number of samples increases. This is because the periodicity in the second-order statistics of the DT SOCS random process naturally leads to a sequence of block Toeplitz covariance matrices as the number of samples increases, the sequence of block Toeplitz matrices is asymptotically equivalent to a sequence of block circulant matrices, and a block circulant matrix becomes a block matrix with diagonal blocks when pre- and post-multiplied by DFT and inverse DFT matrices, respectively. Since the asymptotic FRESH properizer mimics the DT FRESH properizer and the DT FRESH properizer outputs a DT proper-complex SOCS random process, it naturally becomes of interest to examine the asymptotic property of the frequency-domain covariance matrix of the asymptotic FRESH properizer output. It turns out that the output of the asymptotic FRESH properizer has the same property discovered in [43].

Such properties of the covariance and the complementary covariance matrices may be used in designing, under various optimality criteria, low-complexity post-processors that follow the asymptotic FRESH properizer. In particular, a



post-processor can be developed that approximates the output of the asymptotic FRESH properizer by a proper-complex random vector having the block matrix with diagonal blocks that is asymptotically equivalent to the exact frequency-domain covariance matrix as its frequency-domain covariance matrix. Of course, this technique makes the post-processor suboptimal that performs most of the main operations in the frequency domain. As the two asymptotic properties strongly suggest, however, if the block size is large enough, then the performance degradation may be negligible. It is already shown in [43] that this is the case for the asymptotic property only of the covariance matrix, where a suboptimal frequency-domain equalizer is proposed that approximates the frequency-domain covariance matrix of a proper-complex SOCS interference by an asymptotically equivalent block matrix with diagonal blocks. It turns out that this equalizer not only achieves significantly lower computational complexity than the exact linear minimum mean-square error (LMMSE) equalizer by exploiting the block structure of the frequency-domain covariance matrix, but also is asymptotically optimal in the sense that its average mean-squared error (MSE) approaches that of the LMMSE equalizer as the number of samples tends to infinity.

To demonstrate that asymptotic optimality and low complexity can be simultaneously achievable by employing the asymptotic FRESH properizer, we consider two representative estimation and detection problems. A conventional technique for the estimation and the detection of CT real-valued random processes with finite-time observation is to use the Karhunen-Loève (KL) expansion of the observation [39]. In [38], the estimation and the detection of CT improper-complex random processes with finite-time observation are considered, and the KL expansion of the augmented observation is proposed. Similarly, the estimation and the detection of DT improper-complex random processes with finite-time observation can be approached by representing the augmented observation vector with a linear combination of the eigenvectors of its



correlation matrix. However, as shown in [43] for the equalization in a proper-complex SOCS random process, such a straightforward approach without exploiting the cyclostationarity results in a high computational complexity in general for a large sample size.

First, for a DT improper-complex SOCS random signal in additive proper-complex white noise, a low-complexity signal estimator is proposed that is a linear function of the output of the asymptotic FRESH properizer. It is shown that the average MSE performance of the estimator approaches that of the widely linear minimum mean-squared error (WLMMSE) estimator as the number of samples tends to infinity. Second, for a DT improper-complex SOCS Gaussian random signal in additive proper-complex white Gaussian noise, a low-complexity signal presence detector is proposed whose test statistic is a quadratic function of the output of the asymptotic FRESH properizer. It is shown that the test statistic converges to the exact likelihood ratio test (LRT) statistic that is a quadratic function of the augmented observation vector with probability one (w.p. 1) as the number of samples tends to infinity. Note that in both cases the asymptotic FRESH properizer as the pre-processor utilizes only the information about the cycle period. Thus, the adoption of adaptive estimation and detection algorithms may be possible that are developed for the processing of proper-complex random vectors. This advantage of employing the asymptotic FRESH properizer may be taken in other communications and signal processing problems involving the block processing of DT improper-complex SOCS random processes.

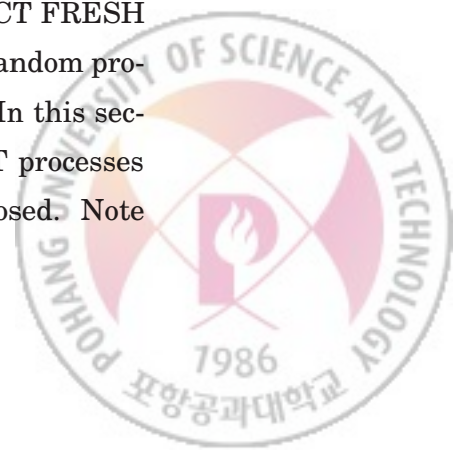
As mentioned earlier, the LCL-type augmentation of the signal mainly used in this chapter is not the only way to WL filtering. We provide a brief discussion on how the proposed WL block processing can be realized by an alternative WL block processing that utilizes the real part of the signal augmented by the imaginary part. In particular, the same estimation and detection problems are examined now with this real-valued signal representation of the complex sig-



nal. The optimal estimator and detector and their computational complexities are derived. It is shown that the all real-valued augmented signal after being properly permuted has a similar asymptotic property in the frequency domain to the LCL-type augmented signal. It is also shown that the redundancy in the augmented signal can be removed as it is done in the asymptotic FRESH properization. By exploiting these properties, we propose asymptotically optimal estimator and detector whose computational complexities are the same as those adopting the asymptotic FRESH properizer as the pre-processor. However, this alternative approach to the block processing of DT improper-complex SOCS random processes may not directly adopt the conventional signal processing techniques and algorithms that are already developed for the filtering of proper-complex random processes. Moreover, the WL processing using complex-valued representation of the signal provides more mathematical elegance and implementational advantage, as pointed out in [17], [18, Ch. 1], and [19].

### 3.1 DT FRESH Properizer

In this section, an LCL PTV operator is proposed that always outputs an equivalent DT proper-complex random process regardless of the propriety of the input DT SOCS random process, under the assumption that the parameter called the reference frequency of the operator satisfies a certain condition. In what follows, all SOCS random processes are DT processes unless otherwise specified. In [21], the notion of CT second-order cyclostationarity is introduced and an LCL PTV operator named p-FRESH vectorizer is proposed that converts an input CT SOCS random process to an equivalent CT proper-complex WSS vector random process. In [44], another LCL PTV operator named CT FRESH properizer is proposed that converts a CT improper-complex SOCS random process into an equivalent CT proper-complex SOCS random process. In this section, the notion of second-order cyclostationarity is extended to DT processes and the DT counterpart of the CT FRESH properizer is also proposed. Note



that, unlike the p-FRESH vectorizer, the CT and the DT FRESH properizers do not vectorize but only properize the input improper-complex SOCS random process. Similar to the CT FRESH properizer, the DT FRESH properizer as a pre-processor enables the adoption of the conventional signal processing techniques and algorithms that utilize only the correlation but not the complementary correlation structure of the signal.

To proceed, the following frequency-selective filter is defined that has half of the entire frequency band as its stopband.

**Definition 14** *Given a reference frequency  $1/M$ , a linear time-invariant system with impulse response  $g_M[n]$  is called the frequency-domain raised square wave (FD-RSW) filter if its frequency response  $G_M(f) = \mathcal{F}\{g_M[n]\}$  is given by*

$$G_M(f) \triangleq \begin{cases} 0, & \text{for } -\frac{1}{2M} \leq f < 0, \\ 1, & \text{for } 0 \leq f < \frac{1}{2M}, \end{cases} \quad (3.1)$$

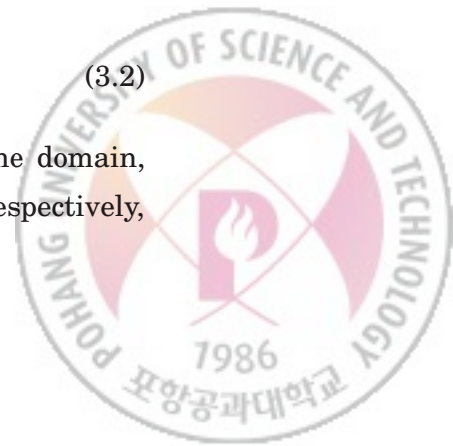
and satisfying  $G_M(f) \triangleq G_M(f + 1/M)$ .

Fig. 3.1 shows the frequency response of the FD-RSW filter with reference frequency  $1/M$ , which alternately passes the frequency components of the input signal in every other interval of bandwidth  $1/(2M)$ . Hereafter,  $\mathcal{G}_M$  denotes the support of this FD-RSW filter. By using the impulse response  $g_M[n]$  of the FD-RSW filter with reference frequency  $1/M$ , we can define an LCL PTV filter as follows.

**Definition 15** *Given a reference frequency  $1/M$  and an input  $X[n]$ , the DT FRESH properizer is defined as a single-input single-output LCL PTV system, whose output is given by*

$$Y[n] \triangleq X[n] * g_M[n] + (X[n]^* * g_M[n]) e^{-j2\pi n/(2M)}. \quad (3.2)$$

Fig. 3.2 shows how the DT FRESH properizer works in the time domain, where  $X[n]$  is the input,  $Y[n]$  is the output, and  $X_1[n]$  and  $X_2[n]$  are, respectively,





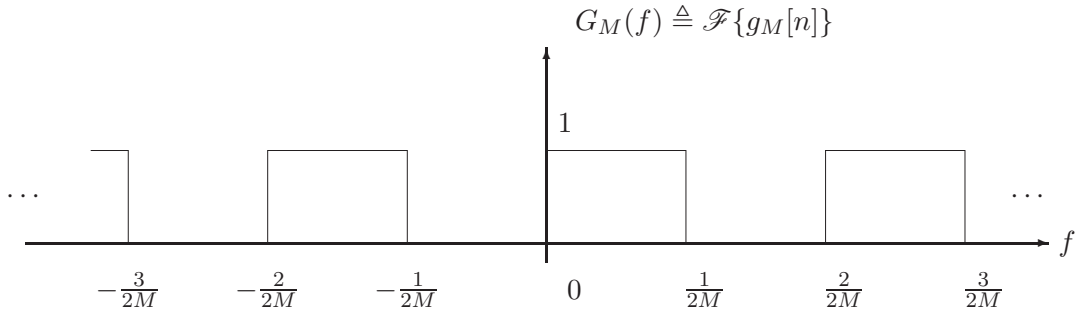


**Fig. 3.1** Frequency response of the FD-RSW filter with reference frequency  $1/M$ .

the first and the second terms on the right side of (3.2). Note that, unlike the upper branch where  $X[n]$  is processed by the FD-RSW filter to generate  $X_1[n]$ ,  $X[n]^*$  is processed in the lower branch by the FD-RSW filter and multiplied by a complex-exponential function  $e^{-j2\pi n/(2M)}$  to generate  $X_2[n]$ . Even though  $-1/(2M)$  is chosen as the frequency of the complex-exponential function, any  $(2k+1)/(2M)$  for  $k \in \mathbb{Z}$  can be chosen. The reason why this is so becomes clear once the DT FRESH properization is viewed in the frequency domain.

The following lemma makes this invertibility argument more precise.

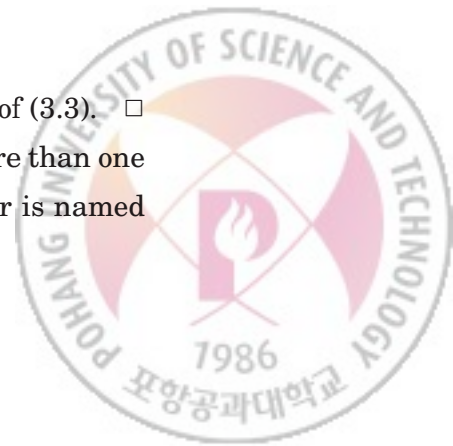
**Lemma 6** *The DT FRESH properizer with reference frequency  $1/M$  is identical to its inverse mapping, i.e.,*

$$X[n] = Y[n] * g_M[n] + (Y[n]^* * g_M[n])e^{-j2\pi n/(2M)}, \quad (3.3)$$

where  $Y[n]$  is the output of the DT FRESH properizer with reference frequency  $1/M$  when its input is  $X[n]$ .

*Proof:* Straightforward by substituting (3.2) into the right side of (3.3).  $\square$

Note that, at this point, the DT FRESH properizer may not be more than one of many possible invertible operators. The reason why this operator is named





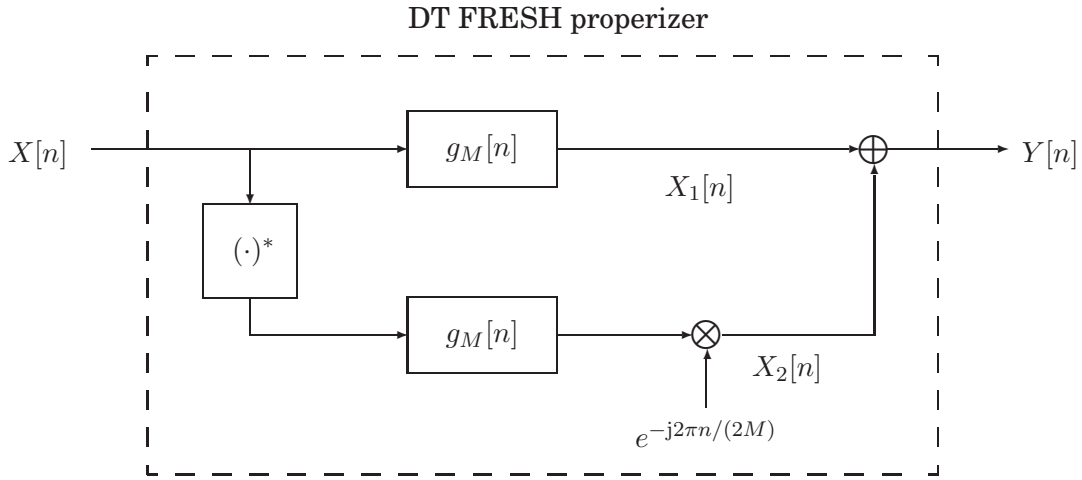


**Fig. 3.2** DT FRESH properizer with reference frequency  $1/M$  viewed in the time domain.

the properizer will become clear once the second-order property of the output is analyzed as follows when its input is a zero-mean SOCS random process. In [44], similar property of band-limited CT SOCS random processes and its proof can be found. Thus, we omit the detailed proof of the following theorem, which can be straightforwardly obtained by substituting CT parameters in [44] with DT parameters.

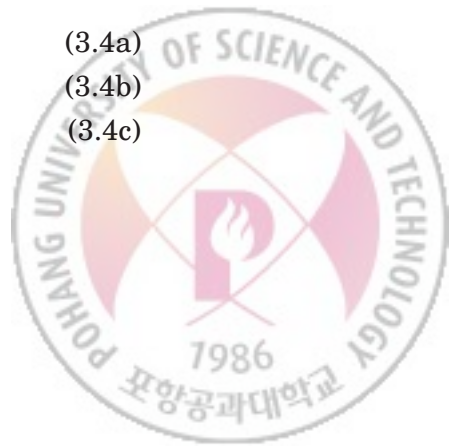
**Theorem 1** *If the input  $X[n]$  to the DT FRESH properizer with reference frequency  $1/M$  is a zero-mean SOCS random process with cycle period  $M$ , then the output  $Y[n]$  becomes a zero-mean proper-complex SOCS random process with cycle period  $2M$ , i.e., the mean, the auto-correlation, and the complementary auto-correlation functions of  $Y[n]$  satisfy*

$$\mu_Y[n] \triangleq \mathbb{E}\{Y[n]\} = 0, \quad (3.4a)$$

$$r_Y[n, m] \triangleq \mathbb{E}\{Y[n]Y[m]^*\} = r_Y[n+2M, m+2M], \text{ and} \quad (3.4b)$$

$$\tilde{r}_Y[n, m] \triangleq \mathbb{E}\{Y[n]Y[m]\} = 0, \quad (3.4c)$$

$\forall m, \forall n$ , respectively.



*Proof:* See the proof of [44, Proposition 1].  $\square$

It is already shown that the amount of the frequency shift in the second term of (3.2) can be any  $(2k + 1)/(2M)$ , for  $k \in \mathbb{Z}$ , to satisfy the invertibility of the DT FRESH properizer. It can be also shown that Theorem 1 holds for any frequency shift  $(2k + 1)/(2M)$ , for  $k \in \mathbb{Z}$ . Moreover, since any integer multiple of  $M$  is also a cycle period of an SOCS random process with cycle period  $M$ , the random process can be FRESH properized by using any reference frequency  $1/(kM)$ ,  $\forall k \in \mathbb{N}$ . Thus, it is not unique to FRESH properize an SOCS random process.

This theorem shows that the DT FRESH properizer in general doubles the cycle period at the cost of the propriety of the output. However, it does not double the cycle period if the input is already proper.

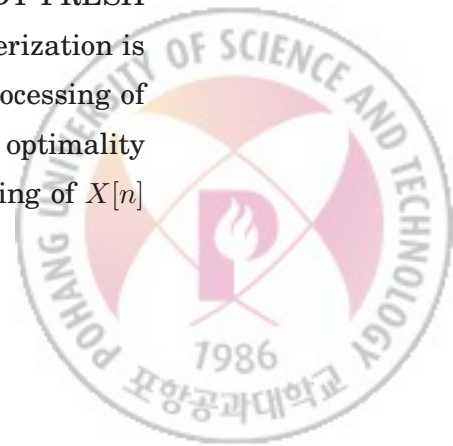
**Corollary 2** *If the input  $X[n]$  to the DT FRESH properizer with reference frequency  $1/M$  is a zero-mean proper-complex SOCS random process with cycle period  $M$ , then the output  $Y[n]$  is a zero-mean proper-complex SOCS random process with cycle period  $M$ .*

*Proof:* See the proof of [44, Corollary 1]. Due to the same reason as Theorem 1, we again omit the detailed proof.  $\square$

Theorem 1 also has the following consequence.

**Corollary 3** *An optimal linear processing of the output of the DT FRESH properizer always leads to the same result as the optimal widely linear processing of the input of the DT FRESH properizer does.*

*Proof:* Let  $X[n]$  and  $Y[n]$  be the input and the output of the DT FRESH properizer with relation (15) and (6). Because the DT FRESH properization is invertible as shown in Lemma 6, the performance of an optimal processing of  $X[n]$  always equal to that of the processing of  $Y[n]$  under the same optimality criterion [39, pp. 289-290]. Thus, an optimal widely linear processing of  $X[n]$



is equivalent to the widely linear processing of  $Y[n]$  under the same criterion. Therefore, the conclusion follows by the propriety of  $Y[n]$  shown in Theorem 1.  $\square$

It is noteworthy that Theorem 1 does not imply that any FRESH properizer can properize an improper SOCS random process with cycle period  $M$ .

**Corollary 4** *If  $k_1M = k_2M'$  for integers  $k_1$  and  $k_2$  where  $k_1$  is not divisible by  $k_2$ , then the output of the DT FRESH properizer with reference frequency  $1/M'$  becomes an improper-complex SOCS random process with cycle period  $2k_1M$ .*

*Proof:* It can be straightforwardly shown by using the CT version proof of [44, Theorem 1], where we just need to replace the reference frequency of the FRESH properizer by  $k_2/(k_1M)$ .  $\square$

In theory, the DT FRESH properizer is enough to deal with improper-complex SOCS random processes by using conventional linear processing techniques and algorithms. However, the FD-RSW filter is not realizable in practice due to its shape in the frequency domain.

### 3.2 Asymptotic FRESH Properizer

In this section, the block processing of an SOCS random process is considered. Motivated by how the DT FRESH properizer works in the frequency domain, an LCL block operator is proposed that converts a finite number of consecutive samples of an SOCS random process to an equivalent random vector. Unlike the DT FRESH properizer proposed in the previous section, this invertible operator does not directly make the complementary covariance matrix of the output vector vanish. Instead, it is shown that the LCL operator makes the complementary covariance matrix of the output vector approach all-zero matrix as the number of samples tends to infinity. This is why it is named the asymptotic FRESH properizer.



### 3.2.1 Asymptotic FRESH Properizer and Its Inverse Operator

Let  $x$  be the length- $MN$  vector obtained by taking the  $MN$  consecutive samples of a DT signal, where and in what follows it is assumed that  $N$  is a positive even number. Motivated by the DT FRESH properizer, we introduce in this subsection an LCL block operator and its inverse.

To proceed, some definitions are provided.

**Definition 16** *The centered DFT matrix  $\mathbf{W}_{MN}$  is defined as an  $(MN)$ -by- $(MN)$  matrix whose  $(m, n)$ th entry, for  $m, n \in \{1, \dots, MN\}$ , is given by*

$$[\mathbf{W}_{MN}]_{m,n} \triangleq \frac{1}{\sqrt{MN}} e^{-j2\pi(m-c_{MN})(n-c_{MN})/(MN)}, \quad (3.5)$$

where  $c_{MN} \triangleq (MN + 1)/2$ .

It is well known that the matrix-vector multiplication with a centered DFT matrix can be implemented with low computational complexity [45], as the multiplication with an ordinary DFT matrix is efficiently implemented by using the fast Fourier transform algorithm.

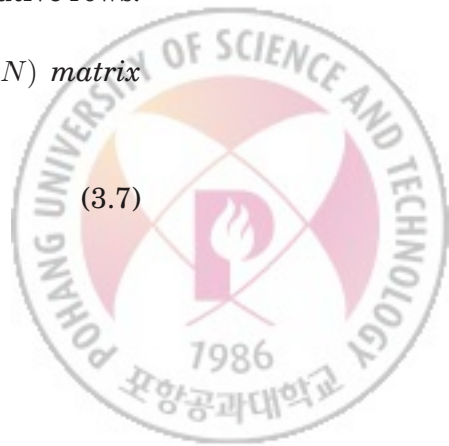
**Definition 17** *Given  $M$  and an even number  $N$ , the  $(MN)$ -by- $(MN)$  matrix  $\mathbf{G}_{M,N}$  is defined as*

$$\mathbf{G}_{M,N} \triangleq \mathbf{I}_M \otimes \begin{bmatrix} \mathbf{O}_{N/2} & \mathbf{O}_{N/2} \\ \mathbf{O}_{N/2} & \mathbf{I}_{N/2} \end{bmatrix}. \quad (3.6)$$

Similar to the FD-RSW pulse, the matrix  $\mathbf{G}_{M,N}$  will be called the raised square wave (RSW) matrix because, when pre-multiplied to a column vector or a matrix, it turns the  $((m-1)N+n)$ th row, for  $m = 1, \dots, M$  and  $n = 1, \dots, N/2$ , into all zeros, i.e., it alternately nulls every other band of  $N/2$  consecutive rows.

**Definition 18** *Given  $M$  and an even number  $N$ , the  $(MN)$ -by- $(MN)$  matrix  $\mathbf{S}_{M,N}$  is defined as*

$$\mathbf{S}_{M,N} \triangleq \begin{bmatrix} \mathbf{O}_{MN-N/2, N/2} & \mathbf{I}_{MN-N/2} \\ \mathbf{I}_{N/2} & \mathbf{O}_{N/2, MN-N/2} \end{bmatrix}. \quad (3.7)$$



Note that the matrix  $S_{M,N}$ , when pre-multiplied to a column vector or a matrix, circularly shifts the rows by  $N/2$ , which corresponds to multiplying  $e^{-j2\pi n/(2M)}$  in the second term of the right side of (3.2). Now, we are ready to introduce an LCL operator that is the block-processing counterpart to the DT FRESH properizer.

**Definition 19** *Given  $M$  and an even number  $N$ , the LCL operator  $f$  with input  $x$  and output  $y = f(x)$ , both of length  $MN$ , is called the asymptotic FRESH properizer if*

$$f(x) \triangleq \mathbf{W}_{MN}^H (\mathbf{G}_{M,N} \mathbf{W}_{MN} x + \mathbf{S}_{M,N} \mathbf{G}_{M,N} \mathbf{W}_{MN} x^*). \quad (3.8)$$

Note that the input  $x$  is pre-multiplied by the centered DFT matrix  $\mathbf{W}_{MN}$  and the RSW matrix  $\mathbf{G}_{M,N}$ , while the complex conjugate  $x^*$  is multiplied additionally by the circular shift matrix  $\mathbf{S}_{M,N}$  to generate the frequency-domain output  $\mathbf{W}_{MN} y$ .

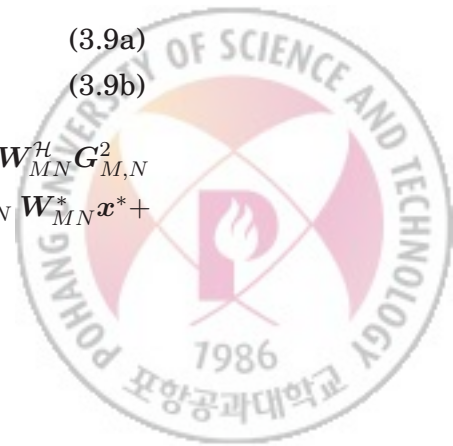
Fig. 3.3 shows  $\mathbf{W}_{MN} x$ ,  $\mathbf{G}_{M,N} \mathbf{W}_{MN} x$ , and  $\mathbf{S}_{M,N} \mathbf{G}_{M,N} \mathbf{W}_{MN} x^*$ , when the  $l$ th entry of the  $\mathbf{W}_{MN} x$  is denoted by  $x'_l$ . Note that, similar to the DT FRESH properization, the locations of all possible non-zero rows of  $\mathbf{G}_{M,N} \mathbf{W}_{MN} x$  and  $\mathbf{S}_{M,N} \mathbf{G}_{M,N} \mathbf{W}_{MN} x^*$  do not overlap, which makes  $\mathbf{W}_{MN} y$  contain all the entries of  $\mathbf{W}_{MN} x$  without any distortion. Note also that the amount of the circular shift of  $\mathbf{S}_{M,N} \mathbf{G}_{M,N} \mathbf{W}_{MN} x^*$  by any  $kN$  for  $k \in \mathbb{Z}$  generates the signal that contains the same information as  $\mathbf{S}_{M,N} \mathbf{G}_{M,N} \mathbf{W}_{MN} x^*$  does. The following lemma makes this invertibility argument more precise.

**Lemma 7** *From the output  $y$  of the asymptotic FRESH properizer with parameters  $M$  and  $N$ , the input  $x$  of the asymptotic FRESH properizer can be recovered as*

$$x = \mathbf{W}_{MN}^H (\mathbf{G}_{M,N} \mathbf{W}_{MN} y + \mathbf{P}_{MN} \mathbf{G}_{M,N} \mathbf{S}_{M,N}^T \mathbf{W}_{MN}^* y^*) \quad (3.9a)$$

$$\triangleq f^{-1}(y) \quad (3.9b)$$

*Proof:* By substituting (3.8) into the right side of (3.9a), we have  $\mathbf{W}_{MN}^H \mathbf{G}_{M,N}^2 \mathbf{W}_{MN} x + \mathbf{W}_{MN}^H \mathbf{G}_{M,N} \mathbf{S}_{M,N} \mathbf{G}_{M,N} \mathbf{W}_{MN} x^* + \mathbf{W}_{MN}^H \mathbf{P}_{MN} \mathbf{G}_{M,N} \mathbf{S}_{M,N}^T \mathbf{G}_{M,N} \mathbf{W}_{MN}^* x^* +$



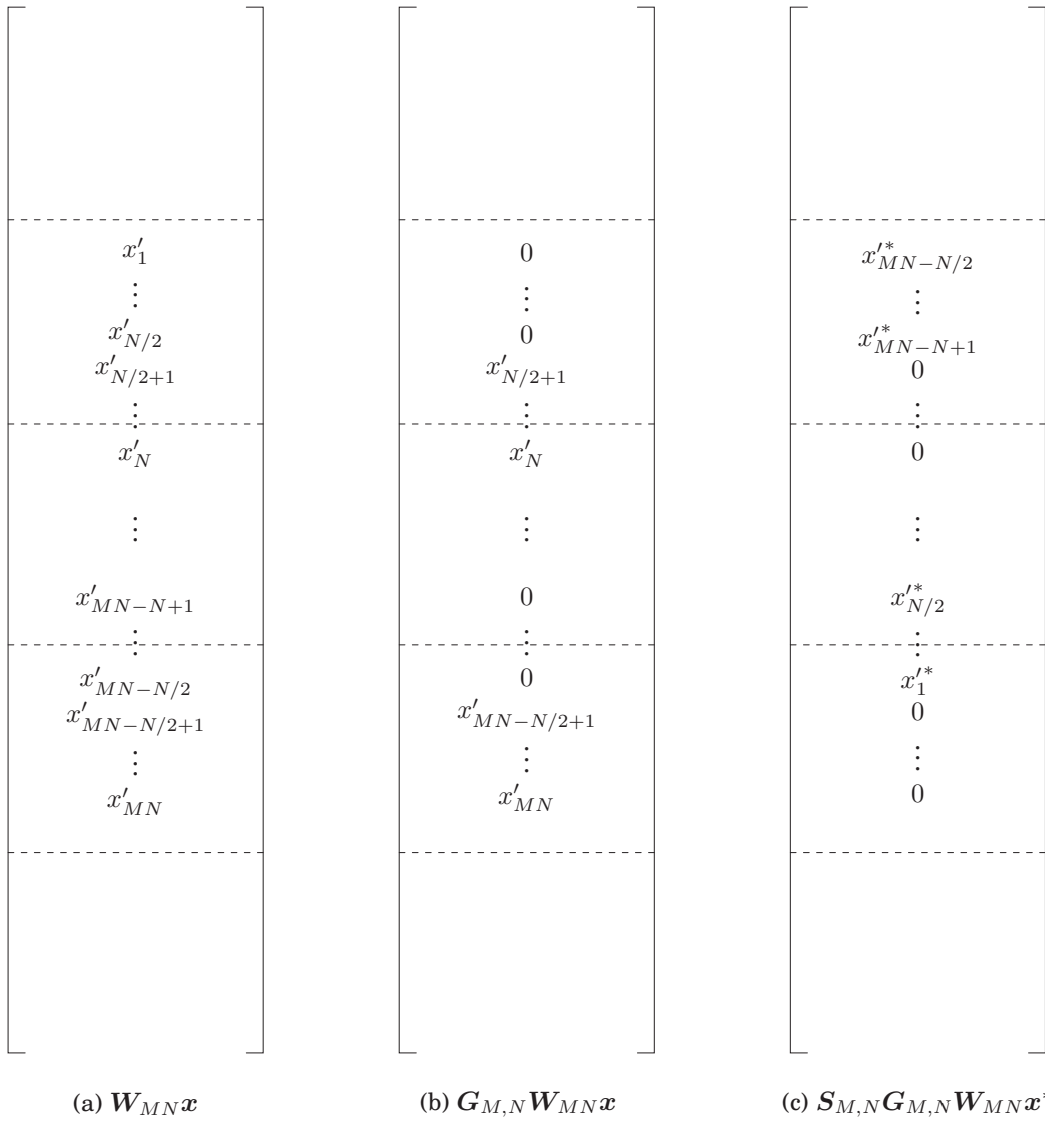


**Fig. 3.3** Illustration that shows how the asymptotic FRESH properizer works in the frequency domain.



$\mathbf{W}_{MN}^H \mathbf{P}_{MN} \mathbf{G}_{M,N} \cdot \mathbf{S}_{M,N}^T \mathbf{S}_{M,N} \mathbf{G}_{M,N} \mathbf{W}_{MN}^* \mathbf{x}$ . The second and the third terms vanish since  $\mathbf{G}_{M,N} \mathbf{S}_{M,N} \mathbf{G}_{M,N} = \mathbf{O}_{MN}$  and  $\mathbf{G}_{M,N} \mathbf{S}_{M,N}^T \mathbf{G}_{M,N} = \mathbf{O}_{MN}$ , respectively. Thus, the right side of (3.9a) becomes  $\mathbf{W}_{MN}^H (\mathbf{G}_{M,N}^2 + \mathbf{P}_{MN} \mathbf{G}_{M,N}^2 \mathbf{P}_{MN}) \mathbf{W}_{MN} \mathbf{x}$ . Moreover, it can be easily shown that  $\mathbf{G}_{M,N}^2 = \mathbf{G}_{M,N}$  and  $\mathbf{G}_{M,N} + \mathbf{P}_{MN} \mathbf{G}_{M,N} \mathbf{P}_{MN} = \mathbf{I}_{MN}$ , because  $\mathbf{P}_{MN} = \mathbf{P}_M \otimes \mathbf{P}_N$  by the properties of the Kronecker product. Therefore, the conclusion follows.  $\square$

Note that, at this point, the asymptotic FRESH properizer may not be more than one of many possible invertible operators. The reason why this operator is named the asymptotic properizer will become clear once the second-order property of the output is analyzed in the next subsection when its input is a finite number of consecutive samples of a zero-mean SOCS random process.

### 3.2.2 Second-Order Properties of Output of Asymptotic FRESH Properizer

Let  $\bar{\mathbf{x}}$  be the length- $2MN$  augmented vector defined as

$$\bar{\mathbf{x}} \triangleq \begin{bmatrix} \mathbf{x} \\ \mathbf{x}^* \end{bmatrix}, \quad (3.10)$$

where and in what follows it is assumed that  $\mathbf{x}$  consists of a finite number of consecutive samples of a *zero-mean* SOCS random process  $X[n]$  with cycle period  $M \in \mathbb{N}$ . Then, the output  $\mathbf{y} = \mathbf{f}(\mathbf{x})$  in (3.8) of the asymptotic FRESH properizer can be rewritten as

$$\mathbf{y} = \mathbf{W}_{MN}^H \bar{\mathbf{G}}_{M,N} \bar{\mathbf{W}}_{MN} \bar{\mathbf{x}} \quad (3.11a)$$

$$\triangleq \mathbf{W}_{MN}^H \hat{\mathbf{y}}, \quad (3.11b)$$

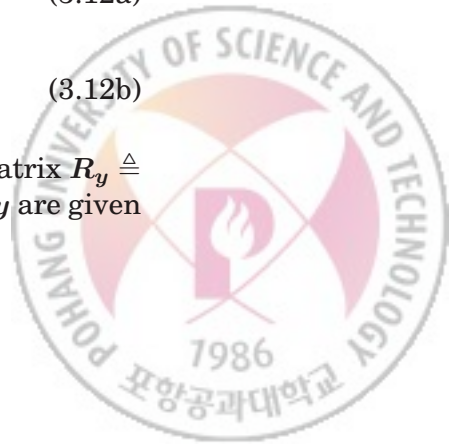
where the  $(MN)$ -by- $(2MN)$  matrix  $\bar{\mathbf{G}}_{M,N}$  and the  $(2MN)$ -by- $(2MN)$  matrix  $\bar{\mathbf{W}}_{MN}$  are given by

$$\bar{\mathbf{G}}_{M,N} \triangleq \begin{bmatrix} \mathbf{G}_{M,N} & \mathbf{S}_{M,N} \mathbf{G}_{M,N} \end{bmatrix} \quad (3.12a)$$

and

$$\bar{\mathbf{W}}_{MN} \triangleq \begin{bmatrix} \mathbf{W}_{MN} & \mathbf{O}_{MN} \\ \mathbf{O}_{MN} & \mathbf{W}_{MN} \end{bmatrix}, \quad (3.12b)$$

respectively, and  $\hat{\mathbf{y}}$  is the centered DFT of  $\mathbf{y}$ . Thus, the covariance matrix  $\mathbf{R}_{\hat{\mathbf{y}}} \triangleq \mathbb{E}\{\mathbf{y}\mathbf{y}^H\}$  and the complementary covariance matrix  $\bar{\mathbf{R}}_{\hat{\mathbf{y}}} \triangleq \mathbb{E}\{\mathbf{y}\mathbf{y}^T\}$  of  $\mathbf{y}$  are given





by

$$\mathbf{R}_y = \mathbf{W}_{MN}^H \bar{\mathbf{G}}_{M,N} \bar{\mathbf{W}}_{MN} \mathbf{R}_{\bar{x}} \bar{\mathbf{W}}_{MN}^H \bar{\mathbf{G}}_{M,N}^H \mathbf{W}_{MN} \quad (3.13a)$$

and

$$\tilde{\mathbf{R}}_y = \mathbf{W}_{MN}^H \bar{\mathbf{G}}_{M,N} \bar{\mathbf{W}}_{MN} \tilde{\mathbf{R}}_{\bar{x}} \bar{\mathbf{W}}_{MN}^T \bar{\mathbf{G}}_{M,N}^T \mathbf{W}_{MN}^*, \quad (3.13b)$$

respectively, where  $\mathbf{R}_{\bar{x}} \triangleq \mathbb{E}\{\bar{x}\bar{x}^H\}$  and  $\tilde{\mathbf{R}}_{\bar{x}} \triangleq \mathbb{E}\{\bar{x}\bar{x}^T\}$  denote the covariance and the complementary covariance matrices of the augmented vector  $\bar{x}$ , respectively.

Throughout this chapter, we call

$$\mathbf{R}_{\hat{y}} \triangleq \mathbb{E}\{\hat{y}\hat{y}^H\} = \mathbf{W}_{MN} \mathbf{R}_y \mathbf{W}_{MN}^H \quad (3.14a)$$

and

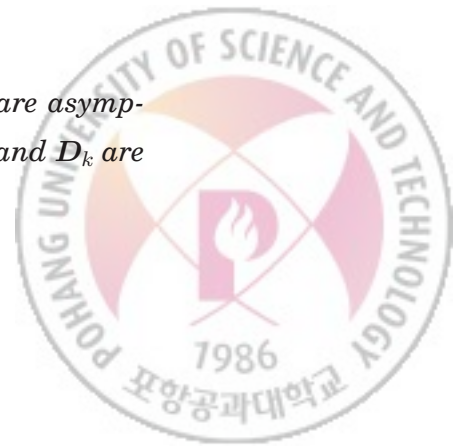
$$\tilde{\mathbf{R}}_{\hat{y}} \triangleq \mathbb{E}\{\hat{y}\hat{y}^T\} = \mathbf{W}_{MN} \tilde{\mathbf{R}}_y \mathbf{W}_{MN}^T \quad (3.14b)$$

the frequency-domain covariance and the frequency-domain complementary covariance matrices, respectively.

To analyze the asymptotic second-order properties of  $y$ , we briefly review definitions and related lemmas for asymptotic equivalence between two sequences of matrices.

**Definition 20** [42] Let  $(\mathbf{A}_k)_k$  and  $(\mathbf{B}_k)_k$  be two sequences of  $N_k$ -by- $N_k$  matrices with  $N_k \rightarrow \infty$  as  $k \rightarrow \infty$ . Then,  $(\mathbf{A}_k)_k$  and  $(\mathbf{B}_k)_k$  are asymptotically equivalent and denoted by  $\mathbf{A}_k \sim \mathbf{B}_k$  if 1) the strong norms of  $\mathbf{A}_k$  and  $\mathbf{B}_k$  are uniformly bounded, i.e., there exists a constant  $c$  such that  $\|\mathbf{A}_k\|, \|\mathbf{B}_k\| \leq c < \infty, \forall k$ , and 2) the weak norm of  $\mathbf{A}_k - \mathbf{B}_k$  vanishes asymptotically, i.e.,  $\lim_{k \rightarrow \infty} |\mathbf{A}_k - \mathbf{B}_k| = 0$ , where the strong norm  $\|\mathbf{A}\|$  and the weak norm  $|\mathbf{A}|$  of an  $N_k$ -by- $N_k$  matrix  $\mathbf{A}$  are defined as  $\|\mathbf{A}\| \triangleq \max_{x \neq 0} \sqrt{x^H \mathbf{A}^H \mathbf{A} x / x^H x}$  and  $|\mathbf{A}| \triangleq \sqrt{\text{tr}(\mathbf{A} \mathbf{A}^H) / N_k}$ , respectively.

**Lemma 8** If two sequences  $(\mathbf{A}_k)_k$  and  $(\mathbf{B}_k)_k$  of  $N_k$ -by- $N_k$  matrices are asymptotically equivalent and if the strong norms of  $N_k$ -by- $N_k$  matrices  $\mathbf{C}_k$  and  $\mathbf{D}_k$  are uniformly bounded, then  $\mathbf{C}_k \mathbf{A}_k \mathbf{D}_k \sim \mathbf{C}_k \mathbf{B}_k \mathbf{D}_k$ .



*Proof:* Since  $C_k \sim C_k$  and  $D_k \sim D_k$ , it is straightforward to show the conclusion by applying [42, Theorem 1-(3)] twice.  $\square$

**Lemma 9** *If  $A_k \sim B_k$  and  $C_k \sim D_k$ , then  $(A_k + C_k) \sim (B_k + D_k)$ .*

*Proof:* By applying the triangle inequality, it is straightforward to show that the strong norms of  $A_k + C_k$  and  $B_k + D_k$  are uniformly bounded and that the weak norm of  $A_k + C_k - B_k - D_k$  vanishes asymptotically. Therefore, the conclusion follows.  $\square$

For brevity, in what follows, two square matrices  $A_k$  and  $B_k$  of the same size will be said to be asymptotically equivalent if  $A_k \sim B_k$ . Now, we introduce our definition of asymptotic propriety.

**Definition 21** *A sequence  $(y_k)_k$  of length- $N_k$  complex-valued random vectors is asymptotically proper if the complementary covariance matrix of  $y_k$  is asymptotically equivalent to the  $N_k$ -by- $N_k$  all-zero matrix.*

For brevity, a random vector  $y_k$  will be said to be asymptotically proper if the sequence  $(y_k)_k$  is asymptotically proper. Before showing that the output  $y$  of the asymptotic FRESH properizer is asymptotically proper, the second-order properties of the augmented vector  $\bar{x}$  are examined as follows.

**Proposition 2** *If the random vector  $x$  is obtained by taking the  $MN$  consecutive samples from a zero-mean SOCS random process with cycle period  $M$ , then the covariance matrix  $R_{\bar{x}}$  and the complementary covariance matrix  $\tilde{R}_{\bar{x}}$  of the augmented vector  $\bar{x}$  defined in (3.10) satisfy*

$$\bar{W}_{MN} R_{\bar{x}} \bar{W}_{MN}^H \sim \Omega \quad (3.15a)$$

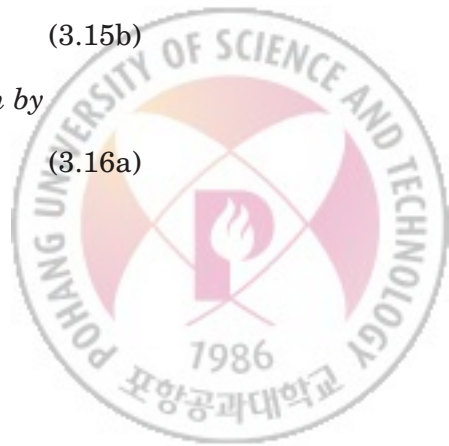
and

$$\bar{W}_{MN} \tilde{R}_{\bar{x}} \bar{W}_{MN}^T \sim \tilde{\Omega}, \quad (3.15b)$$

respectively, where the  $(2MN)$ -by- $(2MN)$  matrices  $\Omega$  and  $\tilde{\Omega}$  are given by

$$\Omega \triangleq (\bar{W}_{MN} R_{\bar{x}} \bar{W}_{MN}^H) \odot (\mathbf{1}_{2M} \otimes I_N) \quad (3.16a)$$

and



$$\tilde{\Omega} \triangleq (\bar{\mathbf{W}}_{MN} \tilde{\mathbf{R}}_{\bar{x}} \bar{\mathbf{W}}_{MN}^T) \odot (\mathbf{1}_{2M} \otimes \mathbf{P}_N), \quad (3.16b)$$

respectively.

*Proof:* By definition, the left sides of (3.15a) and (3.15b) can be rewritten, respectively, as

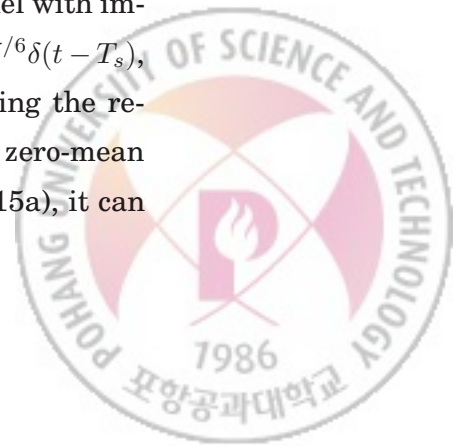
$$\bar{\mathbf{W}}_{MN} \mathbf{R}_{\bar{x}} \bar{\mathbf{W}}_{MN}^H = \begin{bmatrix} \mathbf{W}_{MN} \mathbf{R}_x \mathbf{W}_{MN}^H & \mathbf{W}_{MN} \tilde{\mathbf{R}}_x \mathbf{W}_{MN}^H \\ \mathbf{W}_{MN} \tilde{\mathbf{R}}_x^* \mathbf{W}_{MN}^H & \mathbf{W}_{MN} \mathbf{R}_x^* \mathbf{W}_{MN}^H \end{bmatrix} \quad (3.17a)$$

and

$$\bar{\mathbf{W}}_{MN} \tilde{\mathbf{R}}_{\bar{x}} \bar{\mathbf{W}}_{MN}^T = \begin{bmatrix} \mathbf{W}_{MN} \tilde{\mathbf{R}}_x \mathbf{W}_{MN}^T & \mathbf{W}_{MN} \mathbf{R}_x \mathbf{W}_{MN}^T \\ \mathbf{W}_{MN} \mathbf{R}_x^* \mathbf{W}_{MN}^T & \mathbf{W}_{MN} \tilde{\mathbf{R}}_x^* \mathbf{W}_{MN}^T \end{bmatrix}. \quad (3.17b)$$

Since both  $\mathbf{R}_x$  and  $\tilde{\mathbf{R}}_x$  are  $(MN)$ -by- $(MN)$  block Toeplitz matrices with block size  $M$ -by- $M$ , each submatrix on the right side of (3.17a) is asymptotically equivalent to the Hadamard product of  $(\mathbf{1}_M \otimes \mathbf{I}_N)$  and the submatrix itself as shown in [43, Proposition 1]. Thus, by using the fact that  $\mathbf{A} \sim \mathbf{B}$  if each submatrix of  $\mathbf{A}$  is asymptotically equivalent to the corresponding submatrix of  $\mathbf{B}$  [43, Lemma 5], we obtain (3.15a). Similar to (3.15a), it can be shown by using the property  $\mathbf{W}_{MN}^T = \mathbf{W}_{MN}^H \mathbf{P}_{MN}$  of the centered DFT matrix that each submatrix on the right side of (3.17b) is asymptotically equivalent to Hadamard product of  $(\mathbf{1}_M \otimes \mathbf{P}_N)$  and the submatrix itself. Thus, we obtain (3.15b). Therefore, the conclusion follows.  $\square$

Figs. 3.4 and 3.5 show the entry-by-entry magnitudes of the exemplary frequency-domain covariance and complementary covariance matrices. To generate a zero-mean improper-complex SOCS random process, equally-likely BPSK symbols are linearly modulated with the square-root raised cosine (SRRC) pulse having roll-off factor 0.5 and transmitted at the symbol rate of  $1/T_s$  [symbols/sec]. After the BPSK signal passes through the frequency selective channel with impulse response  $h(t) = 0.22e^{j\pi/3}\delta(t - 5T_s) + 0.44e^{j\pi/2}\delta(t - 3T_s) + 0.87e^{j\pi/6}\delta(t - T_s)$ , the SOCS random process  $X[n]$  is obtained by 2-times over-sampling the received signal, i.e., the sampling rate is  $2/T_s$  [samples/sec]. Thus, the zero-mean SOCS random process  $X[n]$  has the cycle period 2. As shown in (3.15a), it can



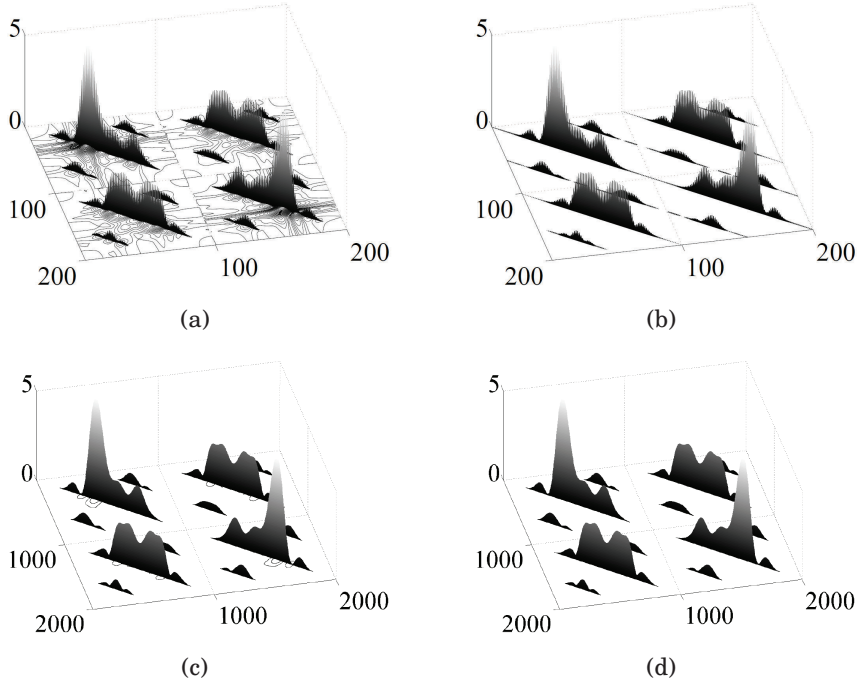


**Fig. 3.4** Magnitudes of exemplary (a)  $\bar{W}_{MN} R_{\bar{x}} \bar{W}_{MN}^H$  for  $N = 50$ , (b)  $\Omega$  for  $N = 50$ , (c)  $\bar{W}_{MN} R_{\bar{x}} \bar{W}_{MN}^H$  for  $N = 500$ , and (d)  $\Omega$  for  $N = 500$ , when  $M = 2$ .

be seen in Fig. 3.4 that  $\bar{W}_{MN} R_{\bar{x}} \bar{W}_{MN}^H$  approaches  $\Omega$  as  $N$  increases. Similarly, as shown in (3.15b), it can be seen in Fig. 3.5 that  $\bar{W}_{MN} \tilde{R}_{\bar{x}} \bar{W}_{MN}^T$  approaches  $\tilde{\Omega}$  as  $N$  increases.

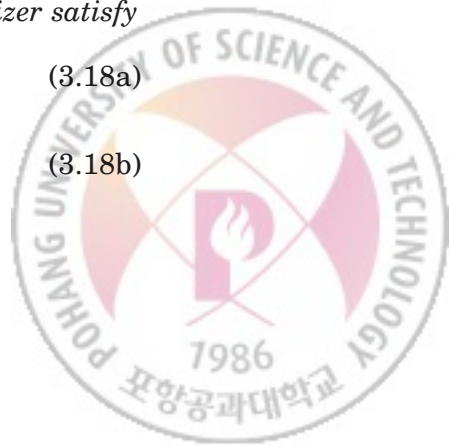
Now, the asymptotic second-order properties of the output  $y$  of the asymptotic FRESH properizer are examined as follows.

**Theorem 2** *If the input  $x$  to the asymptotic FRESH properizer with parameters  $M$  and  $N$  is obtained by taking the  $MN$  consecutive samples from an SOCS random process with cycle period  $M$ , then the covariance and the complementary covariance matrices of the output  $y$  of the asymptotic FRESH properizer satisfy*

$$R_y \sim W_{MN}^H \Sigma W_{MN} \quad (3.18a)$$

and

$$\tilde{R}_y \sim O_{MN}, \quad (3.18b)$$



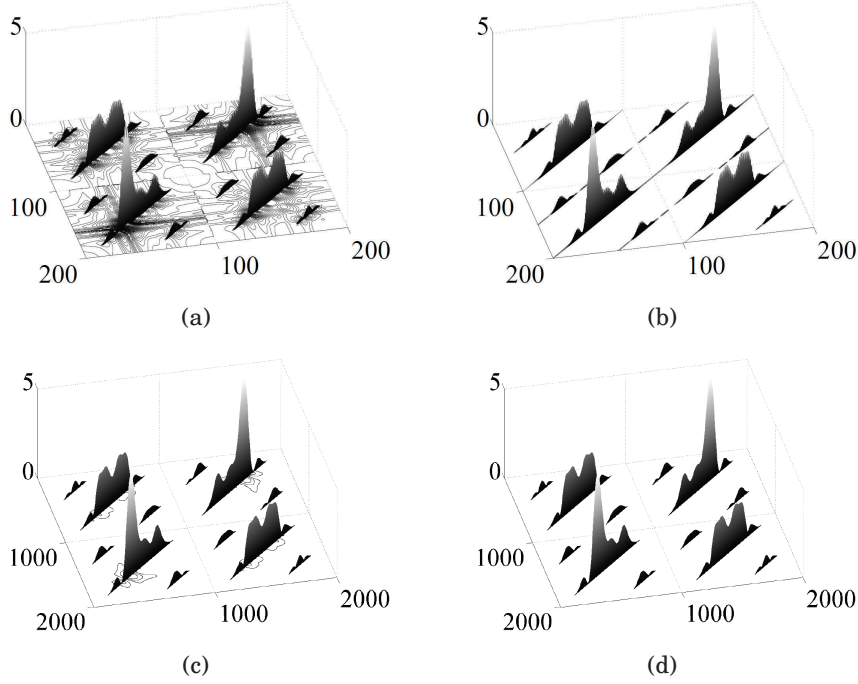


**Fig. 3.5** Magnitudes of exemplary (a)  $\bar{W}_{MN} \tilde{R}_x \bar{W}_{MN}^T$  for  $N = 50$ , (b)  $\tilde{\Omega}$  for  $N = 50$ , (c)  $\bar{W}_{MN} \tilde{R}_x \bar{W}_{MN}^T$  for  $N = 500$ , and (d)  $\tilde{\Omega}$  for  $N = 500$ , when  $M = 2$ .

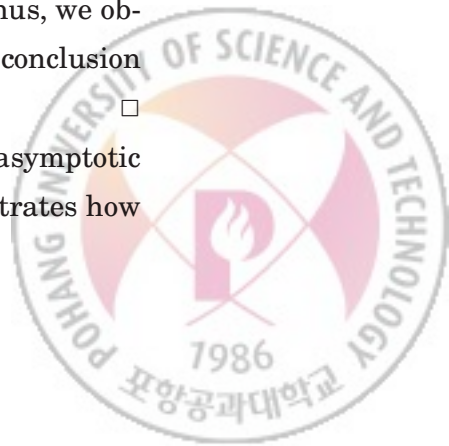
where an  $(MN)$ -by- $(MN)$  matrix  $\Sigma$  is given by

$$\Sigma \triangleq \bar{G}_{M,N} \Omega \bar{G}_{M,N}^H \quad (3.19a)$$

$$= R_{\hat{y}} \odot (1_{2M} \otimes I_{N/2}). \quad (3.19b)$$

*Proof:* By applying Lemmas 8 and 9 to (3.13a) and (3.15a), we obtain  $R_{\hat{y}} \sim \bar{G}_{M,N} \Omega \bar{G}_{M,N}^H$ . Since  $\bar{G}_{M,N} \Omega \bar{G}_{M,N}^H$  can be rewritten as  $(\bar{G}_{M,N} \bar{W}_{MN} \tilde{R}_x \bar{W}_{MN}^H \bar{G}_{M,N}^H) \odot (\bar{G}_{M,N} (1_{2M} \otimes I_N) \bar{G}_{M,N}^H)$  by the definition (3.16a), we obtain  $R_{\hat{y}} \sim \Sigma$  from  $\bar{G}_{M,N} (1_{2M} \otimes I_N) \bar{G}_{M,N}^H = 1_{2M} \otimes I_{N/2}$ . Similarly,  $\tilde{R}_{\hat{y}} \sim (\bar{G}_{M,N} \bar{W}_{MN} \tilde{R}_x \bar{W}_{MN}^T \bar{G}_{M,N}^T) \odot (\bar{G}_{M,N} (1_{2M} \otimes P_N) \bar{G}_{M,N}^T)$  by (3.13b), (3.15b), and (3.16b). Thus, we obtain  $\tilde{R}_{\hat{y}} \sim O_{MN}$  from  $\bar{G}_{M,N} (1_{2M} \otimes P_N) \bar{G}_{M,N}^T = O_{MN}$ . Therefore, the conclusion follows by Lemma 8.  $\square$

By Definition 21 and the above theorem, the output  $y$  of the asymptotic FRESH properizer is indeed asymptotically proper. Fig. 3.6-(a) illustrates how



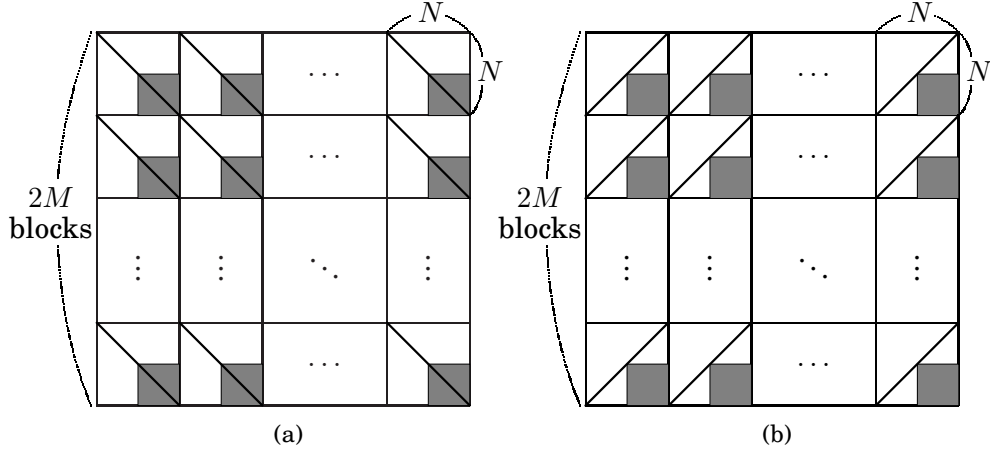
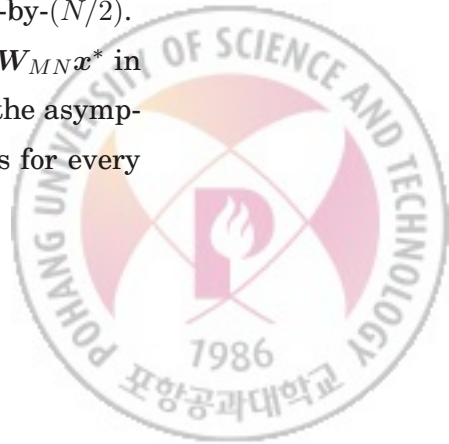


**Fig. 3.6** Illustrations that show how to construct (a)  $R_{\hat{y}}$  and (b)  $\tilde{R}_{\hat{y}}$  from  $\bar{W}_{MN} R_{\bar{x}} \bar{W}_{MN}^H \sim \Omega$  and  $\bar{W}_{MN} \tilde{R}_{\bar{x}} \bar{W}_{MN}^T \sim \tilde{\Omega}$ , respectively. Thick diagonal and anti-diagonal lines represent all possible non-zero entries of  $\Omega$  and  $\tilde{\Omega}$ , respectively.

the frequency-domain covariance matrix  $R_{\hat{y}}$  of the output  $y$  of the asymptotic FRESH properizer is constructed from  $\bar{W}_{MN} R_{\bar{x}} \bar{W}_{MN}^H$ . The thick diagonal lines in each block of size  $N$ -by- $N$  represent all possible non-zero entries of  $\Omega$  that is asymptotically equivalent to  $\bar{W}_{MN} R_{\bar{x}} \bar{W}_{MN}^H$ . Then,  $R_{\hat{y}}$  that is asymptotically equivalent to  $\Sigma$  is obtained by collecting the shaded sub-blocks of size  $(N/2)$ -by- $(N/2)$ . Fig. 3.6-(b) illustrates how the frequency-domain complementary covariance matrix  $\tilde{R}_{\hat{y}}$  of the output  $y$  of the asymptotic FRESH properizer is constructed from  $\bar{W}_{MN} \tilde{R}_{\bar{x}} \bar{W}_{MN}^T$ . The thick anti-diagonal lines in each block of size  $N$ -by- $N$  represent all possible non-zero entries of  $\tilde{\Omega}$  that is asymptotically equivalent to  $\bar{W}_{MN} \tilde{R}_{\bar{x}} \bar{W}_{MN}^T$ . Then,  $\tilde{R}_{\hat{y}}$  that is asymptotically equivalent to  $O_{MN}$  is obtained by collecting the shaded sub-blocks of size  $(N/2)$ -by- $(N/2)$ .

It is already shown that the amount of the circular shift of  $G_{M,N} W_{MN} x^*$  in (3.6) can be any  $N(2k+1)/2$ , for  $k \in \mathbb{Z}$ , to satisfy the invertibility of the asymptotic FRESH properizer. It can be also shown that Theorem 2 holds for every





circular shift by  $N(2k + 1)/2$ , for  $k \in \mathbb{Z}$ . Moreover, since  $R_x$  and  $\tilde{R}_x$  that are  $(MN)$ -by- $(MN)$  block Toeplitz matrices with block size  $M$ -by- $M$  can be viewed as block Toeplitz matrices with block size  $(lM)$ -by- $(lM)$ ,  $\forall l \in \mathbb{N}$ , the sampled vector  $x$  can be asymptotically properized by using any parameters  $lM$  and  $N/l$ , for all  $l \in \mathbb{N}$  such that  $N/l$  is even. Thus, similar to the DT FRESH properizer, it is not unique to asymptotically properize a finite number of consecutive samples of a zero-mean SOCS random process with cycle period  $M$ .

In the following two sections, two representative estimation and detection problems are presented to demonstrate that low-complexity asymptotically optimal post-processors can be easily designed by exploiting the asymptotic second-order properties of the output of the asymptotic FRESH properizer.

### **3.3 Application of Asymptotic FRESH Properizer to Signal Estimation Problem**

In this section, given a finite number of consecutive samples of a zero-mean improper-complex SOCS random process in additive proper-complex white noise, the minimum mean squared error estimation of the random process is considered when only the second-order statistics of the observation vector are provided. It is well known [18] that an optimal estimator is the WLMMSE estimator that linearly processes the observation vector augmented by its complex conjugate. This optimality of the use of the augmented vector still holds even if the output of the asymptotic FRESH properizer is processed, because the output as an equivalent observation vector is still improper. Instead, motivated by Theorem 2, we propose to use the LMMSE estimator that processes the output of the asymptotic FRESH properizer as if the signal component is a proper-complex random vector with its frequency-domain covariance matrix being equal to the masked version of the exact frequency-domain covariance matrix. It turns out that this suboptimal linear estimator is asymptotically optimal in the sense that the difference of its average MSE performance from that





of the WLMSE estimator having higher computational complexity converges to zero as the number of samples tends to infinity.

### 3.3.1 Asymptotically Optimal Low-Complexity Estimator

Let  $\mathbf{r}$  be the length- $MN$  observation vector modeled by

$$\mathbf{r} = \mathbf{x} + \mathbf{v}, \quad (3.20)$$

where  $\mathbf{x}$  is the desired signal to be estimated that consists of the  $MN$  consecutive samples of a zero-mean improper-complex SOCS random process with cycle period  $M \in \mathbb{N}$ , and  $\mathbf{v}$  is the additive proper-complex white noise vector.

Given the observation model (3.20) with the first- and second-order moments  $\mathbb{E}\{\mathbf{x}\} = \mathbf{0}_{MN}$ ,  $\mathbb{E}\{\mathbf{x}\mathbf{x}^H\} = \mathbf{R}_x$ ,  $\mathbb{E}\{\mathbf{x}\mathbf{x}^T\} = \tilde{\mathbf{R}}_x$ ,  $\mathbb{E}\{\mathbf{v}\} = \mathbf{0}_{MN}$ ,  $\mathbb{E}\{\mathbf{v}\mathbf{v}^H\} = \sigma^2 \mathbf{I}_{MN}$ , and  $\mathbb{E}\{\mathbf{v}\mathbf{v}^T\} = \mathbf{O}_{MN}$  of  $\mathbf{x}$  and  $\mathbf{v}$ , the WLMSE estimation problem can be formulated as

$$\begin{aligned} & \underset{\mathbf{x}_{\text{wl}}}{\text{minimize}} && \varepsilon^{(N)} \\ & \text{subject to} && \mathbf{x}_{\text{wl}} = \mathbf{F}_1 \mathbf{r} + \mathbf{F}_2 \mathbf{r}^*, \end{aligned} \quad (3.21)$$

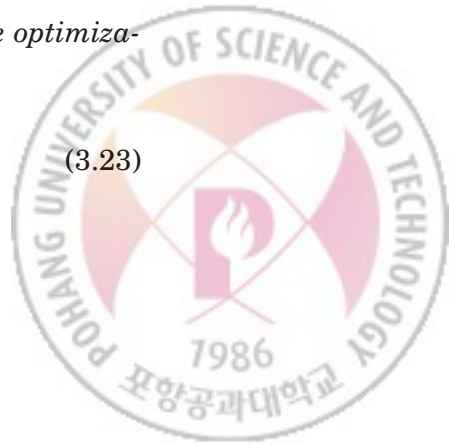
where the average MSE  $\varepsilon^{(N)}$  is defined as

$$\varepsilon^{(N)} \triangleq \frac{1}{MN} \mathbb{E}\{\|\mathbf{x} - \mathbf{x}_{\text{wl}}\|^2\}. \quad (3.22)$$

In the following lemma, the optimal solution to the above estimation problem is provided along with its average MSE performance. It is well known [18] that the optimal estimator that minimizes the average MSE without the wide linearity constraint becomes this WLMSE estimator if the desired signal vector and the additive noise vector are both Gaussian.

**Lemma 10** *The WLMSE estimator  $\mathbf{x}_{\text{opt}}$  of  $\mathbf{x}$  as the solution to the optimization problem (3.21) is given by*

$$\mathbf{x}_{\text{opt}} = \mathbf{F}_{1,\text{opt}} \mathbf{r} + \mathbf{F}_{2,\text{opt}} \mathbf{r}^* \quad (3.23)$$



where

$$\mathbf{F}_{1,\text{opt}} \triangleq (\mathbf{R}_x - \tilde{\mathbf{R}}_x \mathbf{R}_r^{-1*} \tilde{\mathbf{R}}_x^*)(\mathbf{R}_r - \tilde{\mathbf{R}}_x \mathbf{R}_r^{-1*} \tilde{\mathbf{R}}_x^*)^{-1} \quad (3.24a)$$

and

$$\mathbf{F}_{2,\text{opt}} \triangleq (\tilde{\mathbf{R}}_x - \mathbf{R}_x \mathbf{R}_r^{-1} \tilde{\mathbf{R}}_x)(\mathbf{R}_r^* - \tilde{\mathbf{R}}_x^* \mathbf{R}_r^{-1} \tilde{\mathbf{R}}_x)^{-1}. \quad (3.24b)$$

with  $\mathbf{R}_r \triangleq \mathbb{E}\{\mathbf{r}\mathbf{r}^H\} = \sigma^2 \mathbf{I}_{MN} + \mathbf{R}_x$ . Moreover, the average MSE  $\varepsilon_{\text{opt}}^{(N)} \triangleq \mathbb{E}\{\|\mathbf{x} - \mathbf{x}_{\text{opt}}\|^2\}/(MN)$  is given by

$$\varepsilon_{\text{opt}}^{(N)} = \frac{1}{MN} \text{tr}(\mathbf{R}_x - \mathbf{F}_{1,\text{opt}} \mathbf{R}_x - \mathbf{F}_{2,\text{opt}} \tilde{\mathbf{R}}_x^*). \quad (3.25)$$

*Proof:* See [18, Section 5.4] and the references therein.  $\square$

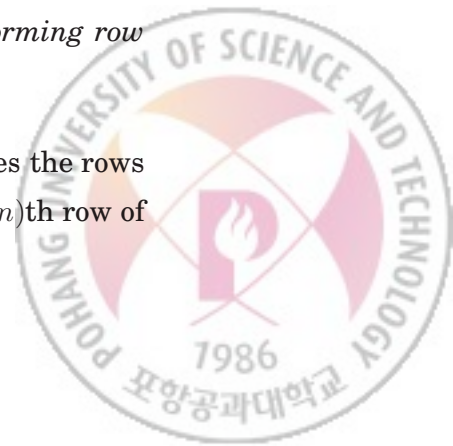
Apparently, the WLMSE estimator in (3.23) requires the computation of two matrices  $\mathbf{F}_{1,\text{opt}}$  and  $\mathbf{F}_{2,\text{opt}}$  to be pre-multiplied to  $\mathbf{r}$  and  $\mathbf{r}^*$ , respectively. In this brute-force approach, as it can be seen from (3.24a) and (3.24b), the major burden in computing these matrices comes from the multiplications and the inversions of  $(MN)$ -by- $(MN)$  matrices, which require  $\mathcal{O}(M^3 N^3)$  complex-valued scalar multiplications. Instead, we may take an alternative approach to reduce the computational complexity. Similar to  $\bar{\mathbf{x}}$  in (3.10), let  $\bar{\mathbf{r}}$  be the augmented observation vector of  $\mathbf{r}$ . Then, it can be shown [18, Result 5.3] that  $\mathbf{x}_{\text{opt}}$  given by (3.23) is identical to the upper  $MN$  elements of the LMMSE estimate

$$\mathbf{R}_{\bar{\mathbf{x}}} (\sigma^2 \mathbf{I}_{2MN} + \mathbf{R}_{\bar{\mathbf{x}}})^{-1} \bar{\mathbf{r}} \quad (3.26)$$

of  $\bar{\mathbf{x}}$ , where  $\mathbf{R}_{\bar{\mathbf{x}}}$  denotes the covariance matrix of  $\bar{\mathbf{x}}$ . Now, the following lemma enables us to reduce the complexity in computing  $\mathbf{x}_{\text{opt}}$  to  $\mathcal{O}(M^3 N^2)$ .

**Lemma 11** *The covariance matrix  $\mathbf{R}_{\bar{\mathbf{x}}}$  of  $\bar{\mathbf{x}}$  can be converted into a  $(2MN)$ -by- $(2MN)$  block Toeplitz matrix with block size  $(2M)$ -by- $(2M)$  by performing row and column permutations.*

*Proof:* Let  $\mathbf{E}_{2,MN}$  be the  $(2MN)$ -by- $(2MN)$  matrix that permutes the rows of the post-multiplied matrix in such a way that the  $(MN(m-1) + n)$ th row of



the post-multiplied matrix becomes the  $(2(n-1) + m)$ th row, for  $m = 1, 2$  and  $n = 1, 2, \dots, MN$ . Since  $\mathbf{x}$  consists of  $MN$  consecutive samples of a zero-mean SOCS random process  $X[n]$  with cycle period  $M$ , if this invertible operator is used to rearrange the order of the augmented vector  $\bar{\mathbf{x}}$  defined in (3.10), then we have

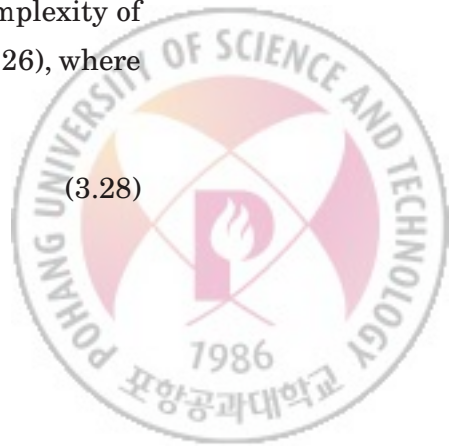
$$\mathbf{E}_{2,MN}\bar{\mathbf{x}} = \begin{bmatrix} [\mathbf{x}]_1 & [\mathbf{x}]_1^* & [\mathbf{x}]_2 & [\mathbf{x}]_2^* & \cdots & [\mathbf{x}]_{MN} & [\mathbf{x}]_{MN}^* \end{bmatrix}^T. \quad (3.27)$$

Note that this is nothing but the vector consisting of  $2MN$  consecutive samples of the random process  $\bar{X}[n]$  defined by using  $X[n]$  as  $\bar{X}[2n] \triangleq X[n]$  and  $\bar{X}[2n+1] \triangleq X[n]^*$  for all  $n$ . It can be straightforwardly shown that  $\bar{X}[n]$  is a zero-mean SOCS random process with cycle period  $2M$ , which implies that  $r_{\bar{X}}[n, m] \triangleq \mathbb{E}\{\bar{X}[n]\bar{X}[m]^*\} = r_X[n+2M, m+2M], \forall m, \forall n$ . Therefore, the conclusion follows.  $\square$

The above lemma combined with the computationally efficient inversion technique in [46] for a block Toeplitz matrix enables us to perform the inversion of  $(\sigma^2 \mathbf{I}_{2MN} + \mathbf{R}_{\bar{\mathbf{x}}})$  in (3.26) now only with  $\mathcal{O}(M^3 N^2)$  complex-valued scalar multiplications. Also, the matrix-vector multiplications  $(\sigma^2 \mathbf{I}_{2MN} + \mathbf{R}_{\bar{\mathbf{x}}})^{-1} \bar{\mathbf{r}}$  and  $\mathbf{R}_{\bar{\mathbf{x}}} \{(\sigma^2 \mathbf{I}_{2MN} + \mathbf{R}_{\bar{\mathbf{x}}})^{-1} \bar{\mathbf{r}}\}$  in (3.26) require only  $\mathcal{O}(M^2 N^2)$  complex-valued scalar multiplications. Therefore, the overall computational complexity of the WLMMSE estimator is  $\mathcal{O}(M^3 N^2)$ .

The WLMMSE estimator can be realized also in the frequency domain. Note, however, that the computational complexity does not decrease. Of course, the frequency-domain conversion of the observation vector requires only  $\mathcal{O}(MN \log(MN))$  of computational complexity when the fast Fourier transform (FFT) is used. It can be shown that the brute-force approach based on (3.23) to the frequency-domain estimation requires the overall computational complexity of  $\mathcal{O}(M^3 N^3)$ . Instead, we may take an alternative approach based on (3.26), where the LMMSE estimate of  $\bar{\mathbf{W}}_{MN} \bar{\mathbf{x}}$  is given by

$$\bar{\mathbf{W}}_{MN} \mathbf{R}_{\bar{\mathbf{x}}} \bar{\mathbf{W}}_{MN}^H (\sigma^2 \mathbf{I}_{2MN} + \bar{\mathbf{W}}_{MN} \mathbf{R}_{\bar{\mathbf{x}}} \bar{\mathbf{W}}_{MN}^H)^{-1} \bar{\mathbf{W}}_{MN} \bar{\mathbf{r}}. \quad (3.28)$$



However, it involves the inversion of a matrix that is not highly structured, which leads to the overall computational complexity of the frequency-domain approach using  $\bar{W}_{MN}\bar{r}$  no better than the time-domain approach using  $\bar{r}$ .

An alternative observation model that is equivalent to the original one in (3.20) can be obtained by applying the asymptotic FRESH properization to  $r$  as

$$s = y + w, \quad (3.29)$$

where  $s = f(r)$ ,  $y = f(x)$ , and  $w = f(v)$ . Since the equivalent observation vector  $s$  is not proper in general, the linear processing of  $s$  and  $s^*$  is still needed for the second-order optimal estimation of  $x$ . Instead, we propose to use a suboptimal linear estimator as follows, which is a function only of  $s$ .

**Definition 22** *The proposed estimate  $x_p$  of  $x$  is defined by*

$$x_p = f^{-1}(F_p s), \quad (3.30)$$

where  $F_p$  is given by

$$F_p \triangleq W_{MN}^H \Sigma (\sigma^2 I_{MN} + \Sigma)^{-1} W_{MN}. \quad (3.31)$$

Note from (3.30) and (3.31) that  $\Sigma(\sigma^2 I_{MN} + \Sigma)^{-1} W_{MN} s$  is the estimate of  $W_{MN} y = W_{MN} f(x)$  and, consequently, that  $F_p s$  is the estimate of  $y = f(x)$ . Let  $y_p \triangleq F_p s$ . Then, the estimate  $x_p$  of  $x = f^{-1}(y)$  is obtained as (3.30) by applying the inverse operation  $f^{-1}$  to  $y_p$ .

It can be immediately seen that  $F_p$  is chosen to make  $y_p$  the LMMSE estimate of  $y$  when the covariance and the complementary covariance matrices of  $y$  are set equal to  $W_{MN}^H \Sigma W_{MN}$  and  $O_{MN}$  appearing in (3.18a) and (3.18b), respectively. This idea of using the asymptotically equivalent matrices is motivated by Theorem 2, which naturally leads to the asymptotic optimality of the proposed estimator as shown in what follows.

First, the invariance of the Euclidean norm under the asymptotic FRESH properization is shown.



**Lemma 12** *The input  $x$  and the output  $y = f(x)$  of the asymptotic FRESH properizer have the same Euclidean norm, i.e.,  $\|x\| = \|y\|$ .*

*Proof:* Since the centered DFT matrix  $W_{MN}$  is unitary, we have  $\|x\| = \|W_{MN}x\|$ . Let  $y_l$  and  $y'_l$  denote the  $l$ th entries of  $y$  and  $W_{MN}x$ , respectively. Then, we have  $\|W_{MN}x\|^2 = \sum_{l=1}^{MN} |y'_l|^2 = \sum_{l=1}^{MN} |y_l|^2 = \|y\|^2$  by Definition 19 of  $f(x)$  in (3.8), which is illustrated in Fig. 3.3. Therefore, the conclusion follows.  $\square$

Second, the average MSE of the proposed estimator is derived.

**Lemma 13** *The average MSE  $\varepsilon_p^{(N)} \triangleq \mathbb{E}\{\|x - x_p\|^2\}/(MN)$  of the proposed estimator is given by*

$$\varepsilon_p^{(N)} = \frac{1}{MN} \text{tr}\{\Sigma - \Sigma(\sigma^2 I_{MN} + \Sigma)^{-1} \Sigma\}. \quad (3.32)$$

*Proof:* The linearity of the asymptotic FRESH properizer leads to  $y - y_p = f(x - x_p)$ . Then, by Lemma 12, the average MSE performance can be written as  $\varepsilon_p^{(N)} = \mathbb{E}\{\|y - y_p\|^2\}/(MN)$ . Since  $W_{MN}$  is unitary and  $y_p = F_p s$ , it can be shown that we have

$$\begin{aligned} \varepsilon_p^{(N)} &= \frac{1}{MN} \text{tr}\{R_{\hat{y}} - 2\Sigma(\sigma^2 I_{MN} + \Sigma)^{-1} R_{\hat{y}} \\ &\quad + \Sigma(\sigma^2 I_{MN} + \Sigma)^{-1} (\sigma^2 I_{MN} + R_{\hat{y}}) (\sigma^2 I_{MN} + \Sigma)^{-1} \Sigma\}. \end{aligned} \quad (3.33)$$

It can be also shown that if  $\tilde{A} \triangleq A \odot (1_{2M} \otimes I_{N/2})$  and  $\tilde{B} \triangleq B \odot (1_{2M} \otimes I_{N/2})$  for  $(MN)$ -by- $(MN)$  matrices  $A$  and  $B$  then  $\text{tr}(A) = \text{tr}(\tilde{A})$  and  $\text{tr}(\tilde{A}\tilde{B}) = \text{tr}(\tilde{A}\tilde{B})$ . Thus, the right side of (3.33) is invariant under replacing  $R_{\hat{y}}$  with  $\Sigma = R_{\hat{y}} \odot (1_{2M} \otimes I_{N/2})$  in (3.19b). Therefore, (3.33) can be simplified to (3.32).  $\square$

Now, the asymptotic optimality of the proposed estimator is provided.

**Theorem 3** *The average MSE of the proposed estimator approaches that of the WLM MSE estimator as the number of samples tends to infinity in the sense that*

$$\lim_{N \rightarrow \infty} (\varepsilon_p^{(N)} - \varepsilon_{\text{opt}}^{(N)}) = 0. \quad (3.34)$$



*Proof:* It is shown in [18, Section 5.4] that the average MSE  $\varepsilon_{\text{opt}}^{(N)}$  in (3.25) of the WMMSE estimator can be simplified as

$$\varepsilon_{\text{opt}}^{(N)} = \frac{1}{2MN} \text{tr}\{\mathbf{R}_{\bar{x}} - \mathbf{R}_{\bar{x}}(\sigma^2 \mathbf{I}_{2MN} + \mathbf{R}_{\bar{x}})^{-1} \mathbf{R}_{\bar{x}}\}. \quad (3.35)$$

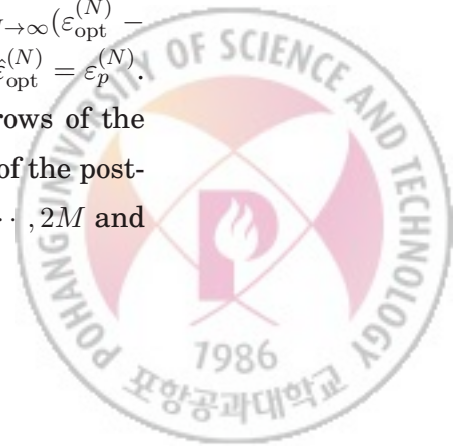
Now, we define  $\hat{\Omega} \triangleq \bar{\mathbf{W}}_{MN}^H \Omega \bar{\mathbf{W}}_{MN}$  and introduce

$$\hat{\varepsilon}_{\text{opt}}^{(N)} \triangleq \frac{1}{2MN} \text{tr}\{\hat{\Omega} - \hat{\Omega}(\sigma^2 \mathbf{I}_{2MN} + \hat{\Omega})^{-1} \hat{\Omega}\} \quad (3.36a)$$

$$= \frac{1}{2MN} \text{tr}\{\Omega - \Omega(\sigma^2 \mathbf{I}_{2MN} + \Omega)^{-1} \Omega\}, \quad (3.36b)$$

which is obtained by replacing  $\mathbf{R}_{\bar{x}}$  in (3.35) with  $\hat{\Omega}$  and by using the fact that  $\bar{\mathbf{W}}_{MN}$  is unitary. Note that  $\bar{\mathbf{W}}_{MN} \mathbf{R}_{\bar{x}} \bar{\mathbf{W}}_{MN}^H \sim \Omega$  as shown in (3.15a). This introduction of  $\hat{\varepsilon}_{\text{opt}}^{(N)}$  is motivated by the result in [43, Theorem 1], where a sub-optimal estimator is proposed for the estimation of a proper-complex cyclostationary random signal and its average MSE is shown to approach that of the LMMSE estimator as the number of samples tends to infinity. Since  $\mathbf{R}_{\bar{x}}$  is a covariance matrix, it is positive semidefinite, which implies that all the eigenvalues of  $(\sigma^2 \mathbf{I}_{2MN} + \mathbf{R}_{\bar{x}})^{-1}$  in (3.35) are upper bounded by  $1/\sigma^2$ . Note that  $\Omega$  and  $\hat{\Omega}$  are also positive semidefinite because  $(\mathbf{1}_{2M} \otimes \mathbf{I}_{N/2})$  in (3.16a) is positive semidefinite. Similarly, all the eigenvalues of  $(\sigma^2 \mathbf{I}_{2MN} + \hat{\Omega})^{-1}$  in (3.36a) are also upper bounded by  $1/\sigma^2$ . Thus, the strong norms  $\|(\sigma^2 \mathbf{I}_{2MN} + \mathbf{R}_{\bar{x}})^{-1}\|$  and  $\|(\sigma^2 \mathbf{I}_{2MN} + \hat{\Omega})^{-1}\|$  are uniformly upper bounded by  $1/\sigma^2$  for any matrix size. Recall that if  $\mathbf{A}_k \sim \mathbf{B}_k$  and  $\|\mathbf{A}_k^{-1}\|, \|\mathbf{B}_k^{-1}\| \leq c < \infty, \forall k$ , for a positive constant  $c$ , then  $\mathbf{A}_k^{-1} \sim \mathbf{B}_k^{-1}$  [42, Theorem 1-(4)]. Thus, we have  $(\sigma^2 \mathbf{I}_{2MN} + \mathbf{R}_{\bar{x}})^{-1} \sim (\sigma^2 \mathbf{I}_{2MN} + \hat{\Omega})^{-1}$ . Recall also that if two sequences  $(\mathbf{A}_k)_k$  and  $(\mathbf{B}_k)_k$  of  $N_k$ -by- $N_k$  matrices are asymptotically equivalent then  $\lim_{k \rightarrow \infty} \text{tr}(\mathbf{A}_k - \mathbf{B}_k)/N_k = 0$  [42, Corollary 1]. Thus, combined with Lemmas 8 and 9, we have  $\lim_{N \rightarrow \infty} (\varepsilon_{\text{opt}}^{(N)} - \hat{\varepsilon}_{\text{opt}}^{(N)}) = 0$ . Therefore, in order to show (3.34), it now suffices to show  $\hat{\varepsilon}_{\text{opt}}^{(N)} = \varepsilon_p^{(N)}$ .

Let  $\mathbf{E}_{2M,N}$  be the  $(2MN)$ -by- $(2MN)$  matrix that permutes the rows of the post-multiplied matrix in such a way that the  $(N(m-1) + n)$ th row of the post-multiplied matrix becomes the  $(2M(n-1) + m)$ th row for  $m = 1, 2, \dots, 2M$  and



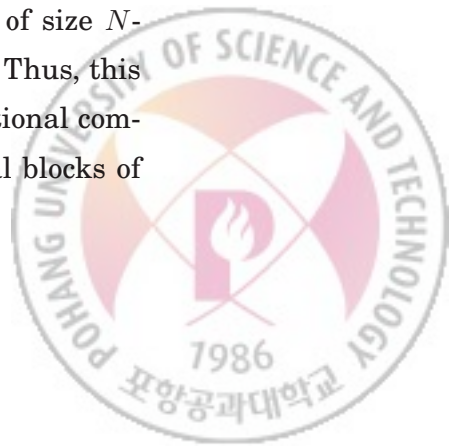


$n = 1, 2, \dots, N$ , i.e., the rows having indexes  $(N(m-1)+n)$ , for  $m = 1, 2, \dots, 2M$ , are grouped for each  $n$ . Then,  $\mathbf{E}_{2M,N} \mathbf{\Omega} \mathbf{E}_{2M,N}^T$  is a  $(2MN)$ -by- $(2MN)$  block diagonal matrix with block size  $(2M)$ -by- $(2M)$ , because  $\mathbf{\Omega}$  is a  $(2MN)$ -by- $(2MN)$  block matrix with diagonal blocks of block size  $N$ -by- $N$ . Similarly, the  $(MN)$ -by- $(MN)$  matrix  $\mathbf{E}_{2M,N/2}$  is defined. Let  $\mathbf{E}_1$  and  $\mathbf{E}_2$  be the  $(MN)$ -by- $(MN)$  matrix that are defined as  $\mathbf{E}_1 \triangleq \mathbf{P}_{MN}(\mathbf{I}_{N/2} \otimes \hat{\mathbf{E}}_{2M})\mathbf{E}_{2M,N/2}$  and  $\mathbf{E}_2 \triangleq (\mathbf{I}_{N/2} \otimes \hat{\mathbf{E}}_{2M})\mathbf{E}_{2M,N/2}$ , respectively, where the  $(2M)$ -by- $(2M)$  matrix  $\hat{\mathbf{E}}_{2M}$  permutes the rows of the post-multiplied matrix in such a way that the  $(2m)$ th row becomes the  $m$ th row and that the  $(2m-1)$ th row becomes the  $(M+m)$ th row for  $m = 1, 2, \dots, M$ . Then, the definition  $\mathbf{\Sigma} \triangleq \tilde{\mathbf{G}}_{M,N} \mathbf{\Omega} \tilde{\mathbf{G}}_{M,N}^H$  in (3.19a) leads to

$$\mathbf{E}_{2M,N} \mathbf{\Omega} \mathbf{E}_{2M,N}^T = \begin{bmatrix} \mathbf{E}_1 \mathbf{\Sigma}^* \mathbf{E}_1^T & \mathbf{O}_{MN} \\ \mathbf{O}_{MN} & \mathbf{E}_2 \mathbf{\Sigma} \mathbf{E}_2^T \end{bmatrix}. \quad (3.37)$$

Since  $\mathbf{E}_{2M,N}$ ,  $\mathbf{E}_1$ , and  $\mathbf{E}_2$  are all permutation matrices,  $\hat{\varepsilon}_{\text{opt}}^{(N)}$  in (3.36a) can be rewritten as  $\hat{\varepsilon}_{\text{opt}}^{(N)} = \text{tr}\{\mathbf{\Sigma}^* - \mathbf{\Sigma}^*(\sigma^2 \mathbf{I}_{2MN} + \mathbf{\Sigma}^*)^{-1} \mathbf{\Sigma}^* + \mathbf{\Sigma} - \mathbf{\Sigma}(\sigma^2 \mathbf{I}_{2MN} + \mathbf{\Sigma})^{-1} \mathbf{\Sigma}\} / (2MN)$ , which leads to  $\hat{\varepsilon}_{\text{opt}}^{(N)} = \varepsilon_p^{(N)}$  because  $\mathbf{\Sigma}$  is Hermitian symmetric. Therefore, the conclusion follows.  $\square$

The proposed estimator requires the pre-processing of  $\mathbf{r}$  to obtain  $\mathbf{s}$ , the computation and the multiplication of  $\mathbf{F}_p$ , and the inverse operation on  $\mathbf{y}_p$  to obtain  $\mathbf{x}_p$ . As it can be seen from (3.8) and (3.9), the major burden in the asymptotic FRESH properization and its inverse operation comes from the multiplications of the  $(MN)$ -by- $(MN)$  centered DFT matrix. This can be efficiently implemented with only  $\mathcal{O}(MN \log(MN))$  complex-valued scalar multiplications by using, e.g., the fast algorithm in [45]. As it can be seen from (3.31), the major burden in computing  $\mathbf{F}_p$  comes from the inversion of  $(\sigma^2 \mathbf{I}_{2MN} + \mathbf{\Sigma})$ . The inversion of an  $(MN)$ -by- $(MN)$  block matrix with diagonal blocks of size  $N$ -by- $N$  requires  $\mathcal{O}(M^3 N)$  complex-valued scalar multiplications [43]. Thus, this inversion of  $(\sigma^2 \mathbf{I}_{2MN} + \mathbf{\Sigma})$  has the same order  $\mathcal{O}(M^3 N)$  of computational complexity because  $\mathbf{\Sigma}$  is an  $(MN)$ -by- $(MN)$  block matrix with diagonal blocks of size  $(N/2)$ -by- $(N/2)$ .





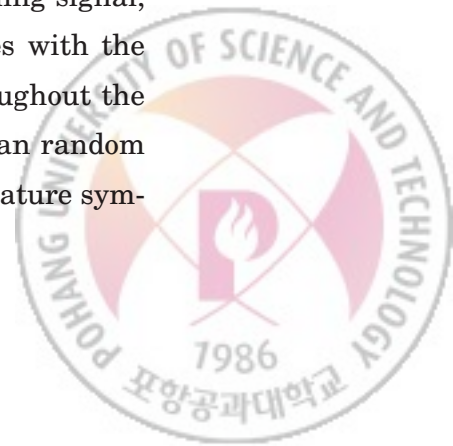
Since we consider the block processing where  $M$  is a fixed small number and  $N$  is much larger than  $M$ , the overall complexities of the WLMMSE and the proposed estimators as functions only of  $N$  can be rewritten now as  $\mathcal{O}(N^2)$  and  $\mathcal{O}(N \log N)$ , respectively. Thus, the computational complexity of the proposed estimator is much lower than that of the WLMMSE estimator. Though not major, an additional complexity reduction comes from the fact that the proposed estimator is linear that requires the computation and multiplication of one matrix  $F_p$  instead of two matrices  $F_{1,\text{opt}}$  and  $F_{2,\text{opt}}$ , all with  $MN(\gg 1)$  columns.

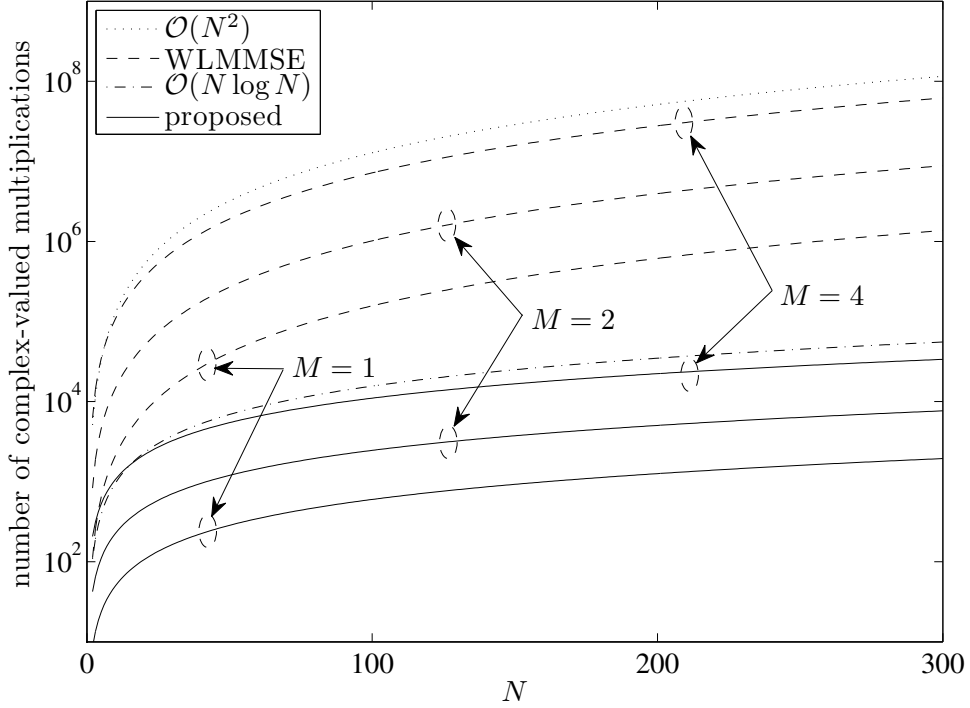
### 3.3.2 Numerical Results

In this subsection, numerical results are provided that show the computational efficiency and the asymptotic optimality of the proposed estimator.

The first result is to compare the complexity of the proposed estimator with that of the WLMMSE estimator. Fig. 3.7 shows that the number of complex-valued multiplications needed in computing the WLMMSE and the proposed estimators for cycle periods  $M = 1, 2$ , and 4. Recall that the computational complexities of the WLMMSE and the proposed estimators are  $\mathcal{O}(N^2)$  and  $\mathcal{O}(N \log N)$  for a fixed integer  $M$ , respectively. It can be seen from Fig. 3.7 that the computational complexity of the proposed estimator is much lower than that of the WLMMSE estimator. As predicted, the approximation motivated by Theorem 2 leads to this significant complexity reduction.

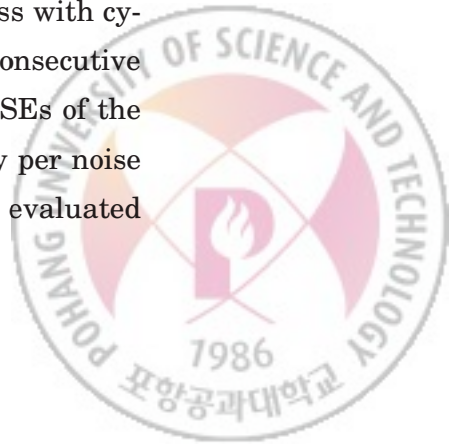
The second result is to show the asymptotic optimality of the proposed estimator. We consider the case where an improper-complex SOCS random process is obtained by uniformly sampling a CT zero-mean improper-complex SOCS random process. The CT random process is, e.g., a Gaussian jamming signal, generated by using two independent real-valued symbol sequences with the SRRC pulse having roll-off factor 0.22 and symbol rate  $1/T_s$ . Throughout the simulations, the data symbols are uncorrelated zero-mean Gaussian random variables with in-phase symbol variance being four-times the quadrature sym-





**Fig. 3.7** Computational complexities of the WMMSE and the proposed estimators.

bol variance. The frequency-selective channel is modeled by a tapped-delay line with impulse response  $h(t) = \sum_{k=1}^5 a_k \delta(t - \tau_k/2)$ , where the tap delay  $\tau_k$ 's are i.i.d. uniform random variables on  $\{0, T_s, 2T_s, \dots, 15T_s\}$  and the tap coefficient  $a_k$ 's are independent proper-complex zero-mean Gaussian random variables with variance  $\mathbb{E}\{|a_k|^2\} = e^{-\tau_k/(3T_s)}$ . The overall channel is then normalized to meet the signal to noise ratio used in the numerical result. The channel output is sampled at 2-times the symbol rate of the OQPSK symbols, which results in the DT zero-mean improper-complex SOCS random process with cycle period  $M = 2$ . Thus, the entries of  $x$  in (3.20) are the  $MN$  consecutive samples of the random process. Fig. 3.8 shows that the average MSEs of the WMMSE and the proposed estimators versus  $N$  for symbol energy per noise density  $E_s/N_0 = 0, 5$ , and  $10$  [dB], where the theoretical results are evaluated



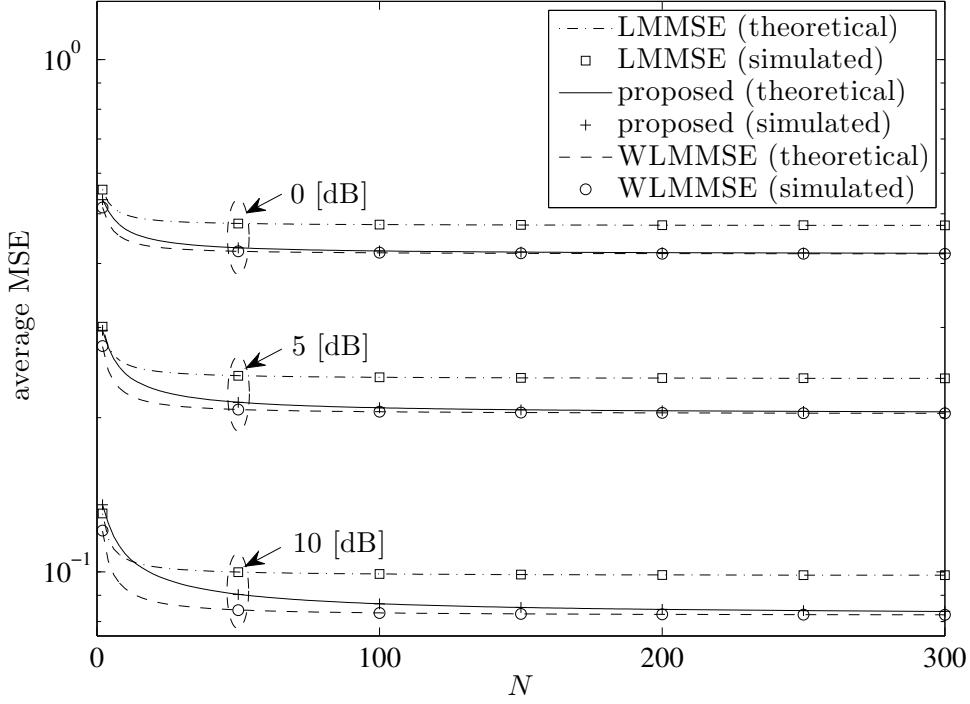


**Fig. 3.8** Average MSEs of the LMMSE, the WLMSE and the propose estimators.

by (3.25) and (3.32) while the simulated results are obtained from  $10^5$  Monte-Carlo runs. It can be seen that, as shown in Theorem 3, the average MSE of the proposed estimator approaches that of the WLMSE estimator as  $N$  increases. It can be also seen that the LMMSE estimator has higher average MSE than the proposed and the WLMSE estimators.

### 3.4 Application of Asymptotic FRESH Properizer to Signal Presence Detection Problem

In this section, again given a finite number of consecutive samples, now the signal presence detection of a zero-mean improper-complex SOCS Gaussian random process is considered in additive proper-complex white Gaussian



noise. It is well known [40] that the likelihood ratio is a sufficient statistic for all binary hypothesis tests under any optimality criterion. In [18], it is shown that the exact LRT statistic can be written as a quadratic function of the augmented observation vector when the improper-complex random process is *Gaussian*. Similar to the estimation problem in the previous section, this optimality of the use of the augmented vector still holds even if the output of the asymptotic FRESH properizer as an equivalent observation vector is processed. Again motivated by Theorem 2, we propose to use this equivalent observation vector of half the length of the augmented vector as if the signal component is a proper-complex random vector with its frequency-domain covariance matrix being equal to the masked version of the exact frequency-domain covariance matrix. It turns out that this suboptimal test statistic is asymptotically optimal in the sense that its difference from the exact LRT statistic having higher computational complexity converges to zero w.p. 1 as the number of samples tends to infinity.

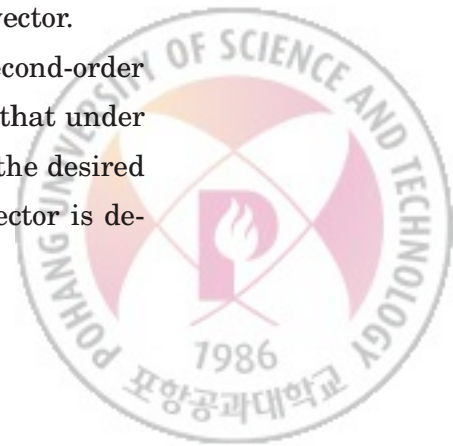
### **3.4.1 Asymptotically Optimal Low-Complexity Detector**

Let  $\mathbf{r}$  be the length- $MN$  observation vector modeled by

$$\begin{aligned} \mathcal{H}_0 : \quad \mathbf{r} &= \mathbf{v} \\ \text{versus} \\ \mathcal{H}_1 : \quad \mathbf{r} &= \mathbf{x} + \mathbf{v}, \end{aligned} \tag{3.38}$$

where  $\mathcal{H}_0$  and  $\mathcal{H}_1$  are the null and the alternative hypotheses, respectively. The desired signal  $\mathbf{x}$  to be detected consists of the  $MN$  consecutive samples of a zero-mean improper-complex SOCS Gaussian random process with cycle period  $M \in \mathbb{N}$ , and  $\mathbf{v}$  is the additive proper-complex white Gaussian noise vector.

Throughout this section, the definitions and the notations of the second-order statistics of  $\mathbf{x}$ ,  $\mathbf{v}$ , and  $\mathbf{r}$  follow those in the previous section except that under the null hypothesis the second-order statistic of  $\mathbf{r}$  does not contain the desired signal component. Similar to (3.10), the augmented observation vector is de-



noted by  $\bar{r}$ . Then, the LRT statistic of the observation vector  $r$  is provided as follows.

**Lemma 14** *Given the observation model (3.38), the LRT statistic is given by*

$$T_{\text{LRT}}^{(N)} = \frac{1}{2MN} \bar{r}^H \bar{R}_{\bar{x}} \bar{r}, \quad (3.39)$$

where  $\bar{R}_{\bar{x}} \triangleq \sigma^{-2} \mathbf{I}_{2MN} - (\sigma^2 \mathbf{I}_{2MN} + \mathbf{R}_{\bar{x}})^{-1}$ .

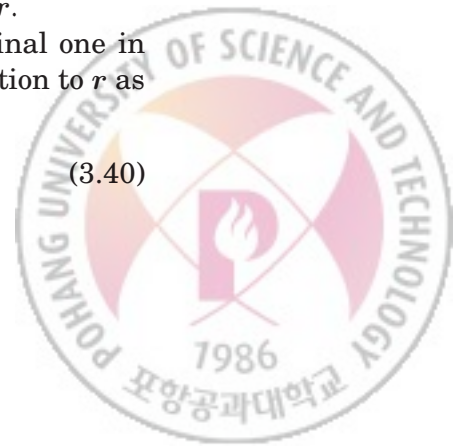
*Proof:* It is straightforward by using the probability density function (PDF) of the augmented improper-complex Gaussian random vector [47]. For details, see [18, Section 7.4].  $\square$

Note that, since the length- $MN$  observation vector  $r$  is improper and Gaussian, the LRT statistic  $T_{\text{LRT}}^{(N)}$  in (3.39) is a quadratic form of the length- $2MN$  augmented observation vector  $\bar{r}$ . Under any optimality criterion such as the Neyman-Pearson, the Bayesian, and the minimax criteria, the optimal detector computes  $T_{\text{LRT}}^{(N)}$ , compares it with an optimal threshold  $\eta$ , and then declares  $\mathcal{H}_1$  if  $T_{\text{LRT}}^{(N)} > \eta$  and  $\mathcal{H}_0$  otherwise.

The computation of  $T_{\text{LRT}}^{(N)}$  requires the matrix inversion of  $(\sigma^2 \mathbf{I}_{2MN} + \mathbf{R}_{\bar{x}})$ , which is the  $(2MN)$ -by- $(2MN)$  covariance matrix of the augmented observation vector  $\bar{r}$  under  $\mathcal{H}_1$ , and the matrix-vector multiplication. The major burden in computing  $T_{\text{LRT}}^{(N)}$  comes from the matrix inversion and it requires  $\mathcal{O}(M^3 N^2)$  complex-valued scalar multiplications when Lemma 11 is used. The matrix-vector multiplication requires only  $\mathcal{O}(M^2 N^2)$  complex-valued scalar multiplications. Thus, the overall computational complexity of the LRT statistic is  $\mathcal{O}(M^3 N^2)$ . Due to the same reason as the frequency-domain WLMMSE estimation in Section 3.3.1, the frequency-domain approach using  $\bar{W}_{MN} \bar{r}$  is no better in computational complexity than the time-domain approach using  $\bar{r}$ .

An alternative observation model that is equivalent to the original one in (3.38) can be obtained by applying the asymptotic FRESH properization to  $r$  as

$$\begin{aligned} \mathcal{H}_0 : & \quad s = w \\ \text{versus} & \\ \mathcal{H}_1 : & \quad s = y + w, \end{aligned} \quad (3.40)$$



where  $s = f(r)$ ,  $y = f(x)$ , and  $w = f(v)$ . Since the equivalent observation vector  $s$  is not proper in general, the augmentation of  $s$  and  $s^*$  is still needed to compute the exact LRT statistic of  $s$ . Instead, we propose to use a suboptimal LRT statistic as follows, which is a quadratic function only of  $s$ .

**Definition 23** *Given the observation model (3.40), the proposed test statistic of  $s$  is defined by*

$$T_p^{(N)} \triangleq \frac{1}{MN} s^H W_{MN}^H \bar{\Sigma} W_{MN} s, \quad (3.41)$$

where  $\bar{\Sigma} \triangleq \sigma^{-2} \mathbf{I}_{MN} - (\sigma^2 \mathbf{I}_{MN} + \Sigma)^{-1}$ .

It can be immediately seen that  $T_p^{(N)}$  can be viewed as the exact LRT statistic of  $s$  when the covariance and the complementary covariance matrices of  $y$  are set equal to  $W_{MN}^H \Sigma W_{MN}$  and  $O_{MN}$  appearing in (3.18a) and (3.18b), respectively. Similar to the estimation problem in the previous section, this idea of using the asymptotically equivalent matrices is again motivated by Theorem 2, which naturally leads to the asymptotic equivalence of the LRT statistic  $T_{\text{LRT}}^{(N)}$  in (3.39) and the proposed test statistic  $T_p^{(N)}$  in (3.41).

Now, the asymptotic optimality of the proposed test statistic is provided.

**Theorem 4** *The proposed test statistic approaches the exact LRT statistic as the number of samples tends to infinity in the sense that*

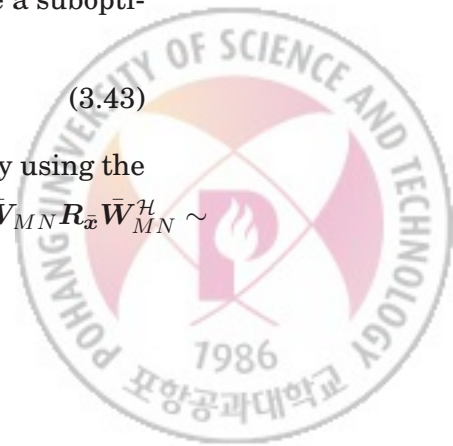
$$\lim_{N \rightarrow \infty} (T_p^{(N)} - T_{\text{LRT}}^{(N)}) = 0, w.p. 1, \quad (3.42)$$

under  $\mathcal{H}_0$  and  $\mathcal{H}_1$ .

*Proof:* We define  $\bar{\Omega} \triangleq \sigma^{-2} \mathbf{I}_{2MN} - (\sigma^2 \mathbf{I}_{2MN} + \Omega)^{-1}$  and introduce a suboptimal test statistic

$$\hat{T}_{\text{LRT}}^{(N)} \triangleq \frac{1}{2MN} \bar{r}^H \bar{W}_{MN}^H \bar{\Omega} \bar{W}_{MN} \bar{r}, \quad (3.43)$$

which is obtained by replacing  $\bar{R}_{\bar{x}}$  in (3.39) with  $\bar{W}_{MN}^H \bar{\Omega} \bar{W}_{MN}$  and by using the fact that  $\bar{W}_{MN}$  is unitary. This introduction of  $\hat{T}_{\text{LRT}}^{(N)}$  is motivated by  $\bar{W}_{MN} R_{\bar{x}} \bar{W}_{MN}^H \sim$





$\Omega$  in (3.15a). Similar to the proof of Theorem 3, it can be shown that  $\bar{\mathbf{R}}_{\bar{x}} \sim \bar{\mathbf{W}}_{MN}^{\mathcal{H}} \bar{\Omega} \bar{\mathbf{W}}_{MN}$ . In [48], the LRT problems are considered where the covariance matrix of a proper-complex Gaussian signal vector is either Toeplitz or block Toeplitz. It is shown under both  $\mathcal{H}_0$  and  $\mathcal{H}_1$  that a suboptimal test statistic, which is obtained by replacing the covariance matrix in the quadratic form of the LRT statistic with its asymptotically equivalent one, converges to the exact LRT statistic w.p. 1 as the number of samples tends to infinity [48, Propositions 1 and 3]. By applying this result, we have  $\lim_{N \rightarrow \infty} (T_{\text{LRT}}^{(N)} - \hat{T}_{\text{LRT}}^{(N)}) = 0$  w.p. 1 because  $\mathbf{R}_{\bar{x}} \sim \bar{\mathbf{W}}_{MN}^{\mathcal{H}} \bar{\Omega} \bar{\mathbf{W}}_{MN}$ . Therefore, in order to show (3.42), it now suffices to show  $\hat{T}_{\text{LRT}}^{(N)} = T_p^{(N)}$ .

Let  $\hat{s}$  be the frequency-domain equivalent observation vector that is defined as  $\hat{s} \triangleq \mathbf{W}_{MN} \mathbf{s}$ . Then, by using the permutation matrices  $\mathbf{E}_{2M,N}$ ,  $\mathbf{E}_1$ , and  $\mathbf{E}_1$  that are defined in the proof of Theorem 3 in Section IV, we have

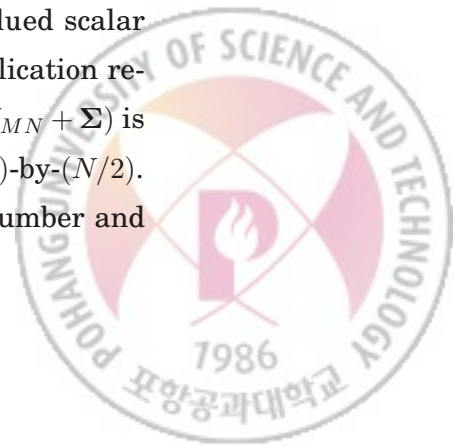
$$\mathbf{E}_{2M,N} \bar{\mathbf{W}}_{MN} \bar{\mathbf{r}} = \begin{bmatrix} \mathbf{E}_1 \hat{s}^* \\ \mathbf{E}_2 \hat{s} \end{bmatrix}. \quad (3.44)$$

By using (3.37) and (3.44), we can rewrite  $\hat{T}_{\text{LRT}}^{(N)}$  defined in (3.43) as  $\hat{T}_{\text{LRT}}^{(N)} = (\hat{s}^{\mathcal{T}} \bar{\Sigma}^* \hat{s}^* + \hat{s}^{\mathcal{H}} \bar{\Sigma} \hat{s}) / (2MN) = T_p^{(N)}$  because  $\hat{s}^{\mathcal{H}} \bar{\Sigma} \hat{s}$  is real-valued and (3.37) leads

$$\mathbf{E}_{2M,N} \bar{\Omega} \mathbf{E}_{2M,N}^{\mathcal{T}} = \begin{bmatrix} \mathbf{E}_1 \bar{\Sigma}^* \mathbf{E}_1^{\mathcal{T}} & \mathbf{O}_{MN} \\ \mathbf{O}_{MN} & \mathbf{E}_2 \bar{\Sigma} \mathbf{E}_2^{\mathcal{T}} \end{bmatrix}. \quad (3.45)$$

Therefore, the conclusion follows.  $\square$

The computation of the proposed test statistic  $T_p^{(N)}$  requires the pre-processing of  $\mathbf{r}$  to obtain  $\mathbf{s}$ , the matrix inversion of  $(\sigma^2 \mathbf{I}_{MN} + \Sigma)$ , and the matrix-vector multiplication to compute the quadratic form. As shown in Section IV, the asymptotic FRESH properization of the length- $MN$  vector  $\mathbf{r}$  and the matrix inversion of  $(\sigma^2 \mathbf{I}_{MN} + \Sigma)$  require  $\mathcal{O}(MN \log(MN))$  and  $\mathcal{O}(M^3 N)$  complex-valued scalar multiplications, respectively. In addition, the matrix-vector multiplication requires  $\mathcal{O}(M^2 N)$  complex-valued scalar multiplications, because  $(\sigma^2 \mathbf{I}_{MN} + \Sigma)$  is an  $(MN)$ -by- $(MN)$  block matrix with diagonal blocks of size  $(N/2)$ -by- $(N/2)$ . Since we consider the block processing where  $M$  is a fixed small number and



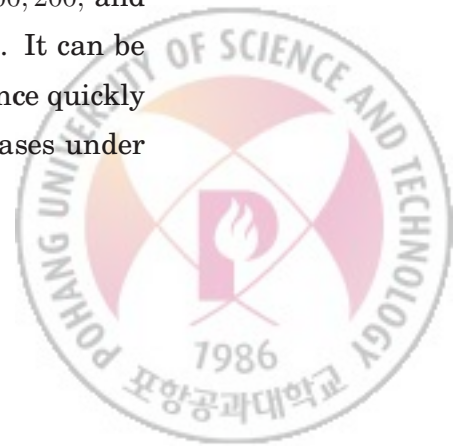


$N$  is much larger than  $M$ , the overall complexity in computing the exact LRT statistic and the proposed test statistic as functions only of  $N$  can be rewritten now as  $\mathcal{O}(N^2)$  and  $\mathcal{O}(N \log N)$ , respectively. Thus, the computational complexity of the proposed test statistic is much lower than that of the exact LRT statistic.

### 3.4.2 Numerical Results

In this subsection, numerical results are provided that show only the asymptotic optimality of the proposed test statistic because its computational efficiency can be similarly shown as Fig. 3.7. Throughout this subsection, the zero-mean improper-complex SOCS Gaussian random process to be detected is obtained by uniformly sampling the OQPSK-like signal generated in a similar way to that described in Section 3.3.2.

The first result is to show the convergence of the proposed test statistic to the exact LRT statistic. Fig. 3.9 shows the statistical average of the exact LRT and that of the proposed test statistics for symbol energy per noise density  $E_s/N_0 = 0, -5$ , and  $-10$  [dB]. It can be seen that the statistical averages of the exact LRT and the proposed test statistics approach the same non-zero value as the number of samples tends to infinity under both hypotheses. In particular, they coincide under  $\mathcal{H}_1$  because the trace of  $\bar{\Sigma}$  are the same as that of  $\bar{R}_{\bar{x}}$ . Since the convergence w.p. 1 is hard to show by using Monte-Carlo simulations, we instead show the convergence in probability that is implied by the convergence w.p. 1 [49]. Fig. 3.10 shows the empirical cumulative distribution function (CDF) of the difference of the proposed test statistic from the exact LRT statistic for symbol energy per noise density  $E_s/N_0 = -5$  [dB] and  $N = 100, 200$ , and  $400$ , where the empirical CDF is obtained by  $10^5$  Monte-Carlo runs. It can be seen that, as implied by Theorem 4, the empirical CDF of the difference quickly converges to the unit step function as the number of samples increases under both hypotheses.



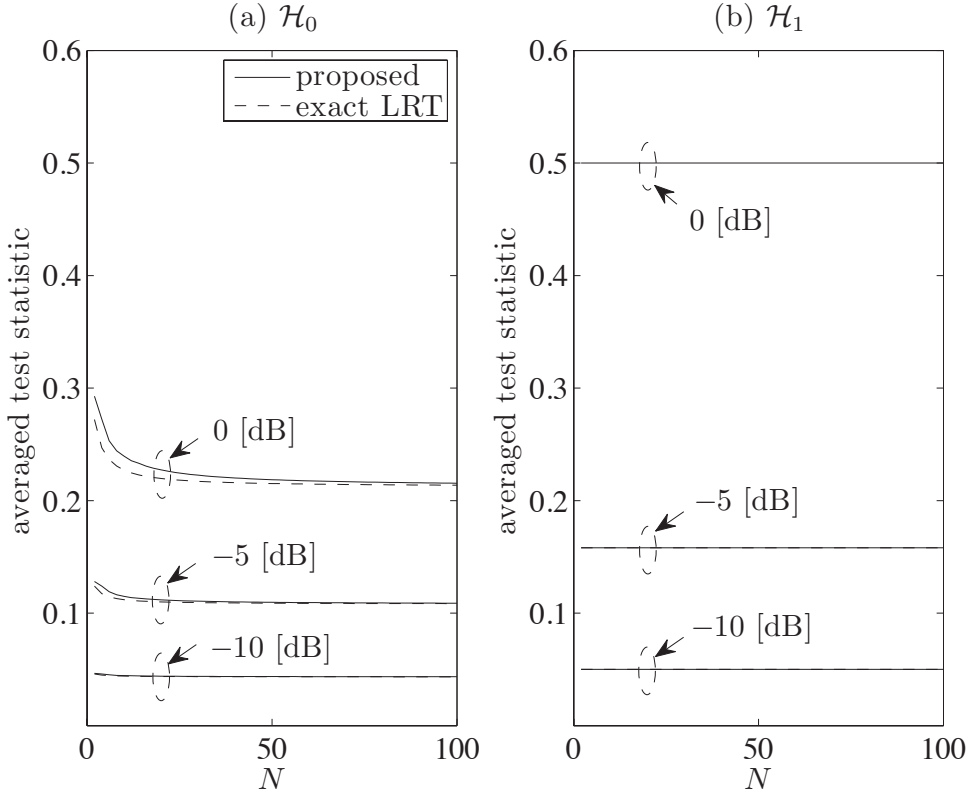


**Fig. 3.9** Statistical averages of the exact LRT and the proposed test statistics versus  $N$  for  $E_s/N_0 = 0, -5$ , and  $-10$  [dB], under (a)  $\mathcal{H}_0$  and (b)  $\mathcal{H}_1$ .

The second result is to compare the receiver operating characteristic (ROC) curves of the optimal detector that uses the exact LRT statistic (3.39) and the proposed detector that uses the proposed test statistic (3.41). As a common practice in computing the PDF of a quadratic function of Gaussian random vectors [50], we approximate the statistics by gamma random variables to obtain the probability of miss  $P_M \triangleq \Pr(\text{declare } \mathcal{H}_0 | \mathcal{H}_1)$  and the probability of false alarm  $P_{FA} \triangleq \Pr(\text{declare } \mathcal{H}_1 | \mathcal{H}_0)$ . The CDF  $F_X(x; a, b)$  of the gamma random variable  $X$  with two parameters  $a$  and  $b$  is given by

$$F_X(x; a, b) = I\left(\frac{ax}{\sqrt{b}}, b-1\right), \quad \forall x > 0, \quad (3.46)$$



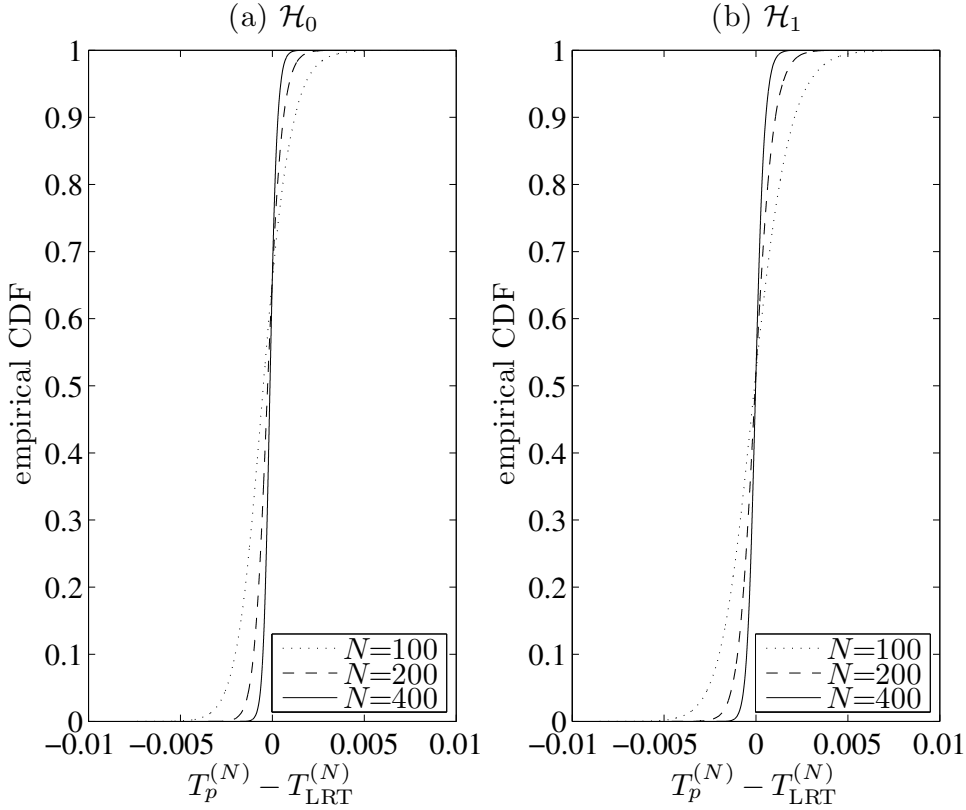
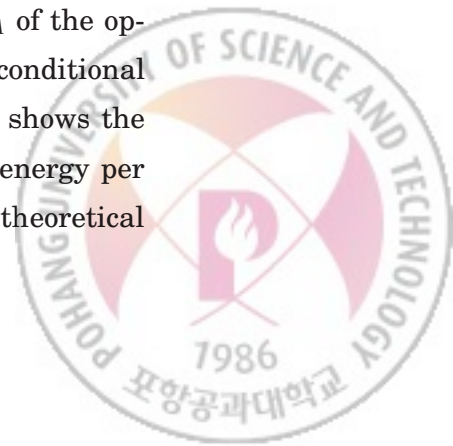


**Fig. 3.10** Empirical CDFs of the difference of the proposed test statistic from the exact LRT statistic for  $N = 100, 200$ , and  $400$ , under (a)  $\mathcal{H}_0$  and (b)  $\mathcal{H}_1$ .

where the Pearson's form of incomplete gamma function  $I(u, p)$  is defined by

$$I(u, p) \triangleq \frac{1}{\Gamma(p+1)} \int_0^{u\sqrt{p+1}} t^p e^{-t} dt, \quad (3.47)$$

and where the gamma function  $\Gamma(x)$  is defined by  $\Gamma(x) \triangleq \int_0^\infty t^{x-1} e^{-t} dt$  [49]. Note that the mean and the variance of the random variable whose CDF is  $F_X(x; a, b)$  are given by  $ab$  and  $ab^2$ , respectively. Thus,  $P_M$  and  $P_{FA}$  of the optimal and the proposed detectors can be computed by using the conditional means and variances of the statistics under  $\mathcal{H}_0$  and  $\mathcal{H}_1$ . Fig. 3.11 shows the ROC curves of the optimal and the proposed detectors for symbol energy per noise density  $E_s/N_0 = -5$  [dB] and  $N = 10, 100$ , and  $250$ , where the theoretical



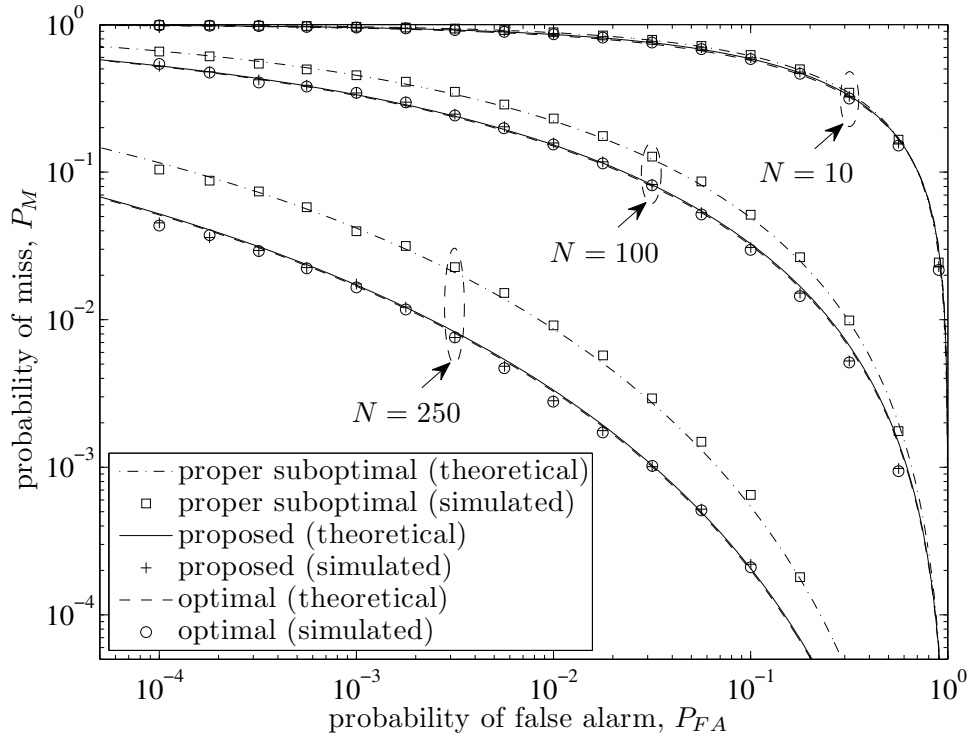
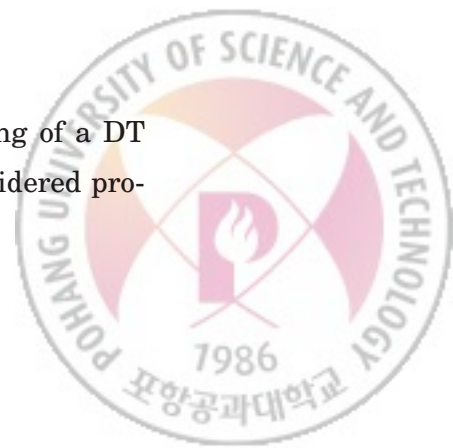


**Fig. 3.11** ROC curves of the optimal and the proposed detectors.

results are evaluated by using (3.46) while the simulated results are obtained from  $10^5$  Monte-Carlo runs. It also shows the ROC curve of a suboptimal detector that utilizes the LRT statistic obtained under the assumption of a proper-complex observed signal. It can be seen that the performance of the detectors is accurately approximated by using the gamma distributions. It can be also seen that the proposed detector performs almost the same as the optimal detector does even when  $N = 10$ .

### 3.5 Discussions

As mentioned earlier, there are two types of WL block processing of a DT improper-complex SOCS random process. So far, we only have considered pro-



cessing the signal vector augmented by its complex conjugate. In this section, we consider the alternative approach of processing the real part of the signal vector augmented by the imaginary part.

Assume again as in Section 3.2.2 that  $x$  consists of a finite number of consecutive samples of a zero-mean SOCS random process  $X[n]$  with cycle period  $M \in \mathbb{N}$ . Following the notation used in [51], let  $\bar{x}_{\mathbb{R}}$  be the length- $2MN$  augmented vector defined as

$$\bar{x}_{\mathbb{R}} \triangleq \begin{bmatrix} \text{Re}\{x\} \\ \text{Im}\{x\} \end{bmatrix}, \quad (3.48)$$

where  $\text{Re}\{\cdot\}$  and  $\text{Im}\{\cdot\}$  denote the real and the imaginary parts. Then, the covariance matrix  $R_{\bar{x}_{\mathbb{R}}} \triangleq \mathbb{E}\{\bar{x}_{\mathbb{R}}\bar{x}_{\mathbb{R}}^H\} = \mathbb{E}\{\bar{x}_{\mathbb{R}}\bar{x}_{\mathbb{R}}^T\}$  of  $\bar{x}_{\mathbb{R}}$  is given by a block matrix

$$R_{\bar{x}_{\mathbb{R}}} = \begin{bmatrix} \mathbb{E}\{\text{Re}\{x\}\text{Re}\{x\}^T\} & \mathbb{E}\{\text{Re}\{x\}\text{Im}\{x\}^T\} \\ \mathbb{E}\{\text{Im}\{x\}\text{Re}\{x\}^T\} & \mathbb{E}\{\text{Im}\{x\}\text{Im}\{x\}^T\} \end{bmatrix}. \quad (3.49)$$

Note that each  $(MN)$ -by- $(MN)$  submatrix in (3.49) is a block Toeplitz matrix with block size  $M$ -by- $M$  because the cycle period of  $X[n]$  is  $M$ .

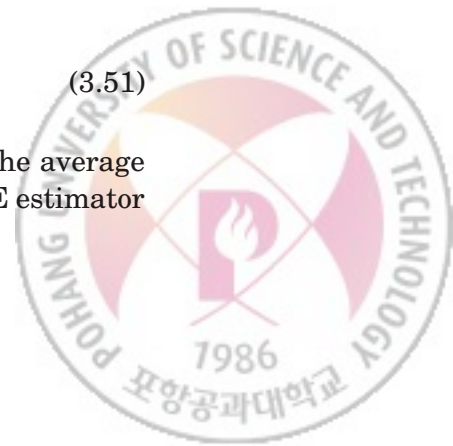
Consider the same estimation and detection problems examined in Sections 3.3 and 3.4 but now by using real-valued augmented vectors. First, in the estimation problem, the observation model (3.20) can be rewritten as

$$\bar{r}_{\mathbb{R}} = \bar{x}_{\mathbb{R}} + \bar{v}_{\mathbb{R}}, \quad (3.50)$$

where  $\bar{r}_{\mathbb{R}}$  and  $\bar{v}_{\mathbb{R}}$  are defined similarly to  $\bar{x}_{\mathbb{R}}$  from  $r$  and  $v$  in (3.20), respectively. Note that, since  $v$  is modeled by an additive proper-complex white noise vector with covariance matrix  $\sigma^2 I_{MN}$ ,  $\bar{v}_{\mathbb{R}}$  is an additive real-valued white noise vector with covariance matrix  $(\sigma^2/2)I_{2MN}$ . Thus, the WLMMSSE estimator  $x_{\text{opt}}$  of  $x$  is obtained as  $x_{\text{opt}} = [I_{MN} \ jI_{MN}]\bar{x}_{\mathbb{R},\text{opt}}$ , where

$$\bar{x}_{\mathbb{R},\text{opt}} = R_{\bar{x}_{\mathbb{R}}} \left( \frac{\sigma^2}{2} I_{2MN} + R_{\bar{x}_{\mathbb{R}}} \right)^{-1} \bar{r}_{\mathbb{R}} \quad (3.51)$$

is the LMMSE estimator of  $\bar{x}_{\mathbb{R}}$ . Of course, it is straightforward that the average MSE of this WLMMSSE estimator is the same as  $\varepsilon_{\text{opt}}^{(N)}$  of the WLMMSSE estimator



in (3.23). Second, in the presence detection problem, the observation model (3.38) can be rewritten as

$$\begin{aligned} \mathcal{H}_0 : \bar{\mathbf{r}}_{\mathbb{R}} &= \bar{\mathbf{v}}_{\mathbb{R}} \\ \text{versus} \\ \mathcal{H}_1 : \bar{\mathbf{r}}_{\mathbb{R}} &= \bar{\mathbf{x}}_{\mathbb{R}} + \bar{\mathbf{v}}_{\mathbb{R}}, \end{aligned} \quad (3.52)$$

where  $\bar{\mathbf{v}}_{\mathbb{R}}$  is an additive real-valued white Gaussian noise vector with covariance matrix  $(\sigma^2/2) \mathbf{I}_{2MN}$ . Then, it can be shown that the LRT statistic  $T_{\text{LRT}}^{(N)}$  in (3.39) now as a function of  $\bar{\mathbf{r}}_{\mathbb{R}}$  is obtained as

$$T_{\text{LRT}}^{(N)} = \frac{1}{2MN} \bar{\mathbf{r}}_{\mathbb{R}}^T \bar{\mathbf{R}}_{\bar{\mathbf{x}}_{\mathbb{R}}} \bar{\mathbf{r}}_{\mathbb{R}}, \quad (3.53)$$

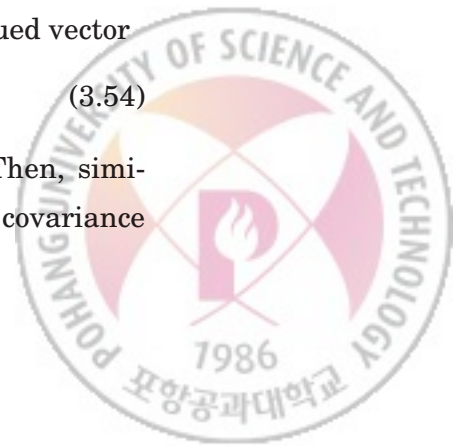
where  $\bar{\mathbf{R}}_{\bar{\mathbf{x}}_{\mathbb{R}}} \triangleq (2/\sigma^2) \mathbf{I}_{2MN} - ((\sigma^2/2) \mathbf{I}_{2MN} + \mathbf{R}_{\bar{\mathbf{x}}_{\mathbb{R}}})^{-1}$ .

The common major burden in computing the LMMSE estimate  $\bar{\mathbf{x}}_{\mathbb{R}, \text{opt}}$  and the exact LRT statistic  $T_{\text{LRT}}^{(N)}$  comes from the inversion of  $((\sigma^2/2) \mathbf{I}_{2MN} + \mathbf{R}_{\bar{\mathbf{x}}_{\mathbb{R}}})$ . Similar to Lemma 11, the covariance matrix  $\mathbf{R}_{\bar{\mathbf{x}}_{\mathbb{R}}}$  can be converted into a  $(2MN)$ -by- $(2MN)$  block Toeplitz matrix with block size  $(2M)$ -by- $(2M)$ , where the permutation matrix  $\mathbf{E}_{2,MN}$  defined in the proof of the lemma is used again for the row and column permutations. Thus, the computationally efficient inversion technique in [46] for a block Toeplitz matrix again enables us to perform the inversion with  $\mathcal{O}(M^3 N^2)$  real-valued scalar multiplications. Therefore, the overall computational complexity is  $\mathcal{O}(M^3 N^2)$ , which is the same as that of the optimal processing by using the complex-valued signal vector augmented by its complex conjugate, though the multiplications are now performed between real-valued scalars.

This computational complexity can be reduced to  $\mathcal{O}(MN \log(MN) + M^3 N)$  if an asymptotic property of  $\mathbf{R}_{\bar{\mathbf{x}}_{\mathbb{R}}}$  is exploited in the frequency-domain. To proceed, we convert the real-valued augmented vector  $\bar{\mathbf{x}}_{\mathbb{R}}$  into a complex-valued vector

$$\bar{\mathbf{W}}_{MN} \bar{\mathbf{x}}_{\mathbb{R}} = \begin{bmatrix} \mathbf{W}_{MN} \text{Re}\{\mathbf{x}\} \\ \mathbf{W}_{MN} \text{Im}\{\mathbf{x}\} \end{bmatrix} \quad (3.54)$$

by pre-multiplying the DFT matrix  $\mathbf{W}_{MN}$  to  $\text{Re}\{\mathbf{x}\}$  and  $\text{Im}\{\mathbf{x}\}$ . Then, similar to Proposition 2, we can derive the asymptotic property of the covariance



matrix  $\bar{\mathbf{W}}_{MN} \mathbf{R}_{\bar{\mathbf{x}}_{\mathbb{R}}} \bar{\mathbf{W}}_{MN}^{\mathcal{H}}$  of  $\bar{\mathbf{W}}_{MN} \bar{\mathbf{x}}_{\mathbb{R}}$  as follows. Since the submatrices of  $\mathbf{R}_{\bar{\mathbf{x}}_{\mathbb{R}}}$  in (3.49) are  $(MN)$ -by- $(MN)$  block Toeplitz matrices with block size  $M$ -by- $M$ , each submatrix is asymptotically equivalent to a block matrix with diagonal blocks when pre- and post-multiplied by DFT and inverse DFT matrices, respectively. Thus, we have

$$\bar{\mathbf{W}}_{MN} \mathbf{R}_{\bar{\mathbf{x}}_{\mathbb{R}}} \bar{\mathbf{W}}_{MN}^{\mathcal{H}} \sim \Omega_{\mathbb{R}}, \quad (3.55)$$

where  $\Omega_{\mathbb{R}}$  is the  $(2MN)$ -by- $(2MN)$  matrix given by

$$\Omega_{\mathbb{R}} \triangleq (\bar{\mathbf{W}}_{MN} \mathbf{R}_{\bar{\mathbf{x}}_{\mathbb{R}}} \bar{\mathbf{W}}_{MN}^{\mathcal{H}}) \odot (\mathbf{1}_{2M} \otimes \mathbf{I}_N). \quad (3.56)$$

Now, this asymptotic property (3.55) leads to the asymptotically optimal estimator and detector. First, in the estimation problem, we propose the suboptimal estimator  $\mathbf{x}_{\text{approx}} = [\mathbf{I}_{MN} \text{ j } \mathbf{I}_{MN}] \bar{\mathbf{x}}_{\mathbb{R}, \text{approx}}$  of  $\mathbf{x}$ , where

$$\bar{\mathbf{x}}_{\mathbb{R}, \text{approx}} = \bar{\mathbf{W}}_{MN}^{\mathcal{H}} \Omega_{\mathbb{R}} \left( \Omega_{\mathbb{R}} + \frac{\sigma^2}{2} \mathbf{I}_{2MN} \right)^{-1} \bar{\mathbf{W}}_{MN} \bar{\mathbf{r}}_{\mathbb{R}}. \quad (3.57)$$

Note that (3.57) is a suboptimal estimator of  $\bar{\mathbf{x}}_{\mathbb{R}}$  obtained by using the property (3.55). It can be easily shown in a similar way to Theorem 3 that the average MSE performance of the proposed estimator approaches that of the WLMMSE estimator  $[\mathbf{I}_{MN} \text{ j } \mathbf{I}_{MN}] \bar{\mathbf{x}}_{\mathbb{R}, \text{opt}}$ , where  $\bar{\mathbf{x}}_{\mathbb{R}, \text{opt}}$  is given by (3.51). Thus, the proposed estimator  $\mathbf{x}_{\text{approx}}$  is asymptotically optimal. Second, in the presence detection problem, we propose by using the property (3.55) the suboptimal test statistic  $T_{\mathbb{R}}^{(N)}$

$$T_{\mathbb{R}}^{(N)} \triangleq \frac{1}{2MN} \bar{\mathbf{r}}_{\mathbb{R}}^{\mathcal{T}} \bar{\mathbf{W}}_{MN}^{\mathcal{H}} \bar{\Omega}_{\mathbb{R}} \bar{\mathbf{W}}_{MN} \bar{\mathbf{r}}_{\mathbb{R}}, \quad (3.58)$$

of  $\bar{\mathbf{r}}_{\mathbb{R}}$ , where  $\bar{\Omega}_{\mathbb{R}} \triangleq (2/\sigma^2) \mathbf{I}_{2MN} - ((\sigma^2/2) \mathbf{I}_{2MN} + \Omega_{\mathbb{R}})^{-1}$ . It can be easily shown in a similar way to Theorem 4 that the proposed test statistic approaches the exact LRT statistic as the number of samples tends to infinity in the sense that

$$\lim_{N \rightarrow \infty} (T_{\mathbb{R}}^{(N)} - T_{\text{LRT}}^{(N)}) = 0, \text{ w.p. } 1, \quad (3.59)$$

under  $\mathcal{H}_0$  and  $\mathcal{H}_1$ .





The common major burden in computing theses asymptotically optimal estimate and test statistic comes from the multiplications of the DFT and the inverse DFT matrices and the inversion of  $((\sigma^2/2)\mathbf{I}_{2MN} + \mathbf{\Omega}_{\mathbb{R}})$ , as it can be seen from (3.57) and (3.58). As already mentioned, the multiplications of the  $(MN)$ -by- $(MN)$  DFT and inverse DFT matrices to a vector of length  $MN$  can be efficiently performed with computational complexity of  $\mathcal{O}(MN \log(MN))$  when the FFT algorithm is used. Since  $\mathbf{\Omega}_{\mathbb{R}}$  is a  $(2MN)$ -by- $(2MN)$  block matrix with diagonal blocks of size  $N$ -by- $N$ , the inversion of  $((\sigma^2/2)\mathbf{I}_{2MN} + \mathbf{\Omega}_{\mathbb{R}})$  requires  $\mathcal{O}(M^3N)$  complex-valued scalar multiplications. Therefore, the overall computational complexity is  $\mathcal{O}(MN \log(MN) + M^3N)$ .

This order of complexity is not only lower than that of the optimal estimator  $\mathbf{x}_{\text{opt}}$  and the exact LRT statistic  $T_{\text{LRT}}^{(N)}$ , but also the same as that of  $\mathbf{x}_p$  and  $T_p^{(N)}$  proposed in Sections 3.3 and 3.4 by using the asymptotic FRESH properizer. However, as it is already advocated in [17], [18, Ch. 1], and [19], the WL processing using complex-valued representation of the signal is preferred to that using real-valued representation in that it provides mathematical elegance such as algebraic economies, evocative geometry, and probabilistic insights, and implementational advantage such as the efficient use of complex FFT. In addition, it is worth noting that the use of the asymptotic FRESH properizer results in complexity reduction roughly by half, which do not appear in the big O notation, compared to the processing proposed in this section by using the real part of the signal vector augmented by the imaginary part. This is because  $\mathbf{x}_p$  and  $T_p^{(N)}$  require the matrix inversion and the matrix-vector multiplications to be performed with  $(MN)$ -by- $(MN)$  block matrices and length- $MN$  vectors. On the other hand,  $\bar{\mathbf{x}}_{\mathbb{R},\text{approx}}$  and  $T_{\mathbb{R}}^{(N)}$  require the operations to be performed with  $(2MN)$ -by- $(2MN)$  block matrices and length- $2MN$  vectors. Thus, the complexity in computing  $\mathbf{x}_p$  and  $T_p^{(N)}$  is approximately only a half of that in computing  $\bar{\mathbf{x}}_{\mathbb{R},\text{approx}}$  and  $T_{\mathbb{R}}^{(N)}$ .

Of course, such complexity gaps in computing  $\bar{\mathbf{x}}_{\mathbb{R},\text{approx}}$  and  $T_{\mathbb{R}}^{(N)}$  against  $\mathbf{x}_p$



and  $T_p^{(N)}$ , respectively, can be removed. Recall that the length of the output  $y = f(x)$  of the asymptotic FRESH properizer is halved by removing the redundant information in  $\bar{W}_{MN}\bar{x}$ . We can do the same for  $\bar{W}_{MN}\bar{x}_{\mathbb{R}}$ . For the length- $MN$  real-valued vector  $\text{Re}\{x\}$ , its DFT  $W_{MN}\text{Re}\{x\}$  has conjugate symmetry, i.e.,  $[W_{MN}\text{Re}\{x\}]_n = [W_{MN}\text{Re}\{x\}]_{MN-n+1}^*$ . Similarly,  $[W_{MN}\text{Im}\{x\}]_n = [W_{MN}\text{Im}\{x\}]_{MN-n+1}^*$ . Thus, these redundancies can be removed to reduce the computational complexities of  $\bar{x}_{\mathbb{R},\text{approx}}$  and  $T_{\mathbb{R}}^{(N)}$  by half. This removal of redundancy in the frequency domain is nothing but what the asymptotic FRESH properizer does in the frequency domain. Note that, as already shown in [18], the real-valued augmented vector  $\bar{x}_{\mathbb{R}}$  can be rewritten by using the complex-valued augmented vector  $\bar{x}$  in (3.10) as

$$\bar{x}_{\mathbb{R}} = \frac{1}{2}T_{MN}^{\mathcal{H}}\bar{x}, \quad (3.60)$$

where the  $(2MN)$ -by- $(2MN)$  invertible matrix  $T_{MN}$  is defined as

$$T_{MN} \triangleq \begin{bmatrix} I_{MN} & jI_{MN} \\ I_{MN} & -jI_{MN} \end{bmatrix}. \quad (3.61)$$

Thus, the output  $y = f(x)$  in (3.11) of the asymptotic FRESH properizer can be rewritten in terms of the DFTs of  $\text{Re}\{x\}$  and  $\text{Im}\{x\}$  as

$$y = W_{MN}^{\mathcal{H}}\bar{G}_{M,N}\bar{W}_{MN}T_{MN}\bar{x}_{\mathbb{R}}, \quad (3.62a)$$

$$= W_{MN}^{\mathcal{H}}\left((I_{MN} + S_{M,N})G_{M,N}W_{MN}\text{Re}\{x\} + j(I_{MN} - S_{M,N})G_{M,N}W_{MN}\text{Im}\{x\}\right). \quad (3.62b)$$

Therefore, the removal of redundancy by the asymptotic FRESH properizer is equivalent to that by pre-multiplying  $G_{M,N}$  to  $W_{MN}\text{Re}\{x\}$  and  $W_{MN}\text{Im}\{x\}$ . However, it still needs to be noted that the use of the asymptotic FRESH properizer is more advantageous in that it enables the adoption of the conventional signal processing techniques and algorithms that are already developed for the block processing of proper-complex random processes.



### 3.6 Summary

In this chapter, the asymptotic FRESH properizer is proposed as a pre-processor for the block processing of a finite number of consecutive samples of a DT improper-complex SOCS random process. It turns out that the output of this pre-processor can be well approximated by a proper-complex random vector that has a highly-structured frequency-domain covariance matrix for sufficiently large block size. The asymptotic propriety of the output allows the direct application with negligible performance degradation of the conventional signal processing techniques and algorithms dedicated to the block processing of proper-complex random vectors. Moreover, the highly-structured frequency-domain covariance matrix of the output facilitates the development of low-complexity post-processors. By solving the signal estimation and the signal presence detection problems, it is demonstrated that the asymptotic FRESH properizer leads to the simultaneous achievement of computational efficiency and asymptotic optimality. The use of the real part of the signal augmented by the imaginary part instead of the signal augmented by its complex conjugate is discussed for the estimation and detection problems as well as for the asymptotic FRESH properization. Further research is warranted to apply this pre-processor to various communications and signal processing problems involving the block processing of a DT improper-complex SOCS random process and to derive such almost optimal low-complexity post-processors. Since the cycle period is assumed known throughout this chapter, the estimation of this parameter and the possible mismatch analysis are interesting future research directions. The convergence-rate analysis of systems employing the asymptotic FRESH properizer is also an interesting research direction.



# CHAPTER 4

---

## Joint Transmitter and Receiver Optimization for Improper-Complex Second-Order Stationary Data Sequence

---

One of the classical problems related to the processing of WSCS random processes is a joint optimization of the transmitter (Tx) and receiver (Rx) in a communication system. In [52–55], real-baseband PAM of a WSS real-valued data symbol sequence is considered with a linear Rx for use over an additive WSS colored noise channel. Under the MMSE optimality criterion and the average transmit power constraint, the jointly optimal transmit and receive waveforms are derived. It is shown that, interestingly, the waveforms have nonzero spectral values only on a generalized Nyquist interval [54] with length equal to the minimum bandwidth required to satisfy the Nyquist condition for zero inter-symbol interference (ISI) [1].

This joint optimization problem is extended in [12] to complex-baseband QAM of a WSS complex-valued data symbol sequence. Under the LMMSE optimality criterion and the average transmit power constraint, the jointly optimal trans-



mit and receive waveforms are derived for use over an additive WSCS noise channel. It is well known that a WSCS noise model is better than a WSS model for the case in which data-like QAM interferences are present as well as an ambient Gaussian noise [1]. In contrast to the previous results only with an additive WSS noise, the optimal waveforms are shown in general to have nonzero spectral values on a frequency interval whose length is greater than that of the generalized Nyquist interval. This is because, unlike a WSS random process, a WSCS random process possesses non-zero correlation in the frequency domain among the components that are spaced integer multiples of the symbol rate apart [3]. To exploit such spectral correlation of the WSCS random process, a VFT technique is employed in [12]. This technique is motivated by the harmonic series representation [3] of a WSCS random process, and the use of that representation for joint Tx and Rx optimizations in cyclostationary interference and noise has been examined in [30] and [31].

The results in [12, 30, 31], however, have considered only the real passband or, equivalently, the complex baseband transmission of a proper-complex data sequence. Hence, these results are not directly applicable to, e.g., the real passband transmission of a BPSK data sequence, which is an improper-complex data sequence in complex baseband. Recall that complex-valued random variables, vectors, and processes are called proper if their complementary covariance, complementary covariance matrix, and complementary auto-covariance function (a.k.a. pseudo-covariance, pseudo-covariance matrix, and pseudo-covariance function) vanish, respectively [14]. Otherwise, they are called improper [18]. Although the complex envelopes of the majority of digitally modulated signals are proper, there still remain other digitally modulated signals whose complex envelopes have non-vanishing complementary auto-covariance functions [18]. For example, the complex envelopes of PAM, vestigial sideband PAM, unbalanced QAM, OQPSK, and Gaussian minimum shift keying are improper.



Among these improper-complex signals, we focus in this chapter on a linear modulation of an improper-complex data sequence using only one transmit waveform. In particular, we consider an improper-complex data sequence that is well modeled by a zero-mean improper-complex SOS random process for which the auto-covariance and the complementary auto-covariance functions depend only on the time difference [18]. This results in an improper-complex SOCS transmitted signal. For example, PAM, vestigial sideband PAM, and unbalanced QAM fall into this category. It is assumed that such an improper-complex SOCS signal is transmitted over a strictly band-limited frequency-selective LTI channel whose output is corrupted by an additive proper-complex SOCS random process. As already mentioned, proper-complex SOCS random processes well model the complex envelopes of the majority of digitally modulated signals as well as the complex envelope of an additive Gaussian noise.

Our objective is to extend the aforementioned joint optimizations of the Tx and Rx for proper-complex WSCS signaling to a joint Tx and Rx optimization problem for improper-complex SOCS signaling under the MMSE optimality criterion and the average transmit power constraint, which can be also seen in [56]. It is well known that the second-order properties of an improper-complex signal are not well captured by a linear Rx, but instead by a class of nonlinear Rx's called widely linear Rx's [18]. Combined with a widely linear Rx, the improper-complex signaling can enhance the performance of a communication system. For example, the interference alignment techniques adopting improper-complex data symbols and widely linear processing have been recently studied in [57–60] to increase the total throughput of users in an interference channel. An improper-complex signaling combined with a widely linear processing has also been recently considered as one of the candidate techniques for the next generation wireless communication systems [61, 62].

There are two types of widely linear Rx's. The first one linearly processes the signal augmented by its complex conjugate, whereas the second one linearly





processes the real part of the signal augmented by the imaginary part. In this chapter, the first type of widely linear processing also referred to as the LCL filtering [20] is employed. It is noteworthy that, unlike the joint optimizations in [12, 30, 31], we now need to find two receive waveforms under the WLMMSE optimality criterion, where one is employed to filter the complex envelope of the received signal and the other to filter its complex conjugate.

The VFT technique again enables us to convert the objective function and the average transmit power constraint described initially in the time domain into those in the frequency domain. Unlike the previous joint optimizations, the objective function is now expressed in terms of the VFT of the transmit waveform augmented by the VFT of its complex conjugate and the VFT of a receive waveform augmented by the VFT of the other receive waveform. Using these augmented vector-valued functions, we derive the optimal waveforms of the WLMMSE Rx in a straightforward way as a function of the transmit waveform. It is shown that the two receive waveforms of the WLMMSE Rx exploit not only the periodic spectral correlation due to the cyclostationarity, but also the symmetric spectral correlation about the origin due to the impropriety [18].

To derive the optimal transmit waveform, we devise the notion of the impropriety frequency function of the transmitted improper-complex SOS data sequence by using the relation between the PSD and the complementary PSD of the random process. This real-valued non-negative function converts the transmit waveform optimization problem into an equivalent convex optimization problem to find the optimal energy density of the transmit waveform. Then, a line search combined with an iterative algorithm is proposed to solve the problem. After finding the optimal energy density, the optimal transmit and receive waveforms are obtained. Numerical results provide an example of joint waveform design and also show the effect of the impropriety frequency function on the MSE performance.





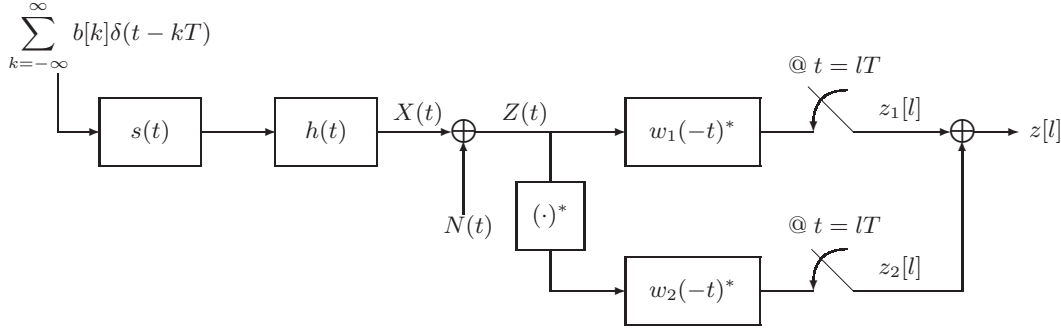


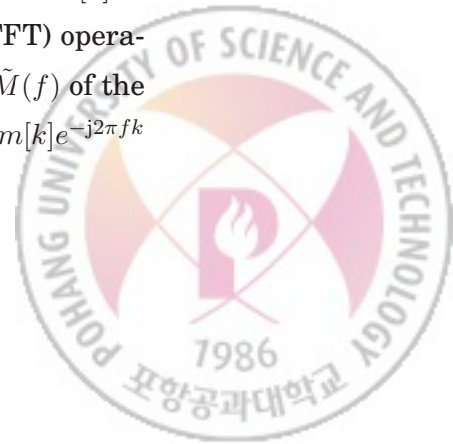
Fig. 4.1 System block diagram.

## 4.1 System Model and Problem Formulation

In this section, we describe the system model and formulate the optimization problem in the time domain. The system model is an extension of that in [12], which only considers the transmission and reception of a proper-complex SOS data sequence, to now allow improper-complex SOS sequences. The optimality criterion of the joint optimization problem is also extended from the LMMSE criterion to the WLMSE criterion.

### 4.1.1 System Model

A Tx and an Rx operate over a real passband to transmit a data sequence  $\{b[l]\}_{l \in \mathbb{Z}}$ . Fig. 4.1 shows the system block diagram in complex baseband. The data sequence  $\{b[l]\}_{l \in \mathbb{Z}}$  is assumed well modeled by a zero-mean improper-complex SOS random process with auto-covariance and complementary auto-covariance functions given, respectively, by  $m[k] \triangleq \mathbb{E}\{b[k+l]b[l]^*\}$  and  $\tilde{m}[k] \triangleq \mathbb{E}\{b[k+l]b[l]\}$ . By applying the discrete-time Fourier transform (DTFT) operations to  $m[k]$  and  $\tilde{m}[k]$ , the PSD  $M(f)$  and the complementary PSD  $\tilde{M}(f)$  of the data sequence  $\{b[l]\}_{l \in \mathbb{Z}}$  are derived, respectively, as  $M(f) \triangleq \sum_{k=-\infty}^{\infty} m[k]e^{-j2\pi fk}$  and  $\tilde{M}(f) \triangleq \sum_{k=-\infty}^{\infty} \tilde{m}[k]e^{-j2\pi fk}$ .



The Tx to be designed employs linear modulation with symbol transmission rate  $1/T$  [symbols/sec], where the transmit waveform is denoted by  $s(t)$ . The transmitted signal  $\sum_{k=-\infty}^{\infty} b[k]s(t-kT)$  is passed through a strictly band-limited channel that is modeled by an LTI system with impulse response  $h(t)$  having the one-sided bandwidth  $B$  [Hz] in complex baseband.

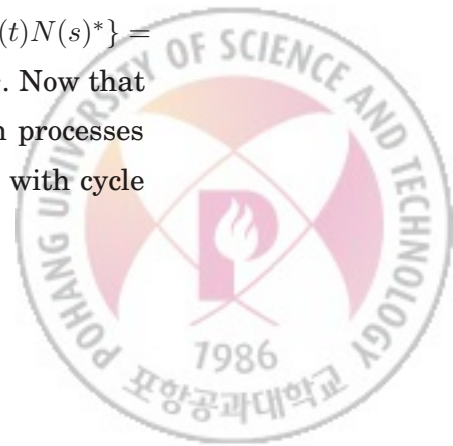
The received signal denoted by  $Z(t)$  consists of the signal from the Tx and an additive interference-plus-noise signal  $N(t)$ , where the latter is modeled by a zero-mean proper-complex SOCS random process with fundamental cycle period  $T_0$ . It is assumed that the multiplicative inverse  $T$  of the symbol transmission rate of the desired signal is chosen as an integer multiple of  $T_0$ . Thus,  $Z(t)$  can be written as

$$Z(t) = \sum_{k=-\infty}^{\infty} b[k]p(t-kT) + N(t), \quad (4.1)$$

where  $p(t) \triangleq h(t) * s(t)$  denotes the overall response.

In (4.1), it can be easily shown that the desired signal component  $X(t) \triangleq \sum_{k=-\infty}^{\infty} b[k]p(t-kT)$  becomes a zero-mean SOCS random process due to the second-order property of the zero-mean SOS data sequence  $\{b[l]\}_{l \in \mathbb{Z}}$ . In other words, the mean, the auto-covariance, and the complementary auto-covariance functions of  $X(t)$  satisfy, respectively,  $\mu_X(t) \triangleq \mathbb{E}\{X(t)\} = 0$ ,  $r_X(t, s) \triangleq \mathbb{E}\{X(t)X(s)^*\} = r_X(t+T, s+T)$ , and  $\tilde{r}_X(t, s) \triangleq \mathbb{E}\{X(t)X(s)\} = \tilde{r}_X(t+T, s+T)$ ,  $\forall t, \forall s$ . In what follows, we also call  $r_X(t, s)$  and  $\tilde{r}_X(t, s)$  the auto-correlation and the complementary auto-correlation functions, respectively, because  $X(t)$  has mean zero.

In (4.1), it can be straightforwardly shown that the interference-plus-noise signal  $N(t)$  is SOCS with mean zero and cycle period  $T$ , because  $T$  is assumed to be an integer multiple of  $T_0$ , i.e.,  $\mu_N(t) \triangleq \mathbb{E}\{N(t)\} = 0$ ,  $r_N(t, s) \triangleq \mathbb{E}\{N(t)N(s)^*\} = r_N(t+T, s+T)$ , and  $\tilde{r}_N(t, s) \triangleq \mathbb{E}\{N(t)N(s)\} = \tilde{r}_N(t+T, s+T)$ ,  $\forall t, \forall s$ . Now that  $Z(t)$  is a summation of two uncorrelated zero-mean SOCS random processes with cycle period  $T$ , it is also a zero-mean SOCS random processes with cycle



period  $T$ .

It is well known [18] that, for a vector-valued signal model, a widely linear Rx employing two linear filters outperforms a linear Rx employing only one linear filter when either the desired signal or the interference-plus-noise signal is improper. Thus, in this chapter, we employ two LTI filters with impulse responses  $w_1(-t)^*$  and  $w_2(-t)^*$  to process the improper-complex SOCS process  $Z(t)$  and its complex conjugate  $Z(t)^*$ , respectively. The two LTI filters are followed by uniform samplers with rate  $1/T$  [samples/sec], and then the sequence of decision statistics  $\{z[l]\}_{l \in \mathbb{Z}}$  is obtained as the sum of the sampler outputs, i.e.,

$$z[l] \triangleq z_1[l] + z_2[l], \quad (4.2)$$

where the sampler outputs  $z_1[l]$  and  $z_2[l]$  are defined, respectively, as

$$z_1[l] \triangleq w_1(-t)^* * Z(t) \big|_{t=lT} = \int_{-\infty}^{\infty} w_1(t - lT)^* Z(t) dt \quad \text{and} \quad (4.3a)$$

$$z_2[l] \triangleq w_2(-t)^* * Z(t)^* \big|_{t=lT} = \int_{-\infty}^{\infty} w_2(t - lT)^* Z(t)^* dt. \quad (4.3b)$$

#### 4.1.2 Problem Formulation in Time Domain

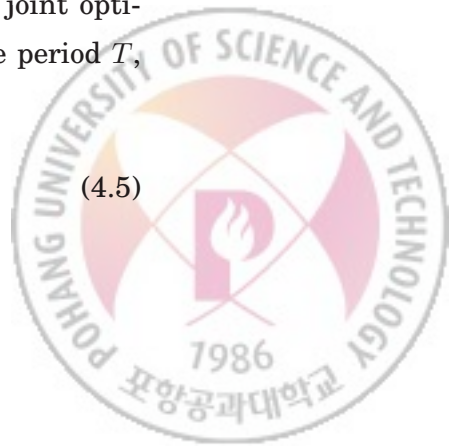
Our objective is to find the transmit and receive waveforms  $s(t)$ ,  $w_1(t)$ , and  $w_2(t)$  that jointly minimize the MSE given by

$$\varepsilon(s(t), w_1(t), w_2(t)) \triangleq \mathbb{E}\{|b[l] - z[l]|^2\}, \quad (4.4)$$

where  $s(t)$ ,  $w_1(t)$ , and  $w_2(t)$  are the parameters to be designed. Since  $T$  is an integer multiple of the fundamental cycle period  $T_0$  of the interference-plus-noise signal, it can be easily shown that the MSE defined in (4.4) as the objective function of the optimization problem is the same regardless of the value of  $l$ .

The average transmit power constraint is then imposed on this joint optimization problem. Since the transmitted signal is SOCS with cycle period  $T$ , the average transmit power  $\bar{P}$  can be defined as

$$\bar{P} \triangleq \mathbb{E} \left\{ \frac{1}{T} \int_{\langle T \rangle} \left| \sum_{k=-\infty}^{\infty} b[k] s(t - kT) \right|^2 dt \right\}, \quad (4.5)$$



where  $\langle T \rangle$  denotes any integration interval of length  $T$  [sec]. Thus, the constraint is given by  $\bar{P} = P_T$  for some  $P_T > 0$ . Therefore, the joint optimization problem is given by

**Problem 1**

$$\underset{s(t), w_1(t), w_2(t)}{\text{minimize}} \quad \varepsilon(s(t), w_1(t), w_2(t)) \quad (4.6a)$$

$$\text{subject to} \quad \bar{P} = P_T. \quad (4.6b)$$

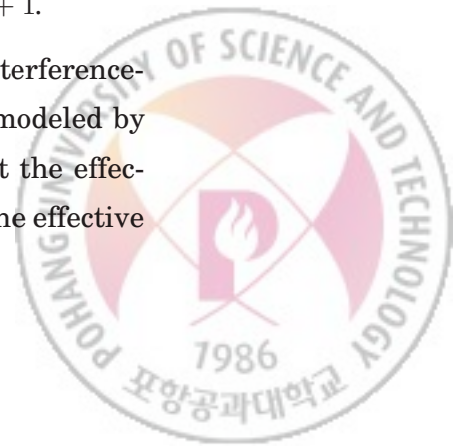
## 4.2 Problem Reformulation in Frequency Domain

In this section, Problem 1 described in the time domain is reformulated in the frequency domain. By proposing the notion of the matrix-valued complementary PSD and the methods to augment the VFTs of the transmit and receive waveforms, we convert the objective function (4.4) and the average transmit power constraint (4.5) to equivalent expressions in the frequency domain.

The objective function and the average transmit power constraint in Problem 1 are converted into equivalent expressions in the frequency domain. To begin with, we propose the notion of the matrix-valued complementary PSD of an improper-complex SOCS random process.

**Definition 24** *Given a pair  $(B, 1/T)$  and an improper-complex SOCS random process  $X(t)$  with cycle period  $T$  and complementary auto-correlation function  $\tilde{r}_X(t, s)$ , let  $\tilde{R}_X^{(k)}(\xi)$  be the CTFT of  $\tilde{r}_X^{(k)}(\tau)$  that is obtained by applying the Fourier series expansion to the periodic signal  $\tilde{r}_X(t, t - \tau) = \tilde{r}_X(t + T, t + T - \tau)$ ,  $\forall t$ , i.e.,  $\tilde{r}_X(t, s) = \sum_{k=-\infty}^{\infty} \tilde{r}_X^{(k)}(t - s) e^{j2\pi kt/T}$ . Then, the matrix-valued complementary PSD  $\tilde{\mathbf{R}}_X(f)$  is defined as a matrix-valued function of  $f \in \mathcal{F}$ , whose  $(k, l)$ th entry is given by  $[\tilde{\mathbf{R}}_X(f)]_{k,l} \triangleq \tilde{R}_X^{(k-l)}(f + (l - L - 1)/T)$  for  $k, l = 1, \dots, 2L + 1$ .*

Note that the matrix-valued complementary PSD  $\tilde{\mathbf{R}}_N(f)$  of the interference-plus-noise signal  $N(t)$  becomes an all-zero matrix because  $N(t)$  is modeled by a zero-mean proper-complex SOCS random process. Note also that the effective matrix-valued complementary PSD can be defined similarly to the effective



matrix-valued PSD. In what follows, each of the VFT, the matrix-valued PSD, and the matrix-valued complementary PSD is an effective one.

By using the above definitions, the matrix-valued PSD and the matrix-valued complementary PSD of the desired signal component in (4.1) are derived as follows.

**Lemma 15** *The  $\mathcal{N}(f)$ -by- $\mathcal{N}(f)$  matrix-valued PSD  $R_X(f)$  and the  $\mathcal{N}(f)$ -by- $\mathcal{N}(-f)$  matrix-valued complementary PSD  $\tilde{R}_X(f)$  of the desired signal  $X(t) = \sum_{l=-\infty}^{\infty} b[l]p(t - lT)$  are given by*

$$R_X(f) = \frac{1}{T} M(fT) p(f) p(f)^{\mathcal{H}} \quad \text{and} \quad (4.7a)$$

$$\tilde{R}_X(f) = \frac{1}{T} \tilde{M}(fT) p(f) (J(-f) p(-f)^*)^{\mathcal{H}}, \quad (4.7b)$$

respectively, where  $p(f)$  denotes the VFT of  $p(t)$  and  $J(f)$  denotes the  $\mathcal{N}(f)$ -by- $\mathcal{N}(f)$  backward identity matrix whose  $(m, n)$ th entry is given by 1 for  $m + n = \mathcal{N}(f) + 1$ , and 0 otherwise.

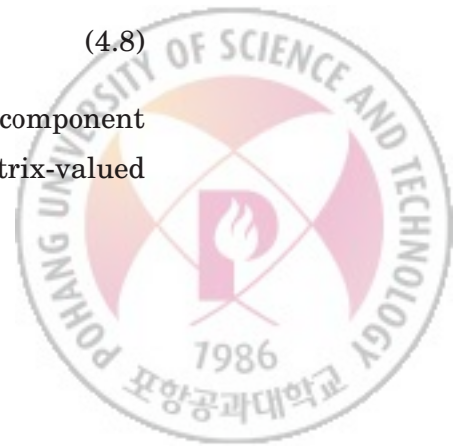
*Proof:* By using the CTFT of  $r_X^{(k)}(\tau)$  and  $\tilde{r}_X^{(k)}(\tau)$ , it can be easily shown that  $R_X^{(k)}(f) = M(fT) P(f + k/T) P(f)^* / T$  and  $\tilde{R}_X^{(k)}(f) = \tilde{M}(fT) P(f + k/T) P(-f) / T$ . Therefore, the conclusion follows from the definitions reviewed in the previous section and Definition 24.  $\square$

Note that  $J(-f) p(-f)^*$  in (4.7) is nothing but the VFT of  $p(t)^*$ . Thus,  $\tilde{R}_X(f)$  can be interpreted as the correlation between the frequency components at  $f$  of  $X(t)$  and  $X(t)^*$ .

Now, we are ready to convert the objective function. The MSE  $\varepsilon \triangleq \varepsilon(s(t), w_1(t), w_2(t))$  defined in (4.4) can be rewritten as

$$\begin{aligned} \varepsilon = & \mathbb{E}\{|b[l]|^2\} - 2\Re\left(\mathbb{E}\{b[l]^* z_1[l]\}\right) + \mathbb{E}\{|z_1[l]|^2\} \\ & - 2\Re\left(\mathbb{E}\{b[l]^* z_2[l]\}\right) + 2\Re\left(\mathbb{E}\{z_1[l] z_2[l]^*\}\right) + \mathbb{E}\{|z_2[l]|^2\}, \end{aligned} \quad (4.8)$$

where  $\Re(\cdot)$  denotes the real part. In the following propositions, each component of the right side of (4.8) is expressed in terms of the VFT, the matrix-valued PSD, and the matrix-valued complementary PSD.



**Proposition 3** *The first three terms of the right side of (4.8) can be rewritten as*

$$\mathbb{E}\{|b[l]|^2\} = \int_{\mathcal{F}} TM(fT)df, \quad (4.9a)$$

$$\mathbb{E}\{b[l]^* z_1[l]\} = \int_{\mathcal{F}} \mathbf{w}_1(f)^H M(fT) \mathbf{p}(f) df, \text{ and} \quad (4.9b)$$

$$\mathbb{E}\{|z_1[l]|^2\} = \int_{\mathcal{F}} \mathbf{w}_1(f)^H \mathbf{R}(f) \mathbf{w}_1(f) df, \quad (4.9c)$$

respectively, where  $\mathbf{w}_1(f)$  is the VFT of  $w_1(t)$  and  $\mathbf{R}(f) \triangleq \mathbf{R}_N(f) + \mathbf{R}_X(f)$ .

*Proof:* See [12, Proposition 1-4].  $\square$

**Proposition 4 .** *The last three terms of the right side of (4.8) can be rewritten as*

$$\mathbb{E}\{b[l]^* z_2[l]\} = \int_{\mathcal{F}} \mathbf{w}_2(f)^H \tilde{M}(fT)^* \mathbf{J}(-f) \mathbf{p}(-f)^* df, \quad (4.10a)$$

$$\mathbb{E}\{z_1[l] z_2[l]^*\} = \int_{\mathcal{F}} \mathbf{w}_1(f)^H \tilde{\mathbf{R}}(f) \mathbf{w}_2(f) df, \text{ and} \quad (4.10b)$$

$$\mathbb{E}\{|z_2[l]|^2\} = \int_{\mathcal{F}} \mathbf{w}_2(f)^H \mathbf{J}(-f) \mathbf{R}(-f)^* \mathbf{J}(-f) \mathbf{w}_2(f) df, \quad (4.10c)$$

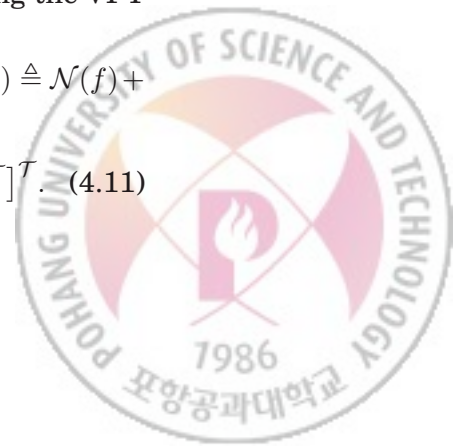
respectively, where  $\mathbf{w}_2(f)$  is the VFT of  $w_2(t)$  and  $\tilde{\mathbf{R}}(f) \triangleq \tilde{\mathbf{R}}_X(f)$ .

*Proof:* It can be shown similarly to Proposition 3.  $\square$

Note in  $\mathbb{E}\{|z_2[l]|^2\} = \int_{\mathcal{F}} \mathbf{w}_2(f)^H \mathbf{J}(-f) \mathbf{R}(-f)^* \mathbf{J}(-f) \mathbf{w}_2(f) df$  that the pre-multiplication of the backward identity matrix  $\mathbf{J}(f)$  reverses the order of the rows whereas the post-multiplication reverses that of the columns. Note also that  $\mathbf{p}(f) = \mathbf{H}(f) \mathbf{s}(f)$ ,  $\forall f \in \mathcal{F}$ , where  $\mathbf{s}(f)$  is the VFT of the transmit waveform  $s(t)$  and  $\mathbf{H}(f)$  is defined as  $\mathbf{H}(f) \triangleq \text{diag}\{\mathbf{h}(f)\}$  with  $\mathbf{h}(f)$  representing the VFT of  $h(t)$ .

To simplify the expression of the objective function, we define  $\bar{\mathcal{N}}(f) \triangleq \mathcal{N}(f) + \mathcal{N}(-f)$ ,

$$\bar{\mathbf{s}}(f) \triangleq [\mathbf{s}(f)^T, (\mathbf{J}(-f) \mathbf{s}(-f)^*)^T]^T \quad \text{and} \quad \bar{\mathbf{w}}(f) \triangleq [\mathbf{w}_1(f)^T, \mathbf{w}_2(f)^T]^T. \quad (4.11)$$





Here, the length- $\bar{\mathcal{N}}(f)$  vector-valued functions  $\bar{s}(f)$  and  $\bar{w}(f)$  are the VFT of the transmit waveform augmented by the VFT of its complex conjugate and the VFT of a receive waveform augmented by the VFT of the other receive waveform, respectively. Also, let the  $\bar{\mathcal{N}}(f)$ -by- $\bar{\mathcal{N}}(f)$  matrices  $\bar{H}(f)$ ,  $\bar{M}(f)$ , and  $\bar{R}(f)$  be defined, respectively, as  $\bar{H}(f) \triangleq \text{diag}\{H(f), J(-f)H(-f)^*J(-f)\}$ ,  $\bar{M}(f) \triangleq \text{diag}\{M(f)I(f), \tilde{M}(f)^*I(-f)\}$ , and

$$\bar{R}(f) \triangleq \begin{bmatrix} R(f) & \tilde{R}(f) \\ \tilde{R}(f)^H & J(-f)R(-f)^*J(-f) \end{bmatrix} \quad (4.12)$$

with  $I(f)$  denoting the  $\mathcal{N}(f)$ -by- $\mathcal{N}(f)$  identity matrix and  $\text{diag}\{A, B\}$  denoting the block diagonal matrix whose diagonal blocks are the matrices  $A$  and  $B$ . These notions enable us to derive the optimal receive waveforms in a straightforward way.

By substituting the results of Propositions 3 and 4 into (4.8), we can rewrite the objective function  $\varepsilon$  as

$$\varepsilon(\bar{s}(f), \bar{w}(f)) = \int_{\mathcal{F}} \left( TM(fT) + \bar{w}(f)^H \bar{R}(f) \bar{w}(f) - 2\Re\{\bar{w}(f)^H \bar{H}(f) \bar{M}(fT) \bar{s}(f)\} \right) df, \quad (4.13)$$

which is a function of  $\bar{s}(f)$  and  $\bar{w}(f)$ . Also, by using [12, Eq. (32)] and the definition of  $\bar{s}(f)$ , we can rewrite the average transmit power  $\bar{P}$  defined in (4.5) as

$$\bar{P} = \frac{1}{T} \int_{\mathcal{F}} M(fT) s(f)^H s(f) df = \frac{1}{2T} \int_{\mathcal{F}} M(fT) \bar{s}(f)^H \bar{s}(f) df. \quad (4.14)$$

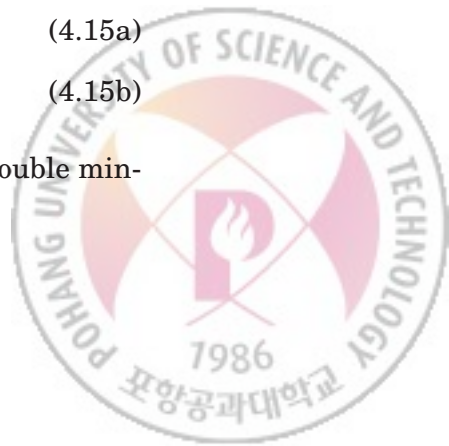
This leads to the equivalent joint optimization problem to find  $\bar{s}(f)$  and  $\bar{w}(f)$  as

**Problem 2 (a)**

$$\underset{\bar{s}(f), \bar{w}(f)}{\text{minimize}} \quad \varepsilon(\bar{s}(f), \bar{w}(f)) \quad (4.15a)$$

$$\text{subject to} \quad \bar{P} = P_T. \quad (4.15b)$$

This joint optimization problem can be converted to an equivalent double minimization problem given by





**Problem 2 (b)**

$$\underset{\bar{s}(f)}{\text{minimize}} \quad \underset{\bar{w}(f)}{\text{minimize}} \quad \varepsilon(\bar{s}(f), \bar{w}(f)) \quad (4.16a)$$

$$\text{subject to} \quad \bar{P} = P_T. \quad (4.16b)$$

In the next section, we solve this optimization problem to obtain the VFTs of the optimal receive and transmit waveforms.

### 4.3 Optimization of Transmit and Receive Waveforms

In this section, we first derive the optimal  $\bar{w}(f)$  that minimizes the objective function of the inner optimization in (4.16a) for given  $\bar{s}(f)$ . By substituting this  $\bar{w}(f)$  and introducing the notion of the propriety frequency function for the data sequence, we reduce the joint optimization problem to an equivalent problem to be solved only for  $s(f)$ . Then, by defining the energy density function for  $s(f)$ , this problem is converted to an equivalent double minimization problem, where the inner problem is to find the optimal  $s(f)$  for a given energy density function and the outer problem is to find the optimal energy density function. Once the optimal energy density function is found, it is straightforward to construct the jointly optimal  $s(f)$  and  $w(f)$ .

#### 4.3.1 Optimization of Widely Linear Receiver

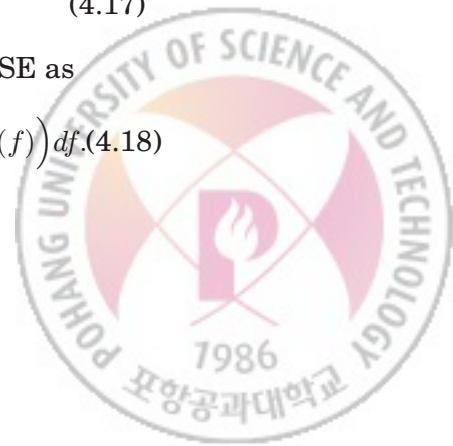
As in [12, Theorem 2], to find the optimal  $\bar{w}(f)$  for given  $\bar{s}(f)$ , an unconstrained quadratic optimization problem needs to be solved. This can be done simply by using the first-order necessary condition as

$$\bar{w}(f) = \bar{R}(f)^{-1} \bar{H}(f) \bar{M}(fT) \bar{s}(f), \quad \forall f \in \mathcal{F}. \quad (4.17)$$

By substituting the above solution into (4.13), we can rewrite the MSE as

$$\varepsilon(\bar{s}(f)) = \int_{\mathcal{F}} \left( TM(fT) - \bar{s}(f)^{\mathcal{H}} \bar{M}(fT)^{\mathcal{H}} \bar{H}(f)^{\mathcal{H}} \bar{R}(f)^{-1} \bar{H}(f) \bar{M}(fT) \bar{s}(f) \right) df. \quad (4.18)$$

which is a function only of  $\bar{s}(f)$ .



### 4.3.2 Improprity Frequency Function

To convert  $\varepsilon(\bar{s}(f))$  into a function only of  $s(f)$ , the notion of the impropriety frequency function is introduced as follows.

**Definition 25** *Given a discrete-time improper-complex SOS random process with PSD  $M(f)$  and complementary PSD  $\tilde{M}(f)$ , its impropriety frequency function  $k(f)$  is defined as*

$$k(f) \triangleq \begin{cases} 0, & \text{if } M(f)M(-f) = 0, \\ \frac{|\tilde{M}(f)|}{\sqrt{M(f)M(-f)}}, & \text{otherwise.} \end{cases} \quad (4.19)$$

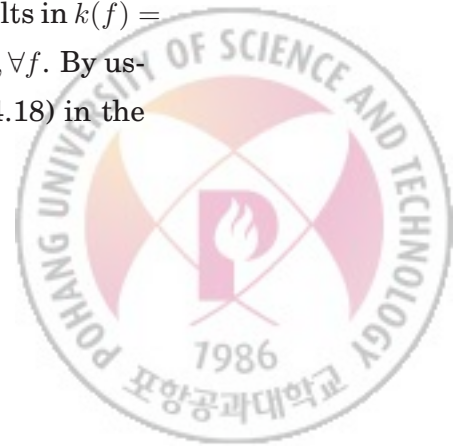
The above definition is motivated by the impropriety coefficient of an improper-complex random variable [18, Definition 3.1] and by a relation between  $M(f)$  and  $\tilde{M}(f)$  shown in [29, Eq. (5)]. By using the phase  $\phi(f)$  of  $\tilde{M}(f)$ , we can rewrite the complementary PSD as  $\tilde{M}(f) = |\tilde{M}(f)|e^{j\phi(f)} = k(f)\sqrt{M(f)M(-f)}e^{j\phi(f)}$ , where  $0 \leq \phi(f) \leq 2\pi$ . In the next lemma, the properties of the impropriety frequency and the phase functions are provided.

**Lemma 16** *The impropriety frequency function  $k(f)$  and the phase function  $\phi(f)$  satisfy*

$$0 \leq k(f) \leq 1, \quad k(-f) = k(f), \quad \text{and} \quad \phi(-f) = \phi(f), \quad \forall f. \quad (4.20)$$

*Proof:* Since  $\tilde{m}[-k] = \tilde{m}[k]$  by definition, we have  $\tilde{M}(-f) = \tilde{M}(f)$ , which implies  $\phi(-f) = \phi(f)$ . This also leads to  $k(-f) = k(f)$  by (4.19). By using the property  $|\tilde{M}(f)|^2 \leq M(f)M(-f)$  shown in [29, Eq. (5)], we have  $0 \leq k(f) \leq 1$ .  $\square$

For example, an uncorrelated real-valued PAM data sequence results in  $k(f) = 1, \forall f$ , whereas any proper-complex data sequence results in  $k(f) = 0, \forall f$ . By using the impropriety frequency function, we can rewrite the MSE (4.18) in the form of a function of  $\bar{s}(f)$  as a function of  $s(f)$ .



### 4.3. OPTIMIZATION OF TRANSMIT AND RECEIVE WAVEFORMS 100

**Lemma 17** Define  $c(f)$  as

$$c(f) \triangleq \frac{1}{T} M(fT) s(f)^H \mathbf{H}(f)^H \mathbf{R}_N(f)^{-1} \mathbf{H}(f) s(f). \quad (4.21)$$

By using  $c(f)$  and  $k(f)$ , also define  $\mathbf{D}(f)$  and  $\mathbf{k}(f)$ , respectively, as

$$\mathbf{D}(f) \triangleq \begin{bmatrix} c(f) & 0 \\ 0 & \frac{c(-f)}{1+c(-f)(1-k(fT)^2)} \end{bmatrix} \quad \text{and} \quad \mathbf{k}(f) \triangleq \begin{bmatrix} 1 \\ k(f) \end{bmatrix}. \quad (4.22)$$

Then, the MSE  $\varepsilon(\bar{s}(f))$  in (4.18) can be rewritten as

$$\varepsilon(s(f)) = \int_{\mathcal{F}} \frac{TM(fT)}{1 + \mathbf{k}(fT)^T \mathbf{D}(f) \mathbf{k}(fT)} df, \quad (4.23)$$

which is a function of  $s(f)$ .

*Proof:* Define the 2-by-2 matrices  $\hat{\mathbf{M}}(f)$ ,  $\mathbf{M}(f)$ , and  $\mathbf{K}(f)$ , respectively, as

$$\hat{\mathbf{M}}(f) \triangleq \begin{bmatrix} M(f) & \tilde{M}(f) \\ \tilde{M}(f)^* & M(-f)^* \end{bmatrix}, \quad (4.24a)$$

$$\mathbf{M}(f) \triangleq \begin{bmatrix} M(f)e^{j\phi(f)} & 0 \\ 0 & M(-f)e^{-j\phi(f)} \end{bmatrix}^{\frac{1}{2}}, \quad \text{and} \quad (4.24b)$$

$$\mathbf{K}(f) \triangleq \begin{bmatrix} 1 & k(f) \\ k(f) & 1 \end{bmatrix}. \quad (4.24c)$$

Then, we can rewrite  $\hat{\mathbf{M}}(f)$  as  $\hat{\mathbf{M}}(f) = \mathbf{M}(f)\mathbf{K}(f)\mathbf{M}(f)^H$ . Also, define the  $\bar{\mathcal{N}}(f)$ -by- $\bar{\mathcal{N}}(f)$  matrix  $\bar{\mathbf{R}}_N(f)$  and the  $\bar{\mathcal{N}}(f)$ -by-2 matrix  $\bar{\mathbf{S}}(f)$  as

$$\bar{\mathbf{R}}_N(f) \triangleq \text{diag}\{\mathbf{R}_N(f), \mathbf{J}(-f)\mathbf{R}_N(-f)^*\mathbf{J}(-f)\} \quad (4.25a)$$

and

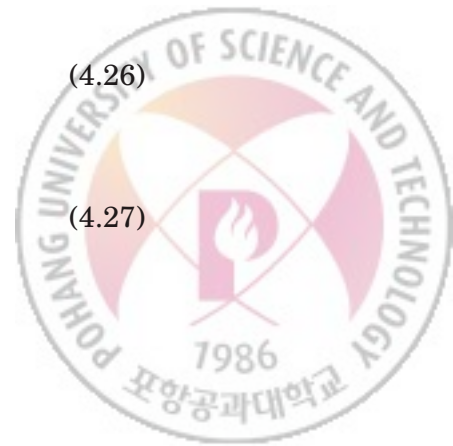
$$\bar{\mathbf{S}}(f) \triangleq \text{diag}\{s(f), \mathbf{J}(-f)s(-f)^*\}, \quad (4.25b)$$

respectively. Due to the ambient noise component in  $N(t)$ ,  $\mathbf{R}_N(f)$  and  $\bar{\mathbf{R}}_N(f)$  are positive definite for all  $f \in \mathcal{F}$ . By using  $\bar{\mathbf{R}}_N(f)^{-1/2}$ , define the  $\bar{\mathcal{N}}(f)$ -by-2 matrix  $\tilde{\mathbf{P}}(f)$  as

$$\tilde{\mathbf{P}}(f) \triangleq \bar{\mathbf{R}}_N(f)^{-1/2} \bar{\mathbf{H}}(f) \bar{\mathbf{S}}(f) \mathbf{M}(fT) / \sqrt{T}. \quad (4.26)$$

Then, it can be shown that

$$\bar{\mathbf{H}}(f) \bar{\mathbf{M}}(fT) \bar{\mathbf{s}}(f) = \sqrt{TM(fT)} e^{-j\phi(fT)/2} \bar{\mathbf{R}}_N(f)^{1/2} \tilde{\mathbf{P}}(f) \mathbf{k}(fT). \quad (4.27)$$



### 4.3. OPTIMIZATION OF TRANSMIT AND RECEIVE WAVEFORMS 101

Thus, the second term of the integrand in (4.18), which contains  $\bar{\mathbf{H}}(f)\bar{\mathbf{M}}(fT)\bar{\mathbf{s}}(f)$ , can be rewritten as

$$\begin{aligned} & \bar{\mathbf{s}}(f)^{\mathcal{H}}\bar{\mathbf{M}}(fT)^{\mathcal{H}}\bar{\mathbf{H}}(f)^{\mathcal{H}}\bar{\mathbf{R}}(f)^{-1}\bar{\mathbf{H}}(f)\bar{\mathbf{M}}(fT)\bar{\mathbf{s}}(f) \\ &= TM(fT)\mathbf{k}(fT)^{\mathcal{T}}\tilde{\mathbf{P}}(f)^{\mathcal{H}}\left(\mathbf{I} + \tilde{\mathbf{P}}(f)\mathbf{K}(fT)\tilde{\mathbf{P}}(f)^{\mathcal{H}}\right)^{-1}\tilde{\mathbf{P}}(f)\mathbf{k}(fT), \end{aligned} \quad (4.28)$$

where  $\mathbf{I}$  conveniently denotes the appropriately sized identity matrix throughout this proof. Let  $\hat{\mathbf{p}}(f) \triangleq \sqrt{M(fT)/T}e^{j\phi(f)/2}\mathbf{R}_N(f)^{-1/2}\mathbf{H}(f)\mathbf{s}(f)$ . Then, we can rewrite  $\tilde{\mathbf{P}}(f)$  and  $c(f)$  defined in (4.21) as  $\tilde{\mathbf{P}}(f) = \text{diag}\{\hat{\mathbf{p}}(f), \mathbf{J}(-f)\hat{\mathbf{p}}(-f)^*\}$  and  $c(f) = \|\hat{\mathbf{p}}(f)\|^2$ , respectively. If  $c(f)c(-f) = 0$ , then it can be shown that (4.28) leads to (4.23) by using the matrix inversion lemma showing  $\mathbf{I} - \mathbf{u}^{\mathcal{H}}(\mathbf{I} + \mathbf{u}\mathbf{u}^{\mathcal{H}})^{-1}\mathbf{u} = (1 + \mathbf{u}^{\mathcal{H}}\mathbf{u})^{-1}$  for any vector  $\mathbf{u}$ . If  $c(f)c(-f) \neq 0$ , then, since  $\tilde{\mathbf{P}}(f)^{\mathcal{H}}\tilde{\mathbf{P}}(f) = \text{diag}\{c(f), c(-f)\}$  is invertible, it can be shown that

$$\tilde{\mathbf{P}}(f)^{\mathcal{H}}(\mathbf{I} + \tilde{\mathbf{P}}(f)\mathbf{K}(fT)\tilde{\mathbf{P}}(f)^{\mathcal{H}})^{-1}\tilde{\mathbf{P}}(f)\tilde{\mathbf{C}}(f) = \mathbf{I}, \quad (4.29)$$

where  $\tilde{\mathbf{C}}(f)$  is defined as

$$\tilde{\mathbf{C}}(f) \triangleq (\tilde{\mathbf{P}}(f)^{\mathcal{H}}\tilde{\mathbf{P}}(f))^{-1} + \mathbf{K}(fT). \quad (4.30)$$

Since  $c(f)$  and  $c(-f)$  are not zero, we can rewrite  $\tilde{\mathbf{C}}(f)$  as  $\tilde{\mathbf{C}}(f) = \text{diag}\{c(f)^{-1}, c(-f)^{-1} + 1 - \mathbf{k}(fT)^{\mathcal{T}}\mathbf{k}(fT)\} + \mathbf{k}(fT)\mathbf{k}(fT)^{\mathcal{T}}$ . Thus, we now can rewrite the right side of (4.28) as

$$TM(fT)\mathbf{k}(fT)^{\mathcal{T}}\tilde{\mathbf{C}}(f)^{-1}\mathbf{k}(fT). \quad (4.31)$$

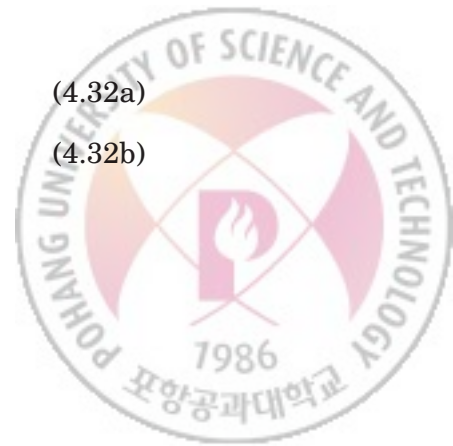
By using the matrix inversion lemma, the conclusion follows.  $\square$

Therefore, the joint optimization problem Problem 2(b) can be reduced to to an equivalent problem to be solved only for  $\mathbf{s}(f)$  as

#### Problem 2 (c)

$$\underset{\mathbf{s}(f)}{\text{minimize}} \quad \varepsilon(\mathbf{s}(f)) \quad (4.32a)$$

$$\text{subject to} \quad \bar{P} = P_T. \quad (4.32b)$$



### 4.3.3 Optimization of Transmitter

Let  $\varepsilon(f)$  denote the integrand in (4.23), i.e.,

$$\varepsilon(f) \triangleq TM(fT)/(1 + \mathbf{k}(fT)^T \mathbf{D}(f) \mathbf{k}(fT)). \quad (4.33)$$

Then, by the definitions of  $c(f)$  and  $\mathbf{D}(f)$  in (4.21) and (4.22), respectively, it can be seen that  $\varepsilon(f_0)$  for some  $f_0$  is affected by the choice of  $s(f)$  at both  $f_0$  and  $-f_0$ . Define the energy density of  $s(f)$  as  $a(f) \triangleq \|s(f)\|^2$ . Then, we can partition the constraint set of Problem 2(c) into disjoint subsets, where each subset contains all feasible transmit waveforms having the same pair  $(a(f), a(-f))$  of the energy density functions for  $f > 0$ . Thus, Problem 2(c) can be rewritten as

#### Problem 3

$$\underset{a(f), a(-f)}{\text{minimize}} \quad \begin{cases} \underset{s(f), s(-f)}{\text{minimize}} & \int_{\mathcal{F}^+} \varepsilon(f) + \varepsilon(-f) df \\ \text{subject to} & \|s(f)\|^2 = a(f), \forall f \in \mathcal{F} \end{cases} \quad (4.34a)$$

$$\text{subject to} \quad \frac{1}{T} \int_{\mathcal{F}^+} M(fT)a(f) + M(-fT)a(-f) df = P_T, \quad (4.34b)$$

where  $\mathcal{F}^+ \triangleq \{f : 0 \leq f < 1/(2T)\}$  denotes the half-Nyquist interval.

Note that similar conversions into equivalent double minimization problems using the energy density function were already adopted in [12, 13] to successfully solve joint Tx-Rx optimization problems. In the next proposition, we present the optimal  $s(f)$  for given  $a(f)$ .

**Proposition 5** *Given  $a(f)$ , the optimal solution to the inner optimization problem in (4.34a) is given by*

$$s(f) = \sqrt{a(f)} \mathbf{v}(f) e^{j\theta(f)}, \quad \forall f \in \mathcal{F}, \quad (4.35)$$

where  $\mathbf{v}(f)$  is the normalized eigenvector corresponding to the largest eigenvalue of  $\mathbf{H}(f)^H \mathbf{R}_N(f)^{-1} \mathbf{H}(f)$ , and  $\theta(f)$  can be chosen arbitrarily.



### 4.3. OPTIMIZATION OF TRANSMIT AND RECEIVE WAVEFORMS 103

*Proof:* Note that the integrand  $\varepsilon(f) + \varepsilon(-f)$  in (4.34a) can be rewritten as

$$\varepsilon(f) + \varepsilon(-f) = T \frac{M(-fT)(1 + c(f)\bar{k}(fT)) + M(fT)(1 + c(-f)\bar{k}(fT))}{1 + c(f) + c(-f) + c(f)c(-f)\bar{k}(fT)}, \quad (4.36)$$

where  $\bar{k}(f) \triangleq 1 - k(f)^2$ . Since  $\varepsilon(f) + \varepsilon(-f)$  evaluated at some  $f_0$  is a function only of  $s(f_0)$  and  $s(-f_0)$  through  $c(f_0)$  and  $c(-f_0)$ , respectively, we just need to minimize by optimizing  $c(f_0)$  and  $c(-f_0)$  in the integrand at each  $f \in \mathcal{F}^+$  subject to the constraint. Let  $c(f_0) = c_1$  and  $c(-f_0) = c_2$ . Then, it can be shown that  $\partial(\varepsilon(f_0) + \varepsilon(-f_0))/\partial c_1 < 0$  and  $\partial(\varepsilon(f_0) + \varepsilon(-f_0))/\partial c_2 < 0$ . Moreover, since  $a(f_0) = s(f_0)^H s(f_0)$ ,  $c(f_0)$  is constrained by  $a(f_0)$  through  $s(f_0)$  and  $c(-f_0)$  is constrained by  $a(-f_0)$  through  $s(-f_0)$ . Thus, we now can separately find  $s(f_0)$  that maximizes  $c(f_0)$  for given  $a(f_0)$  and  $s(-f_0)$  that maximizes  $c(-f_0)$  for given  $a(-f_0)$ . This maximization of  $c(f)$  defined in (4.21) subject to  $a(f) = \|s(f)\|^2$  is exactly the same problem solved in [12, Section IV-B], where the optimal solution is given by (4.35) at each  $f \in \mathcal{F}$ . Therefore, the conclusion follows.  $\square$

According to (4.35), the optimal  $s(f)$  given  $a(f)$  is not affected by the propriety frequency function  $k(f)$ . However, it actually affects the outer optimization of  $a(f)$ , which will be performed in what follows. Let  $\lambda(f)$  denote the largest eigenvalue of  $\mathbf{H}(f)^H \mathbf{R}_N(f)^{-1} \mathbf{H}(f)$ . Then, by (4.35),  $c(f)$  can be simplified as  $c(f) = M(fT)\lambda(f)a(f)/T, \forall f \in \mathcal{F}$ . Thus, the outer minimization problem of Problem 3 to find the optimal energy density  $a_{\text{opt}}(f)$  for  $f \in \mathcal{F}$  becomes

#### Problem 4

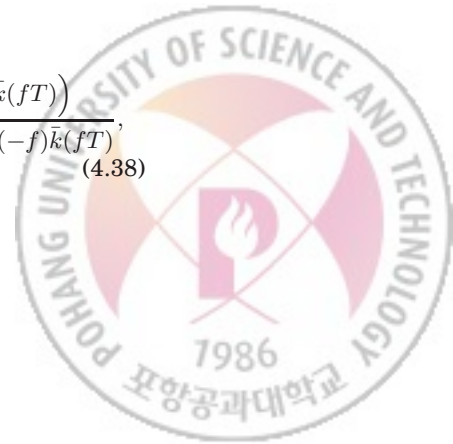
$$\underset{a(f), a(-f)}{\text{minimize}} \quad T^2 \int_{\mathcal{F}^+} \bar{\varepsilon}(f) df \quad (4.37a)$$

$$\text{subject to} \quad \frac{1}{T} \int_{\mathcal{F}^+} M(fT)a(f) + M(-fT)a(-f) df = P_T, \quad (4.37b)$$

where  $\bar{\varepsilon}(f)$  is given by

$$\bar{\varepsilon}(f) \triangleq \frac{\frac{M(-fT)}{T} \left(1 + \frac{M(fT)}{T} \lambda(f)a(f)\bar{k}(fT)\right) + \frac{M(fT)}{T} \left(1 + \frac{M(-fT)}{T} \lambda(-f)a(-f)\bar{k}(fT)\right)}{1 + \frac{M(fT)}{T} \lambda(f)a(f) + \frac{M(-fT)}{T} \lambda(-f)a(-f) + \frac{M(fT)}{T} \lambda(f)a(f) \frac{M(-fT)}{T} \lambda(-f)a(-f)\bar{k}(fT)}, \quad (4.38)$$

with  $\bar{k}(f) \triangleq 1 - k(f)^2$  as already used in (4.36).



### 4.3. OPTIMIZATION OF TRANSMIT AND RECEIVE WAVEFORMS 104

Now, we are ready to present the optimal  $a(f)$ . In what follows,  $\mathcal{F}_M$  and  $\mathcal{F}_\lambda$  denote the supports of  $M(fT)$  and  $\lambda(f)$ , respectively, i.e.,  $\mathcal{F}_M \triangleq \{f \in \mathcal{F} : M(fT) \neq 0\}$  and  $\mathcal{F}_\lambda \triangleq \{f \in \mathcal{F} : \lambda(f) \neq 0\}$ .

**Proposition 6** *The optimal solution to Problem 4 can be found by performing a line search for a parameter  $\nu$  in  $(0, \nu_{\max}]$ , where  $\nu_{\max} \triangleq \max_f \lambda(f)(M(-fT)k(fT)^2 + M(fT))$ . For each  $\nu \in (0, \nu_{\max}]$ , a candidate density function can be constructed by using the algorithm described in Table 4.1, where*

$$u(\nu, f) = \begin{cases} \left[ \frac{1}{\sqrt{\nu}} - \frac{1 + M(-fT)\lambda(-f)a(-f)}{\sqrt{\lambda(f)\nu(f)}} \right]^+ \frac{\sqrt{\lambda(f)\nu(f)}}{\lambda(f)M(fT)g(-f)}, & \text{for } f \in \mathcal{F}_M \cap \mathcal{F}_\lambda, \\ 0, & \text{for } f \in \mathcal{F}_M \cap (\mathcal{F}_\lambda)^c, \\ \text{arbitrary}, & \text{for } f \in (\mathcal{F}_M)^c, \end{cases} \quad (4.39)$$

with  $g(f) \triangleq 1 + M(fT)\lambda(f)a(f)\bar{k}(fT)$ ,  $\nu(f) \triangleq M(-fT)k(fT)^2 + M(fT)g(-f)^2$ , and  $[x]^+ \triangleq \max(x, 0)$ . The candidate function that satisfies the power constraint (4.37b) is the optimal density function  $a_{\text{opt}}(f)$ .

*Proof:* For convenience, the integration interval  $\mathcal{F}^+$  is partitioned into  $N$  equal-length subintervals. Then, the solution can be straightforwardly extended to the original problem by letting  $N$  tend to infinity. Let  $\xi_i \triangleq i/(2NT) - 1/(4NT)$ ,  $a_i \triangleq a(\xi_i)$ ,  $\hat{a}_i \triangleq a(-\xi_i)$ ,  $m_i \triangleq M(\xi_i T)/T$ ,  $\hat{m}_i \triangleq M(-\xi_i T)/T$ ,  $\lambda_i \triangleq \lambda(\xi_i)$ ,  $\hat{\lambda}_i \triangleq \lambda(-\xi_i)$ , and  $k_i \triangleq k(\xi_i T)$ . Then, the original optimization problem can be approximated by

$$\underset{a_i, \hat{a}_i \geq 0}{\text{minimize}} \quad \sum_{i=1}^N f_i(a_i, \hat{a}_i) \quad (4.40a)$$

$$\text{subject to} \quad \sum_{i=1}^N (m_i a_i + \hat{m}_i \hat{a}_i) \leq P_T T, \quad (4.40b)$$

where  $f_i(a_i, \hat{a}_i)$  is given by

$$f_i(a_i, \hat{a}_i) \triangleq \frac{\hat{m}_i(1 + m_i \lambda_i a_i \bar{k}_i) + m_i(1 + \hat{m}_i \hat{\lambda}_i \hat{a}_i \bar{k}_i)}{1 + m_i \lambda_i a_i + \hat{m}_i \hat{\lambda}_i \hat{a}_i + m_i \lambda_i a_i \hat{m}_i \hat{\lambda}_i \hat{a}_i \bar{k}_i}$$

for non-negative real numbers  $m_i, \hat{m}_i, \lambda_i, \hat{\lambda}_i$ , and  $\bar{k}_i \triangleq 1 - k_i^2$  with  $0 \leq k_i < 1$ ,  $\forall i$ . It can be easily shown that, if  $m_i = 0$ ,  $a_i$  can be chosen arbitrarily because  $a_i$  does not affect both the objective function and the constraint. It can be also





### 4.3. OPTIMIZATION OF TRANSMIT AND RECEIVE WAVEFORMS 105

easily shown that  $\lambda_i = 0$  results in  $a_i = 0$  to keep from wasting the transmit power. Similarly, if  $\hat{m}_i = 0$ , then  $\hat{a}_i$  can be chosen arbitrarily, and if  $\hat{\lambda}_i = 0$ , then  $\hat{a}_i = 0$ . The case of  $k_i = 1$  is discussed after solving the optimization problem for  $k_i < 1$ . Thus, in what follows, we assume that  $m_i \hat{m}_i \neq 0$ ,  $\lambda_i \hat{\lambda}_i \neq 0$ , and  $k_i < 1$ ,  $\forall i$ .

Define  $\mathbf{a}$  and  $\mathbf{m}$  as

$$\mathbf{a} \triangleq [a_1, \hat{a}_1, a_2, \hat{a}_2, \dots, a_N, \hat{a}_N]^T$$

and

$$\mathbf{m} \triangleq [m_1, \hat{m}_1, m_2, \hat{m}_2, \dots, m_N, \hat{m}_N]^T,$$

respectively. Then, it can be easily shown that the Hessian  $F_i(\mathbf{a})$  of the objective function  $\sum_{i=1}^N f_i(a_i, \hat{a}_i)$  is a positive definite matrix for each  $\mathbf{a}$  and the equality constraint  $\sum_{i=1}^N (m_i a_i + \hat{m}_i \hat{a}_i) = \mathbf{m}^T \mathbf{a}$  is an affine function of  $\mathbf{a}$ . Thus, the problem in (4.40) is a strictly convex optimization problem. Since the Karush-Kuhn-Tucker (KKT) condition is necessary and sufficient for a point to be the unique solution of a strictly convex optimization problem [63, Theorem 22.9], we first need to find the KKT condition.

The Lagrangian function of (4.40) can be written as

$$l(\mathbf{a}, \nu, \boldsymbol{\mu}) = \sum_{i=1}^N f_i(a_i, \hat{a}_i) + \nu(\mathbf{m}^T \mathbf{a} - P_T T) - \boldsymbol{\mu}^T \mathbf{a}$$

by introducing the multipliers  $\nu$  and

$$\boldsymbol{\mu} \triangleq [\mu_1, \hat{\mu}_1, \mu_2, \hat{\mu}_2, \dots, \mu_N, \hat{\mu}_N]^T.$$

Then, the KKT condition can be written as

$$-m_i \lambda_i (\hat{m}_i k^2 + m_i \hat{g}_i(\hat{a}_i)^2) / h_i(a_i, \hat{a}_i)^2 + m_i \nu - \mu_i = 0$$

and

$$-\hat{m}_i \hat{\lambda}_i (m_i k^2 + \hat{m}_i g_i(a_i)^2) / h_i(a_i, \hat{a}_i)^2 + \hat{m}_i \nu - \hat{\mu}_i = 0$$

with  $a_i \geq 0$ ,  $\hat{a}_i \geq 0$ ,  $\mu_i \geq 0$ ,  $\hat{\mu}_i \geq 0$ ,  $\mu_i a_i = 0$ ,  $\hat{\mu}_i \hat{a}_i = 0$ ,  $\forall i$ , and  $\sum_{i=1}^N (m_i a_i + \hat{m}_i \hat{a}_i) = P_T T$ , where

$$h_i(a_i, \hat{a}_i) \triangleq 1 + m_i \lambda_i a_i + \hat{m}_i \hat{\lambda}_i \hat{a}_i + m_i \lambda_i a_i \hat{m}_i \hat{\lambda}_i \hat{a}_i \bar{k}_i,$$

$$g_i(a_i) \triangleq 1 + m_i \lambda_i a_i \bar{k}_i,$$

and



### 4.3. OPTIMIZATION OF TRANSMIT AND RECEIVE WAVEFORMS 106

$$\hat{g}_i(\hat{a}_i) \triangleq 1 + \hat{m}_i \hat{\lambda}_i \hat{a}_i \bar{k}_i.$$

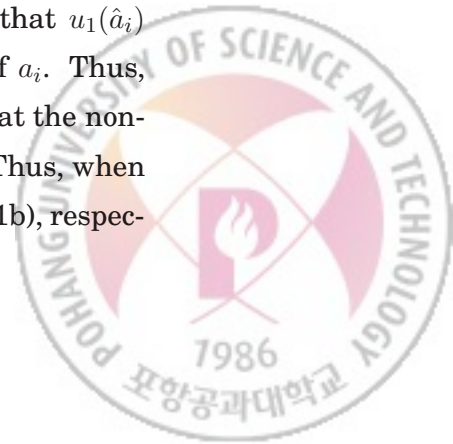
Define  $\nu_i(a_i, \hat{a}_i) \triangleq \lambda_i(\hat{m}_i k^2 + m_i \hat{g}_i(\hat{a}_i)^2)/h_i(a_i, \hat{a}_i)^2$  and  $\hat{\nu}_i(a_i, \hat{a}_i) \triangleq \hat{\lambda}_i(m_i k^2 + \hat{m}_i g_i(a_i)^2)/h_i(a_i, \hat{a}_i)^2$ , respectively. It can be easily shown that  $\partial \nu_i(a_i, \hat{a}_i)/\partial a_i < 0$ ,  $\partial \nu_i(0, \hat{a}_i)/\partial \hat{a}_i < 0$ ,  $\partial \hat{\nu}_i(a_i, \hat{a}_i)/\partial \hat{a}_i < 0$ , and  $\partial \hat{\nu}_i(a_i, 0)/\partial a_i < 0$  for all  $a_i \geq 0$  and  $\hat{a}_i \geq 0$ . Thus,  $\nu_i(a_i, \hat{a}_i) < \nu_i(0, 0)$  and  $\hat{\nu}_i(a_i, \hat{a}_i) < \hat{\nu}_i(0, 0)$ , respectively, for all  $a_i > 0$  and  $\hat{a}_i > 0$ . It can be also shown that, if  $\nu \geq \nu_i(0, 0)$  and  $\nu \geq \hat{\nu}_i(0, 0)$ , then only  $a_i = 0$  and  $\hat{a}_i = 0$  satisfy the KKT condition. It is noteworthy that  $\nu$  satisfying the KKT condition is upper-bounded by  $\nu_{\max}$  that is defined as the largest value among  $\nu_i(0, 0)$  and  $\hat{\nu}_i(0, 0)$ ,  $\forall i$ , which can be easily found and is finite and positive. Thus, to find  $\alpha$ ,  $\nu$ , and  $\mu$  that jointly satisfy the KKT condition, a line search for  $\nu$  can be performed over the interval  $(0, \nu_{\max}]$ , where two steps are needed to construct a candidate solution  $\alpha$  and the multiplier  $\mu$  at each  $\nu$ .

First, a candidate solution  $\alpha$  associated with  $\nu$  is constructed as follows. Given  $\nu$ , we need to find the pair of  $(a_i, \hat{a}_i)$  satisfying the KKT condition, i.e.,  $\nu - \mu_i/m_i = \nu_i(a_i, \hat{a}_i)$  and  $\nu - \hat{\mu}_i/\hat{m}_i = \hat{\nu}_i(a_i, \hat{a}_i)$  with  $a_i \geq 0$ ,  $\hat{a}_i \geq 0$ ,  $\mu_i \geq 0$ ,  $\hat{\mu}_i \geq 0$ ,  $\mu_i a_i = 0$ ,  $\hat{\mu}_i \hat{a}_i = 0$ , which can be rewritten as

$$\begin{aligned} a_i &= u_1(\hat{a}_i) \\ &\triangleq \left[ \sqrt{\frac{\lambda_i(\hat{m}_i k^2 + m_i \hat{g}_i(\hat{a}_i)^2)}{\nu}} - (1 + \hat{m}_i \hat{\lambda}_i \hat{a}_i) \right]^+ \frac{1}{\lambda_i m_i \hat{g}_i(\hat{a}_i)}, \end{aligned} \quad (4.41a)$$

$$\begin{aligned} \hat{a}_i &= u_2(a_i) \\ &\triangleq \left[ \sqrt{\frac{\hat{\lambda}_i(m_i k^2 + \hat{m}_i g_i(a_i)^2)}{\nu}} - (1 + m_i \lambda_i a_i) \right]^+ \frac{1}{\hat{\lambda}_i \hat{m}_i g_i(a_i)}, \end{aligned} \quad (4.41b)$$

$\mu_i = 0$  if  $a_i > 0$ , and  $\hat{\mu}_i = 0$  if  $\hat{a}_i > 0$ . It can be easily shown that  $u_1(\hat{a}_i)$  is a decreasing function of  $\hat{a}_i$  and  $u_2(a_i)$  is a decreasing function of  $a_i$ . Thus,  $(u_2(u_1(\hat{a}_i)))$  becomes an increasing function of  $\hat{a}_i$ . It is noteworthy that the non-negative numbers  $a_i$  and  $\hat{a}_i$  are upper-bounded by  $u_1(0)$  and  $u_2(0)$ . Thus, when we alternately update  $a_i$  and  $\hat{a}_i$  from  $\hat{a}_i = 0$  by using (4.41a) and (4.41b), respec-



### 4.3. OPTIMIZATION OF TRANSMIT AND RECEIVE WAVEFORMS 107

**Table 4.1** An Algorithm to Construct Candidate Density Function at  $\nu \in (0, \nu_{\max}]$

- 
- 1: Choose  $f_0 \in \mathcal{F}^+$ .
  - 2: Construct  $a(f_0)$  and  $a(-f_0)$  as follows.
  - 3:     Set  $a(-f_0) := 0$ .
  - 4:     **REPEAT**
  - 5:         Update  $a(f_0)$  as  $a(f_0) := u(\nu, f_0)$  by using  $u(\nu, f)$  defined in (4.39).
  - 6:         Update  $a(-f_0)$  as  $a(-f_0) := u(\nu, -f_0)$ .
  - 7:     **UNTIL**  $a(f_0)$  and  $a(-f_0)$  converge.
  - 8: Repeat lines 1 – 7 for all  $f_0 \in \mathcal{F}^+$ .
- 

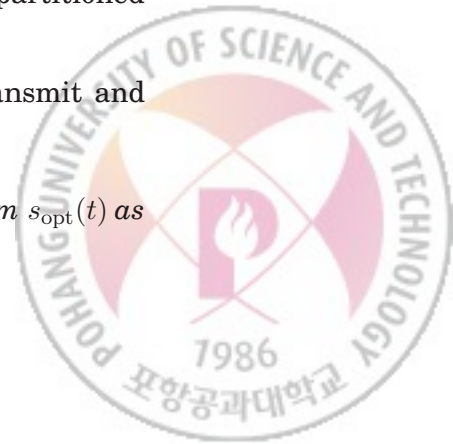
tively, both  $a_i$  and  $\hat{a}_i$  converge to the solution satisfying the KKT conditions. This iteration algorithm can be also used to find the candidate solution  $a_i$  and  $\hat{a}_i$  for the case of  $k_i = 1$ . Note that, if  $k_i = 1$  and  $\lambda_i = \hat{\lambda}_i$ , any pair of  $a_i$  and  $\hat{a}_i$  satisfying  $m_i a_i + \hat{m}_i \hat{a}_i = [\sqrt{(m_i + \hat{m}_i)/(\lambda_i \nu)} - 1/\lambda_i]^+$  can be the candidate solution associated with  $\nu$ . After finding  $a_i$  and  $\hat{a}_i$ ,  $\mu_i$  and  $\hat{\mu}_i$  can be computed by substituting  $a_i$ ,  $\hat{a}_i$ , and  $\nu$  into the KKT condition.

Second, after constructing the candidate solution  $\mathbf{a}$  associated with  $\nu$ , we check whether the candidate solution satisfies the power constraint  $\sum_{i=1}^N (m_i a_i + \hat{m}_i \hat{a}_i) = P_T T$ . If so, then the candidate solution associated with  $\nu_{\text{opt}}$  is the optimal solution  $\mathbf{a}_{\text{opt}}$ . If not, then the line search continues. Therefore, the conclusion follows.  $\square$

Note that any line search algorithm can be used to find  $\mathbf{a}_{\text{opt}}(f)$  in Proposition 6. Note also that the algorithm in Table 4.1 allows the construction of an approximate solution with arbitrary accuracy if the interval  $\mathcal{F}^+$  is partitioned finely enough.

Now, by using  $\mathbf{a}_{\text{opt}}(f)$ , we can find the VFTs of the optimal transmit and receive waveforms as follows.

**Theorem 5** *The VFT  $s_{\text{opt}}(f)$  of the jointly optimal transmit waveform  $s_{\text{opt}}(t)$  as*



the solution to Problem 1 are given by

$$s_{\text{opt}}(f) = \begin{cases} \sqrt{a_{\text{opt}}(f)}v(f)e^{j\theta(f)}, & \text{for } f \in \mathcal{F}_M, \\ \text{arbitrary}, & \text{for } f \in (\mathcal{F}_M)^c, \end{cases} \quad (4.42)$$

where  $\theta(f)$  can be chosen arbitrarily. Then, the VFTs  $w_{1,\text{opt}}(f)$  and  $w_{2,\text{opt}}(f)$  of the jointly optimal receive waveforms  $w_{1,\text{opt}}(t)$  and  $w_{2,\text{opt}}(t)$  can be found by using (4.17).

*Proof:* The conclusion immediately follows from the relation (4.11) among  $s_{\text{opt}}(f)$ ,  $\bar{s}_{\text{opt}}(f)$ ,  $w_{1,\text{opt}}(f)$ ,  $w_{2,\text{opt}}(f)$ , and  $\bar{w}_{\text{opt}}(f)$ , and Propositions 5 and 6.  $\square$

As already mentioned, cyclostationarity and impropriety, respectively, imply the periodic spectral correlation and the symmetric spectral correlation about the origin [18, Ch. 10], [64]. Theorem 1 vividly shows these structures in the optimal transmitted signal. Specifically, the use of the VFT technique and the augmentation of  $s(f)$  and  $s(-f)$  to form  $\bar{s}(f)$  take care of the periodic spectral correlation and the symmetric spectral correlation, respectively.

## 4.4 Numerical Results

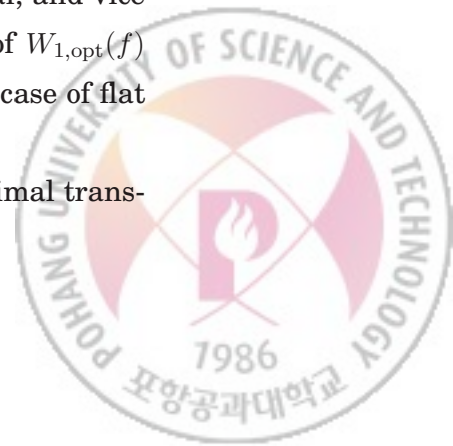
In this section, numerical results are provided that show the magnitude square of the optimal waveforms and that show the performance achieved by the proposed joint optimization. It is assumed throughout this section that the Tx linearly modulates uncorrelated zero-mean improper-complex QAM symbols with uncorrelated in-phase and quadrature components. It is also assumed that an interferer linearly modulates uncorrelated zero-mean proper-complex QPSK symbols having interference-to-signal power ratio (ISR) 5 [dB] and employs a square-root raised cosine transmit waveform having excess bandwidth  $\beta = 0.25$ .

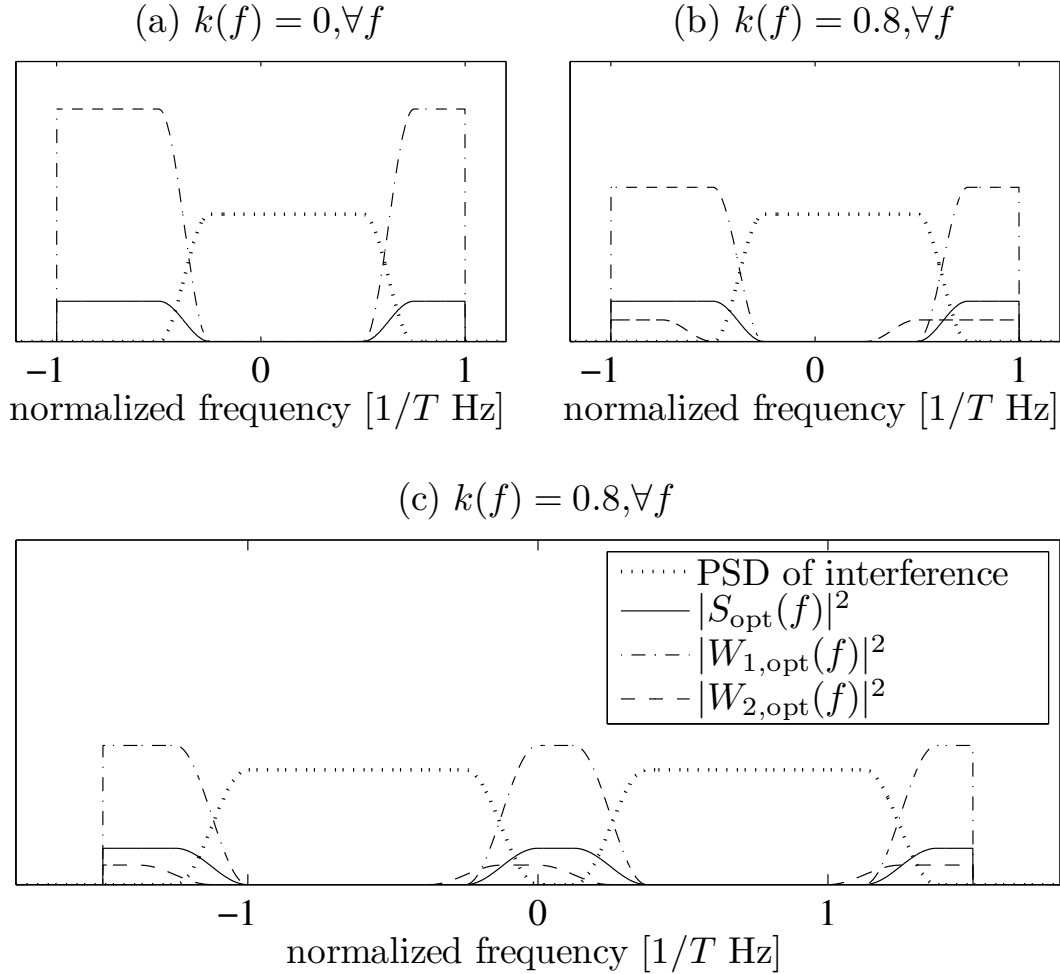
The first results are to compare the PSD of data-like interference with the squared magnitudes of the optimal transmit and receive waveforms. There is a single interferer in Figs. 4.2-(a) and (b), whereas there are two uncorrelated



interferers in Fig. 4.2-(c). The QAM symbols of the Tx have  $E_s/N_0 = 5$  [dB]. For illustrative purposes, it is assumed that all the channels are frequency flat and corrupted by AWGN. In Fig. 4.2-(a), the QAM symbols have the in-phase variance the same as the quadrature variance, which implies  $k(f) = 0, \forall f$ . In Figs. 4.2-(b) and (c), the QAM symbols have the in-phase variance 4-times the quadrature variance, which implies  $k(f) = 0.8, \forall f$ . It is assume that the Tx can emit non-zero power on  $f \in [-1/T, 1/T)$  in both Figs. 4.2-(a) and 4.2-(b) whereas the Tx can emit non-zero power on  $f \in [-2/T, 2/T)$  in both Figs. 4.2-(c). Recall that, when the PSD  $M(f)$  is given, the impropriety function  $k(f)$  at each  $f$  increases as the complementary PSD  $\tilde{M}(f)$  at each  $f$  increases by Definition 25. In addition, the complementary PSD  $\tilde{M}(f)$  has non-zero value if and only if there is non-zero symmetric spectral correlation about the origin in the received signal. As shown in Fig. Fig: spectrum-(a), if the received signal is proper, i.e.,  $k(f) = 0, \forall f$ , then the optimal  $W_{2,\text{opt}}(f)$  becomes zero for all  $t$ . In this proper-complex case, there is no symmetric spectral correlation, so that the WMMSE Rx reduces to the LMMSE Rx. On the other hand, it can be seen in Figs. 2-(b) and 2-(c) that  $W_{2,\text{opt}}(f)$  is non-zero for the data sequence having  $k(f) = 0.8, \forall f$ . This is because the WMMSE Rx is designed to well exploit the impropriety by jointly optimizing  $W_{1,\text{opt}}(f)$  and  $W_{2,\text{opt}}(f)$ . Recall also that a non-zero complementary auto-correlation function in the time domain implies that symmetric components of the signal about the origin in the frequency domain may have non-zero complementary correlation. Thus, if  $f_0$  is in the frequency support of the optimal receive waveform that processes the improper-complex signal, then  $-f_0$  is in the support of the other optimal receive waveform that processes the complex conjugate of the signal, and vice versa. As it can be seen in Figs. 4.2-(b) and 4.2-(c), the support of  $W_{1,\text{opt}}(f)$  and the support of  $W_{2,\text{opt}}(f)$  are symmetric about the origin in this case of flat channels.

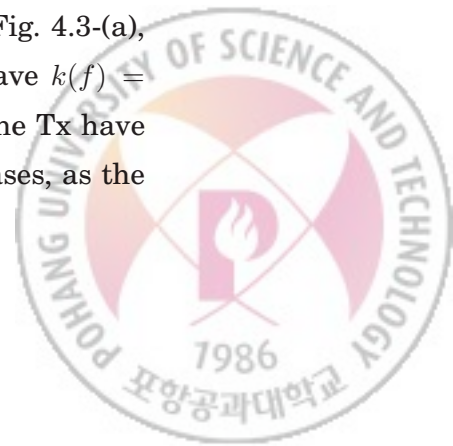
The second results are to compare the MSEs achieved by the optimal trans-





**Fig. 4.2** Comparison of squared-magnitudes of the optimal transmit and receive waveforms for (a)  $k(f) = 0, \forall f$  and single interferer, (b)  $k(f) = 0.8, \forall f$  and single interferer, and (c)  $k(f) = 0.8, \forall f$  and two uncorrelated interferers.

mit and receive waveforms for different levels of impropriety. We consider the same interference and channel parameters as Fig. 4.2-(c). In Fig. 4.3-(a), the QAM symbols of the Tx have  $E_s/N_0$  from 0 to 15 [dB] and have  $k(f) = 0.0, 0.2, 0.4, 0.6, 0.8$ , or  $1.0, \forall f$ . In Fig. 4.3-(b), the QAM symbols of the Tx have  $E_s/N_0 = 0, 5, 10$  or  $15$  [dB] and have  $k(f)$  from 0 to 1,  $\forall f$ . In both cases, as the



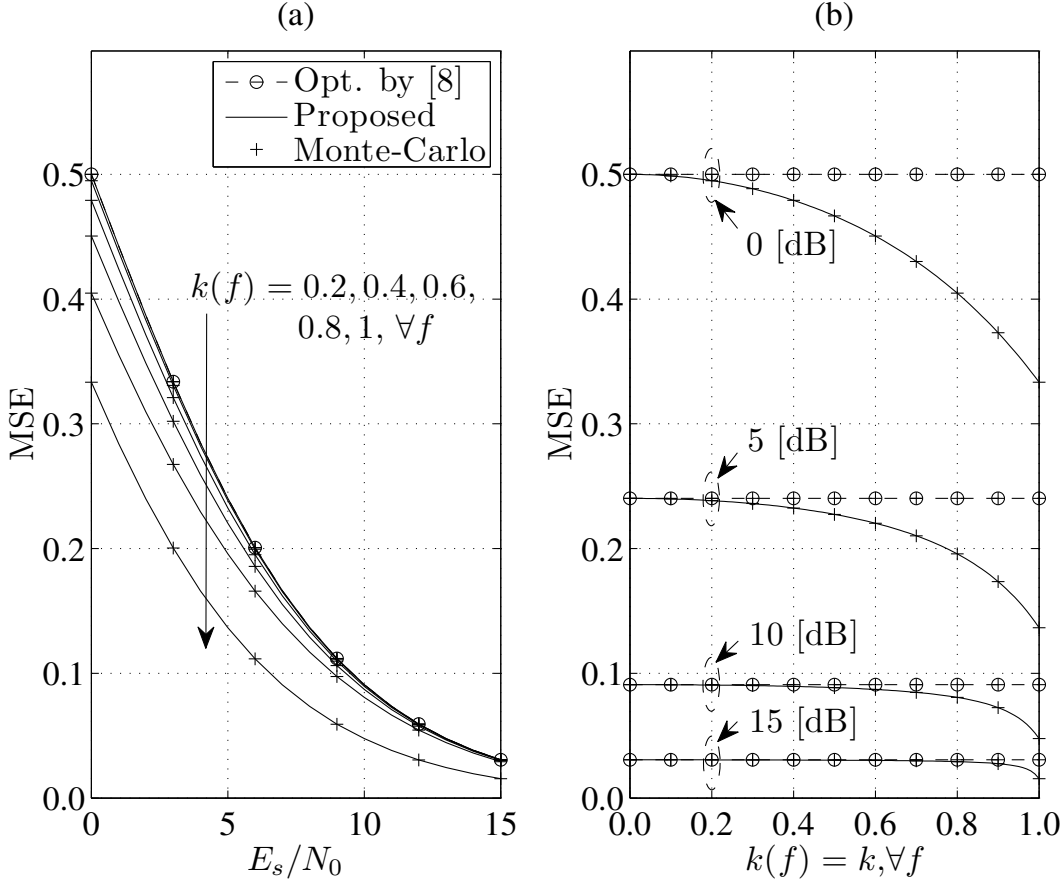


**Fig. 4.3** Comparison of MSE (a) versus  $E_s/N_0$  and (b) versus impropriety  $k(f) = k, \forall f$ .

amount of impropriety increases, the optimal pair of the Tx and Rx more exploits impropriety and cyclostationarity of the desired signal in suppressing the data-like interference and, consequently, the MSE performance monotonically improves.

The final results are to compare the bit error rate (BER) performances achieved by the Rx-only optimization, the Tx-Rx optimization proposed in [12], and the Tx-Rx optimization proposed in this chapter. The BER performances are obtained both by using Gaussian approximation to the interference and by using





Monte-Carlo simulation. We consider the transmission of uncorrelated zero-mean BPSK symbols, i.e.,  $k(f) = 1, \forall f$ , and the same interference parameters as Fig. 4.3. However, the channel from the Tx to the Rx is assumed to be frequency selective with impulse response  $h(t) = 0.6e^{j\pi/4}\delta(t-T/3) + 0.6\delta(t-3T/4) + 0.5e^{j\frac{\pi}{7}}\delta(t-7T/8)$ . It is also assumed that the Tx can emit non-zero power on  $f \in [-2/T, 2/T)$  for Fig. 4.4-(a) and  $f \in [-1.9/T, 1.9/T)$  for Fig. 4.4-(b). In addition, the channels from the interferers to the Rx are chosen to be frequency selective with impulse responses  $h_1(t) = 0.5e^{-j\frac{\pi}{2}}\delta(t-T/2) + 0.8e^{j\pi}\delta(t-5T/11)$  and  $h_2(t) = 0.6e^{-j\pi/5}\delta(t-T/8) + 0.3e^{j\frac{23\pi}{40}}\delta(t-T/3) + 0.2e^{-j\frac{\pi}{3}}\delta(t-8T/7)$ . In the Rx-only optimization, the Rx waveforms are designed to minimize the MSE by using the WLMMSE Rx, while the Tx waveform is fixed as a flat spectrum pulse with bandwidth  $4/T$  and  $3.8/T$  for Figs. 4.4-(a) and 4.4-(b), respectively. It can be seen that the proposed optimization significantly outperforms the joint optimization in [12] because the pair of Tx and Rx proposed in [12] does not utilize the impropriety of the improper-complex data symbols. It can be also seen that the proposed optimization significantly outperforms the Rx-only optimization because the transmit waveforms are drastically different from the jointly optimal one that well exploits the second-order properties of the interfering signal and the channel.

## 4.5 Summary

In this chapter, we have considered a joint optimization of the Tx and Rx for the transmission of an improper-complex SOS data sequence over an additive proper-complex cyclostationary noise channel. An MSE minimization problem is formulated under the average transmit power constraint to find the jointly optimal transmit waveform of a linear modulator and the receive waveforms of a widely linear Rx. This problem is converted into an equivalent problem described in the frequency domain with the help of the VFT technique and solved by introducing the notion of the impropriety frequency function. It is shown



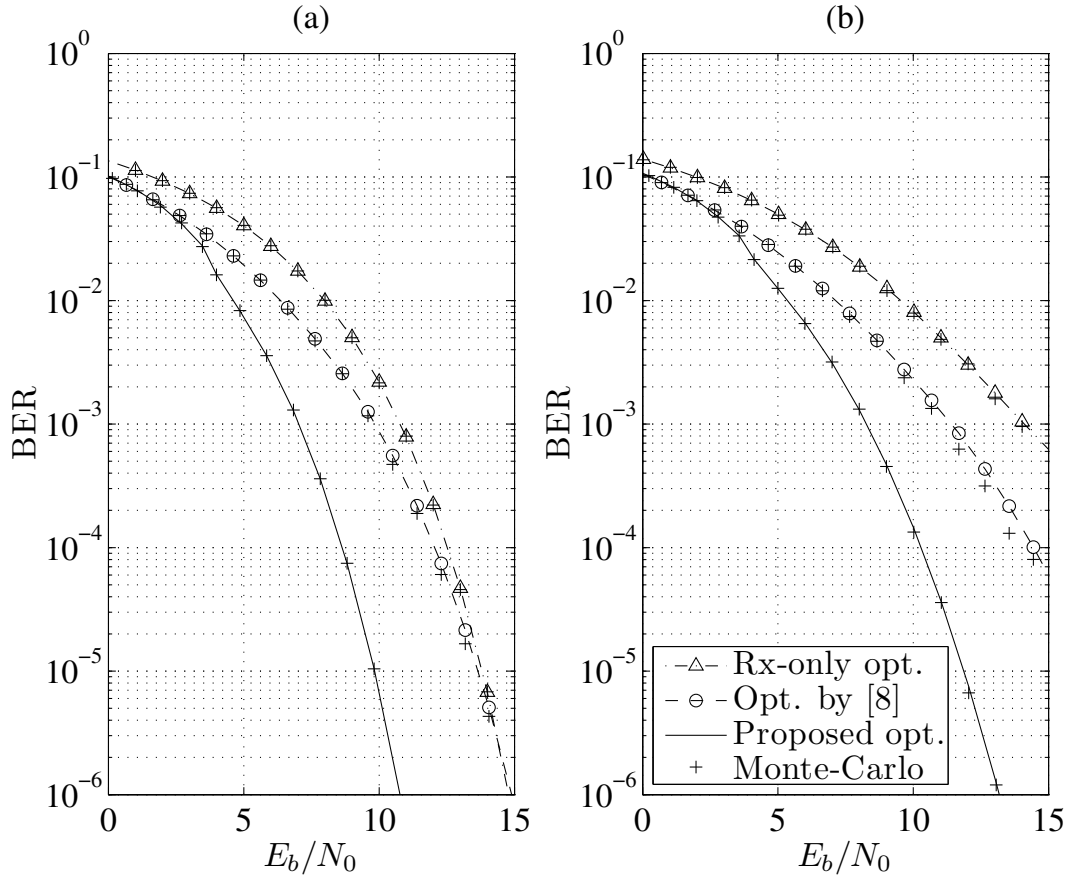


**Fig. 4.4** Comparison of BER versus  $E_b/N_0$  for BPSK data sequence for the transmit band (a)  $[-2/T, 2/T)$  and (b)  $[-1.9/T, 1.9/T)$ .

that the optimal transmit and receive waveforms well exploit the frequency-domain second-order structure of the improper-complex SOS data sequence and the additive proper-complex SOCS noise.



# CHAPTER 5

---

## Conclusions

---

In this thesis, we consider the optimal system design for transmission and reception of the signals that are well modeled as SOCS random processes. First, we propose a simple periodically LCL time-varying operator called a FRESH properizer. It is shown that the FRESH properizer always converts an SOCS random process, whether it is proper or improper, into an equivalent proper-complex SOCS random process. As an application, we consider the detection problem of an improper-complex SOCS Gaussian random process and derive the optimal presence detector that consists of a FRESH properizer followed by an estimator-correlator with a linear periodically time-varying filter. Numerical results show that the proposed detector significantly outperform the conventional linear estimator-correlator.

Then, the asymptotic FRESH properizer is proposed as a pre-processor for the block processing of a finite number of consecutive samples of a DT improper-complex SOCS random process. It turns out that the output of this pre-processor can be well approximated by a proper-complex random vector that has a highly-



structured frequency-domain covariance matrix for sufficiently large block size. The asymptotic propriety of the output allows the direct application with negligible performance degradation of the conventional signal processing techniques and algorithms dedicated to the block processing of proper-complex random vectors. Moreover, the highly-structured frequency-domain covariance matrix of the output facilitates the development of low-complexity post-processors. By solving the signal estimation and the signal presence detection problems, it is demonstrated that the asymptotic FRESH properizer leads to the simultaneous achievement of computational efficiency and asymptotic optimality. The use of the real part of the signal augmented by the imaginary part instead of the signal augmented by its complex conjugate is discussed for the estimation and detection problems as well as for the asymptotic FRESH properization.

Finally, we have considered a joint optimization of the Tx and Rx for the transmission of an improper-complex SOS data sequence over an additive proper-complex cyclostationary noise channel. An MSE minimization problem is formulated under the average transmit power constraint to find the jointly optimal transmit waveform of a linear modulator and the receive waveforms of a widely linear Rx. This problem is converted into an equivalent problem described in the frequency domain with the help of the VFT technique and solved by introducing the notion of the impropriety frequency function. It is shown that the optimal transmit and receive waveforms well exploit the frequency-domain second-order structure of the improper-complex SOS data sequence and the additive proper-complex SOCS noise.

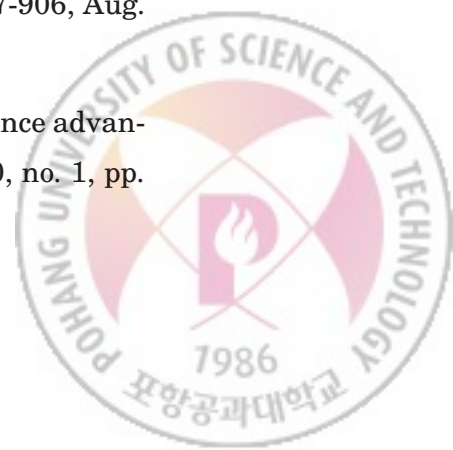


---

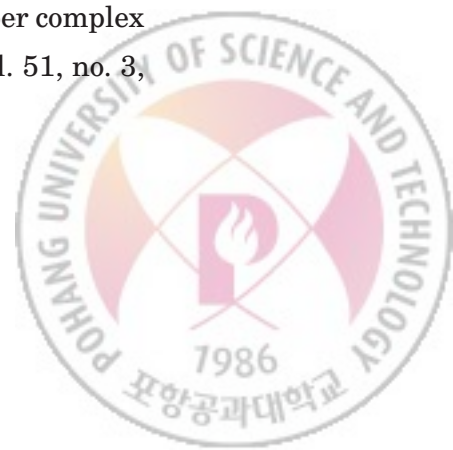
## Bibliography

---

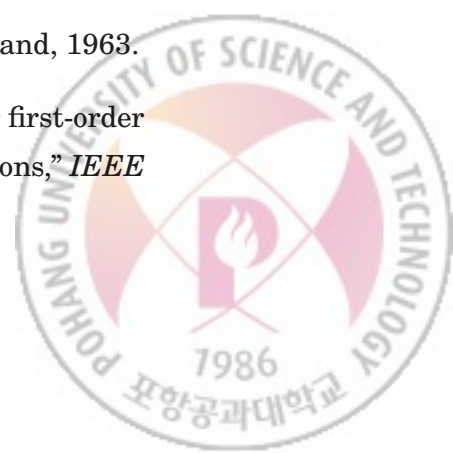
- [1] J. G. Proakis, *Digital Communications*, 4th ed. NY: McGraw Hill, 2001.
- [2] E. G. Gladyshev, "Periodically correlated random sequences," *Sov. Math.*, vol. 2, pp. 385-388, 1961.
- [3] W. A. Gardner and L. E. Franks, "Characterization of cyclostationary random signal processes," *IEEE Trans. Inf. Theory*, vol. 21, no. 1, pp. 4-14, Jan. 1975.
- [4] E. Serpedin, F. Panduru, I. Sari, and G. B. Giannakis, "Bibliography on cyclostationarity," *Signal Process.*, vol. 85, no. 12, pp. 2233-2303, Dec. 2005.
- [5] W. A. Gardner, A. Napolitano, and L. Paura, "Cyclostationarity: Half a century of research," *Signal Process.*, vol. 86, no. 4, pp. 639-697, Apr. 2006.
- [6] W. A. Gardner, "Signal interception: A unifying theoretical framework for feature detection," *IEEE Trans. Commun.*, vol. 36, no. 8, pp. 897-906, Aug. 1988.
- [7] W. A. Gardner and C. M. Spooner, "Signal interception: Performance advantages of cyclic-feature detectors," *IEEE Trans. Commun.*, vol. 40, no. 1, pp. 149-159, Jan. 1992.



- [8] W. A. Gardner, W. A. Brown, and C.-K. Chen, "Spectral correlation of modulated signals: Part II—Digital modulation," *IEEE Trans. Commun.*, vol. 35, no. 6, pp. 595-601, June 1987.
- [9] W. A. Gardner and W. A. Brown, "Frequency-shift filtering theory for adaptive co-channel interference removal," in *Proc. 23rd Asilomar Conf. Signals, Systems, Computers*, vol. 2, Pacific Grove, CA, 30 Oct.-1 Nov. 1989, pp. 562-567.
- [10] G. B. Giannakis, "Filterbanks for blind channel identification and equalization," *IEEE Signal Process. Lett.*, vol. 4, no. 6, pp. 184-187, June 1997.
- [11] A. Sabharwal, U. Mitra, and R. Moses, "MMSE receivers for multirate DS-CDMA systems," *IEEE Trans. Commun.*, vol. 49, no. 12, pp. 2184-2197, Dec. 2001.
- [12] J. H. Cho, "Joint transmitter and receiver optimization in additive cyclostationary noise," *IEEE Trans. Inf. Theory*, vol. 50, no. 12, pp. 3396-3405, Dec. 2004.
- [13] Y. H. Yun and J. H. Cho, "An optimal orthogonal overlay for a cyclostationary legacy signal," *IEEE Trans. Commun.*, vol. 58, no. 5, pp. 1557-1567, May 2010.
- [14] F. D. Neeser and J. L. Massey, "Proper complex random processes with applications to information theory," *IEEE Trans. Inf. Theory*, vol. 39, no. 4, pp. 1293-1302, July 1993.
- [15] P. J. Schreier and L. L. Scharf, "Second-order analysis of improper complex random vectors and processes," *IEEE Trans. Signal Process.*, vol. 51, no. 3, pp. 714-725, Mar. 2003.

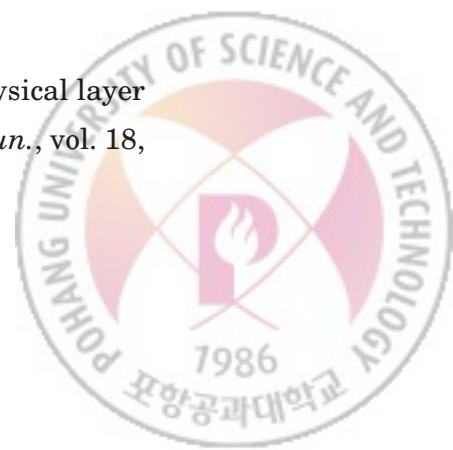


- [16] P. Wahlberg and P. J. Schreier, "Spectral relations for multidimensional complex improper stationary and (almost) cyclostationary processes," *IEEE Trans. Inf. Theory*, vol. 54, no. 4, pp. 1670-1682, Apr. 2008.
- [17] G. Tauböck, "Complex-valued random vectors and channels: Entropy, divergence, and capacity," *IEEE Trans. Inf. Theory*, vol. 58, no. 5, pp. 2729-2744, May 2012.
- [18] P. J. Schreier and L. L. Scharf, *Statistical Signal Processing of Complex-Valued Data: The Theory of Improper and Noncircular Signals*. NY: Cambridge Univ. Press, 2010.
- [19] B. Picinbono and P. Chevalier, "Widely linear estimation with complex data," *IEEE Trans. Signal Process.*, vol. 43, no. 8, pp. 2030-2033, Aug. 1995.
- [20] W. M. Brown and R. B. Crane, "Conjugate linear filtering," *IEEE Trans. Inf. Theory*, vol. 15, no. 4, pp. 462-465, July 1969.
- [21] B. W. Han and J. H. Cho, "Capacity of second-order cyclostationary complex Gaussian noise channels," *IEEE Trans. Commun.*, vol. 60, no. 1, pp. 89-100, Jan. 2012.
- [22] W. A. Gardner, "Cyclic Wiener filtering: Theory and method," *IEEE Trans. Commun.*, vol. 41, no. 1, pp. 151-163, Jan. 1993.
- [23] B. W. Han and J. H. Cho, "Optimal signaling in second-order cyclostationary Gaussian jamming environment," in *Proc. of IEEE Military Communications Conf. (MILCOM)*, Baltimore, MD, 7-10 Nov. 2011, pp. 102-107.
- [24] M. Loève, *Probability Theory*, 3rd ed. Princeton, NJ: Van Nostrand, 1963.
- [25] D. Middleton, "A statistical theory of reverberation and similar first-order scattered fields, Part II: Moments spectra, and special distributions," *IEEE Trans. Inf. Theory*, vol. 13, no. 3, pp. 393-414, July 1967.

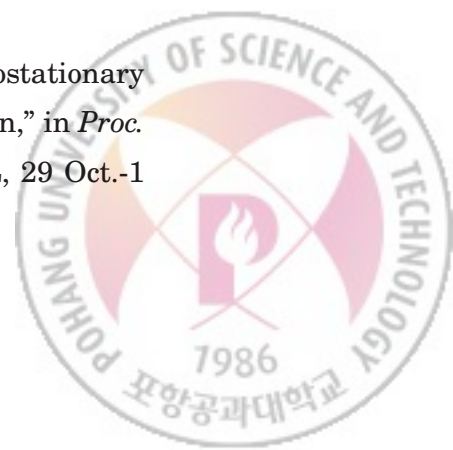




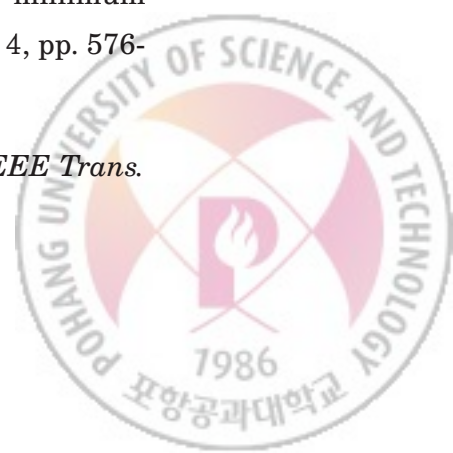
- [26] N. L. Gerr and J. C. Allen, "The Generalized spectrum and spectral coherence of a harmonizable time series," *Digital Signal Process.*, vol. 4, no. 4, pp. 222-238, Oct. 1994.
- [27] A. Napolitano "Uncertainty in measurements on spectrally correlated stochastic processes," *IEEE Trans. Inf. Theory*, vol. 49, no. 9, pp. 2172-2191, Sept. 2003.
- [28] P. J. Schreier and L. L. Scharf, "Stochastic time-frequency analysis using the analytic signal: Why the complementary distribution matters," *IEEE Trans. Signal Process.*, vol. 51, no. 12, pp. 3071-3079, Dec. 2003.
- [29] B. Picinbono and P. Bondon, "Second-order statistics of complex signals," *IEEE Trans. Signal Process.*, vol. 45, no. 2, pp. 411-420, Feb. 1997.
- [30] J. Yang and S. Roy, "On joint transmitter and receiver optimization for multiple-input-multiple-output (MIMO) transmission systems," *IEEE Trans. Commun.*, vol. 42, no. 12, pp. 3221-3231, Dec. 1994.
- [31] G. D. Golden, J. E. Mazo, and J. Salz, "Transmitter design for data transmission in the presence of a data-like interferer," *IEEE Trans. Commun.*, vol. 43, no. 2-4, pp. 837-850, Feb.-Apr. 1995.
- [32] J. H. Cho and W. Gao, "Continuous-time equivalents of Welch bound equality sequences," *IEEE Trans. Inf. Theory*, vol. 51, no. 9, pp. 3176- 3185, Sept. 2005.
- [33] W. A. Gardner, Ed. *Cyclostationarity in Communications and Signal Processing*. Piscataway, NJ: IEEE Press, 1994.
- [34] Y. Shiu, S. Y. Chang, H. Wu, S. C.-H. Huang, and H. Chen "Physical layer security in wireless networks: A tutorial," *IEEE Wireless Commun.*, vol. 18, no. 2, pp. 66-74, Apr. 2011.



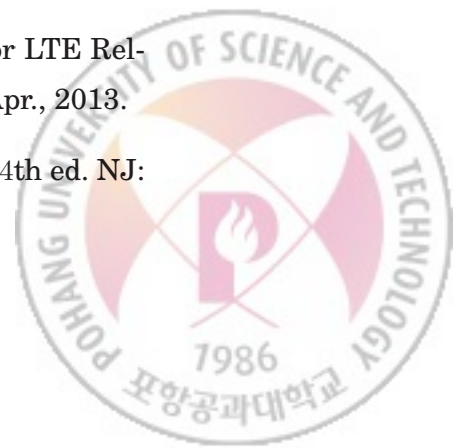
- [35] E. Shi and A. Perrig, "Designing secure sensor networks," *IEEE Wireless Commun.*, vol. 11, no. 6, pp. 38-43, Dec. 2004.
- [36] W. Xu, K. Ma, W. Trappe, and Y. Zhang, "Jamming sensor networks: Attack and defense strategies," *IEEE Network*, vol. 20, no. 3, pp. 41-47, May-June 2006.
- [37] T. Yücek, "A survey of spectrum sensing algorithms for cognitive radio applications," *IEEE Commun. Surveys Tuts.*, vol. 11, no. 1, pp. 116-130, First quarter 2009.
- [38] P. J. Schreier, L. L. Scharf, and C. T. Mullis, "Detection and estimation of improper complex random signals," *IEEE Trans. Inf. Theory*, vol. 51, no. 1, pp. 306-312, Jan. 2005.
- [39] H. L. Van Trees, *Detection, estimation, and modulation theory: Part I*, NY: Wiley, 2001.
- [40] H. V. Poor, *An Introduction to Signal Detection and Estimation*, 2nd ed. NY: Springer-Verlag, 1994.
- [41] B. Picinbono, "On deflection as a performance criterion in detection," *IEEE Trans. Aerosp. Electron. Syst.*, vol. 31, no. 3, pp. 1072-1081, July 1995.
- [42] R. M. Gray, "Toeplitz and circulant matrices: A review," *Found. Trends Commun. Inf. Theory*, vol. 2, no. 3, pp. 155-239, 2006.
- [43] Y. G. Yoo and J. H. Cho, "Asymptotically optimal low-complexity SC-FDE in data-like co-channel interference," *IEEE Trans. Commun.*, vol. 58, no. 6, pp. 1718-1728, June 2010.
- [44] J. H. Yeo and J. H. Cho, "Properization of second-Order cyclostationary random processes and its application to signal presence detection," in *Proc. IEEE Military Communications Conf. (MILCOM)*, Orlando, FL, 29 Oct.-1 Nov. 2012, pp. 1-6.



- [45] G. Bi and Y. Chen, "Fast generalized DFT and DHT algorithms," *Signal Process.*, vol. 65, no. 3, pp. 383-390, Mar. 1998.
- [46] H. Akaike, "Block Toeplitz matrix inversion," *SIAM J. Appl. Math.*, vol. 24, no. 2, pp. 234-241, Mar. 1973.
- [47] A. van den Bos, "The multivariate complex normal distribution—A generalization," *IEEE Trans. Inf. Theory*, vol. 41, no. 2, pp. 537-539, Mar. 1995.
- [48] W. Zhang, H. V. Poor, and Z. Quan, "Frequency-domain correlation: An asymptotically optimum approximation of quadratic likelihood ratio detectors," *IEEE Trans. Signal Process.*, vol. 58, no. 3, pp. 969-979, Mar. 2010.
- [49] A. Papoulis, *Probability, Random Variables, and Stochastic Processes*, 4th ed. New York: McGraw-Hill, 2002.
- [50] U. Grenander, H. O. Pollak, and D. Slepian, "The distribution of quadratic forms in normal variates: A small sample theory with applications to spectral analysis," *J. Soc. Ind. Appl. Math.*, vol. 7, no. 4, pp. 374-401, Dec. 1959.
- [51] J. Eriksson and V. Koivunen, "Complex random vectors and ICA models: Identifiability, uniqueness, and separability," *IEEE Trans. Inf. Theory*, vol. 52, no. 3, pp. 1017-1029, Mar. 2006.
- [52] T. Berger and D. W. Tufts, "Optimum pulse amplitude modulation Part I: Transmitter-receiver design and bounds from information theory," *IEEE Trans. Inf. Theory*, vol. 13, no. 2, pp. 196-208, Apr. 1967.
- [53] E. Hänsler, "Some properties of transmission systems with minimum mean-square error," *IEEE Trans. Commun. Technol.*, vol. 19, no. 4, pp. 576-579, Aug. 1971.
- [54] T. Ericson, "Optimum PAM filters are always band limited," *IEEE Trans. Inf. Theory*, vol. 19, no. 4, pp. 570-573, July 1973.



- [55] T. Ericson and U. Johansson, "A general time-discrete equivalent to a time-continuous Gaussian channel," *IEEE Trans. Inf. Theory*, vol. 20, no. 4, pp. 544-549, July 1974.
- [56] J. Yeo, J. H. Cho, and J. S. Lehnert, "Joint transmitter and receiver optimization for improper-complex second-order stationary data sequence," submitted to *J. Commun. Networking*, also available online at <http://arxiv.org/abs/1405.6450>.
- [57] R. Cadambe, S. A. Jafar, and C. Wang, "Interference alignment with asymmetric complex signaling - Settling the Høst-Madsen–Nosratinia conjecture," *IEEE Trans. Inf. Theory*, vol. 56, no. 9, pp. 4552–4565, Sep. 2010.
- [58] S. H. Park, H. Park, and I. Lee, "Coordinated SINR balancing techniques for multi-cell downlink transmission," in *Proc. VTC 2010-fall*, Ottawa, ON, 6-9 Sept. 2010, pp. 1-5.
- [59] Z. K. M. Ho and E. Jorswieck, "Improper Gaussian signaling on the two-user SISO interference channel," *IEEE Trans. Wireless Commun.*, vol. 11, no. 9, pp. 3194–3203, Sep. 2012.
- [60] Y. Zeng, C. M. Yetis, E. Gunawan, Y. L. Guan, and R. Zhang, "Transmit optimization with improper Gaussian signaling for interference channels," *IEEE Trans. Signal Process.*, vol. 61, no. 11, pp. 2899–2913, June 2013.
- [61] Renesas Mobile Europe Ltd., "Further considerations on advanced receivers," *3GPP TSG-RAN WG4 Meeting R4-66b*, Chicago, IL, 15-19 Apr., 2013.
- [62] Renesas Mobile Europe Ltd., "Receiver structures feasibility for LTE Rel-12," *3GPP TSG-RAN WG4 Meeting R4-66b*, Chicago, IL, 15-19 Apr., 2013.
- [63] E. K. P. Chong and S. H. Zak, *An Introduction to Optimization*, 4th ed. NJ: Wiley, 2013.



- [64] J. Yeo and J. H. Cho, "Asymptotic frequency-shift properizer for block processing of improper-complex second-order cyclostationary random processes," accepted to *IEEE Trans. Inf. Theory*, also available online at <http://arxiv.org/abs/1304.7375>.



# Glossary

## Abbreviations

2-D	two-dimensional
AWGN	additive white Gaussian noise
BER	bit error rate
CDF	cumulative distribution function
CT	continuous-time
DFT	discrete Fourier transform
DT	discrete-time
DTFT	discrete-time Fourier transform
GMSK	Gaussian minimum shift keying
FD-RSW	frequency-domain raised square wave
FFT	fast Fourier transform
FRESH	frequency-shift
HSR	harmonic series representation
i.i.d.	independent and identically distributed
ISI	intersymbol interference



KKT	Karush-Kuhn-Tucker
LCL	linear-conjugate linear
LLR	log-likelihood ratio
LRT	likelihood ratio test
LTl	linear time-invariant
LMMSE	linear minimum mean-squared error
MMSE	minimum mean-squared error
MSE	mean-squared error
MV-PSD	matrix-value power spectral density
OQPSK	offset quaternary phase-shift keying
PAM	pulse amplitude modulation
PDF	probability density function
PSD	power spectral density
PTV	periodically time-varying
QAM	quadrature amplitude modulation
ROC	receiver operating characteristic
RSW	raised square wave
Rx	receiver
SINR	signal-to-interference-plus-noise ratio





SNR	signal-to-noise ratio
SOCS	second-order cyclostationary
SOS	second-order stationary
SRRC	square-root raised cosine
TSR	translation series representation
Tx	transmitter
VFT	vectorized Fourier transform
WSCS	wide-sense cyclostationary
WSS	wide-sense stationary
WL	widely-linear
WLMMSE	widely-linear minimum mean-squared error



## 요 약 문

### 주기정상성과 복소이상성을 이용한 최적 시스템 설계

디지털 변조 신호들은 평균 함수, 자기분산 함수, 상보적 자기분산 함수가 같은 주기로 주기함수들인 이차주기정상적(second-order cyclostationary: SOCS) 랜덤 프로세스로 잘 모델된다. 일차와 이차 통계적 함수들에서 나타나는 주기성과 상보적 자기분산 함수가 0이 되지 않는 특성은 각각 주기정상성(cyclostationarity)과 복소이상성(impropriety)이라고 불린다. 이러한 통계적 특성은 다양한 최적 기준으로 신호 존재 검출기, 신호 추정기, 최적 송수신기와 같은 많은 통신 및 신호처리 시스템 설계에 이용될 수 있다. 본 논문에서는 SOCS 랜덤 프로세스의 주기정상성과 복소이상성을 효율적으로 이용하는 최적 그리고 근사 최적 시스템 설계 방법을 제안한다.

먼저, 연속시간(continuous-time: CT) 주파수 편이(frequency-shift: FRESH) 복소정상화기(properizer)라고 명명된 역연산이 가능한 선형-켈레선형 (linear-conjugate linear: LCL) 또는 광의선형(widely-linear: WL) 주기 시변화 연산기를 제안한다. 이렇게 제안된 연산기는 복소정상적(proper-complex) 또는 복소이상적(improper-complex) SOCS 랜덤 프로세스를 동일하면서 입력 신호 주기의 2배를 주기로 갖는 되는 복소정상적 SOCS 랜덤 프로세스로 변환하는 것을 보인다. 이 연산기의 응용으로서, 복소이상적 SOCS 랜덤 프로세스의 신호 존재 검출 문제가 고려된다. 특히, FRESH properizer를 활용하는 최적의 신호 존재 검출기가 유도되며, 이는 신호 검출 오류확률의 하한을 제시한다.



다음으로 이산시간(discrete-time: DT) SOCS 랜덤 프로세스의 블록 신호처리가 고려된다. CT FRESH properizer를 확장하여 역연산이 가능한 LCL 연산기를 제안하며, 이 연산기는 LCL DT FRESH properizer로 명명되었다. 또한 DT FRESH properizer를 따라하면서도 DT 복소이상적 SOCS 랜덤 프로세스에서 유한개의 연속적인 샘플들을 처리하기 위한 LCL 블록 프로세싱 연산기를 제안하며, 이 연산기는 근사 FRESH properizer라고 명명되었다. 근사 FRESH properizer의 출력은 정확하게는 복소이상적이지만, 근사적으로는 복소정상적이 되며, 샘플 수가 커질 때 대각 행렬을 블록으로 갖는 블록 행렬로 수렴하는 주파수 영역 분산 행렬을 갖는다. 근사 FRESH properizer를 이용하여 근사최적이고 낮은 복잡도를 갖는 신호 처리기가 쉽게 설계될수 있다는 것을 보이기 위해 대표적인 신호 추정 문제와 신호 존재 검출 문제가 제시된다.

마지막으로, 주파수 선택적 채널을 통한 복소이상적이고 이차정상적(second-order stationary: SOS)인 데이터 수열의 전송이 고려된다. 이 문제에서는 선형 변조를 이용하는 송신기와 복소정상적이고 주기정상적인 잡음이 더해지는 채널을 가정한다. 평균 송신 파워 제한하에서 최적의 송수신 파형들을 구하기 위해 LCL 평균 제곱오차(mean-squared error) 최소화 문제가 시간 영역에서 먼저 수식화 된다. 이 최적화 문제는 벡터화된 푸리에 변환 기법을 이용하여 주파수 영역 문제로 변환되고, 이중 최소화 문제 형식으로 놓인다. LCL 수신기가 최적화된 이후에, 복소이상성 주파수 함수를 도입하고 반복 알고리즘이 결합된 선형 검색을 수행하여 최적 송신 파형이 구해진다.



# Publications

## International Journal

- **J. Yeo**, B. W. Han, J. H. Cho, and J. S. Lehnert, "Capacity of an orthogonal overlay channel," in preparation.
- **J. Yeo**, J. H. Cho, and J. S. Lehnert, "Joint transmitter and receiver optimization for improper-complex second-order stationary data sequence," submitted to *Journal of Communications and Networks* (in 2nd review).
- **J. Yeo** and J. H. Cho, "Asymptotic frequency-shift properizer for block processing of improper-complex second-order cyclostationary random processes," *IEEE Trans. Inf. Theory*, vol. 60, no. 7, pp. 4083-4100, July 2014.

## Domestic Journal

- **J. Yeo** and J. H. Cho, "Iterative algorithms for interference alignment in cellular network," *J. Korea Inform. and Commun. Society (J-KICS)*, vol. 37, no. 10, pp. 947-955, Oct. 2012.

## International Conference

- **J. Yeo**, J. H. Cho, and J. S. Lehnert, "An optimal transmission of improper-complex second-order stationary data sequence in cyclostationary interference," submitted to *IEEE Military Commun. Conf. (MILCOM) 2014*.
- **J. Yeo** and J. H. Cho, "Asymptotically optimal low-complexity estimation of sampled improper-complex second-order cyclostationary random



process," in *Proc. of IEEE Wireless Commun. and Netw. Conf. (WCNC)*, Shanghai, China, 7-10 Apr. 2013.

- **J. Yeo** and J. H. Cho, "Properization of second-order cyclostationary random processes and its application to signal presence detection," in *Proc. of IEEE Military Commun. Conf. (MILCOM)*, Orlando, FL, 29 Oct.- 1 Nov. 2012. *Student Travel Grant Awards*
- **J. Yeo** and J. H. Cho, "Optimal presence detection of improper-complex second-order cyclostationary random signal for spectrum sensing in cognitive radio," in *Proc. of IEEE Global Commun. Conf. Workshops (GLOBECOM Workshops)*, Houston, TX, 5-9 Dec., 2011.
- **J. Yeo** and J. H. Cho, "Iterative algorithm for interference alignment in cellular network," in *Proc. of the 26th Int. Technical Conf. on Circuits/Systems, Comput., and Commun. (ITC-CSCC)*, Gyungju, Korea, 19-22 June 2011.
- **J. Yeo** and J. H. Cho, "Low-complexity near-optimal presence detection of linearly modulated signals," in *Proc. of IEEE Global Commun. Conf. (GLOBECOM)*, Honolulu, HI, 29 Nov. - 4 Dec. 2009.

### Domestic Conference

- **J. Yeo**, Y. G. Yoo and J. H. Cho, "Power spectral density of block-transmitted signals for SC-FDE using cyclic prefix, zero padding, and unique word," in *Proc. of the 18th Joint Conf. on Commun. and Inform. (JCCI)*, Jeju, Korea, 23-25 Apr. 2008.

### Patents

- 조준호, 여정호, "무선 인지 기술을 기반으로 하는 무선통신 시스템에서 신호의



존재를 검출하는 방법 및 장치,” 국내 특허 출원, 5/2010, 출원번호: 10-2010-0048074

- 조준호, 여정호, “이차 주기 정상적 신호 특성을 이용하는 신호 추정 방법 및 장치,” 국내 특허 출원, 4/2013, 출원번호: 10-2013-0037538
- 조준호, 여정호, “Method and apparatus for detecting presence of signal in wireless communication system based on CR technology,” 미국, 캐나다, 브라질 특허 출원, 9/2010, 출원번호: 12/885,973 (미국), 2,714,906 (캐나다), PI1004355-1 (브라질)



# Research Projects

- 간섭 제한 다중 안테나 다중 셀룰러 통신 시스템을 위한 새로운 송수신 구조, LG전자, 2012.9 -2013.6
- 간섭 제한 다중 셀룰러 통신 시스템을 위한 스마트 송수신기 구조, LG전자, 2011.6 -2012.5
- 인간의 음성신호 특성 및 각테일 파티 효과를 모방한 새로운 디지털 무선 송수신 방식에 관한 연구, 한국연구재단, 2011.5 - 2013.7
- 무선 통신 및 네트워킹을 위한 새넌/네트워크/내쉬 이론의 융합, 한국연구재단, 2010.9 - 2012.8
- 4세대 무선통신을 위한 새로운 전송 기법 연구, LG전자, 2009.12 -2010.11
- 선형 변조 간섭 채널에서 주파수 효율 향상을 위한 최적의 오버레이 시스템, 한국과학재단, 2008.5 - 2011.2
- FULL-DUPLEX AF 릴레이의 이론적 최적화 연구, 한국전자통신연구원, 2009.5 - 2009.12
- 고속 근거리 무선통신을 위한 FTN 기반의 강인한 송수신 방식에 대한 연구, 한국학술진흥재단, 2008.7 - 2010.6
- 실측데이터를 이용한 통계적 무선공간채널 파라미터 특성연구(2), 한국전자통신연구원, 2008.6 - 2008.11
- 광대역 다중 안테나 이동 통신 시스템의 이론적 최적화 및 이의 실험적 검증, 한국학술진흥재단, 2006.7 - 2008.6
- OFDM기반 100Mbps급 셀룰러 이동통신 기반 기술 연구, 정보통신연구진흥원, 2005.3 - 2012.12

